Models of Mechanics and Growth in Developmental Biology: A Computational Morphodinamics approach

Bozorg, Behruz

2016

Document Version:
Publisher's PDF, also known as Version of record

BEHRUZ BOZORG

MODELS OF MECHANICS AND GROWTH IN DEVELOPMENTAL BIOLOGY:
A COMPUTATIONAL MORPHODYNAMICS APPROACH

Models of Mechanics and Growth in Developmental Biology:
A Computational Morphodynamics approach

Behruz Bozorg

LUNDS UNIVERSITET

2016

Thesis for the degree of Doctor of Philosophy

Computational Biology and Biological Physics
Department of Astronomy and Theoretical Physics
Lund University

Thesis advisor: *Henrik Jönsson*
Faculty opponent: *Christophe Godin*

To be presented, with the permission of the Faculty of Science of Lund University, for public critiscism in Hall A, L317 in Department of Physics, on the 3rd of June 2016, at 13:15.

Organization	Document name
LUND UNIVERSITY Department of Astronomy and Theoretical Physics Sölvegatan 14A SE–223 62 LUND Sweden	**DOCTORAL DISSERTATION**
Author Behruz Bozorg	**Date of issue** June 2016
	Sponsoring organization

Title and subtitle
Models of Mechanics and Growth in Developmental Biology: A Computational Morphodinamics approach

Abstract

Recent evidence has revealed the role of mechanical cues in the development of shapes in organisms. This thesis is an effort to test some of the fundamental hypotheses about the relation between mechanics and patterning in plants. To do this, we develop mechanical models designed to include specific features of plant cell walls. These are heterogeneous stiffness and material anisotropy as well as rates and directions of growth, which we then relate to different domains of the plant tissue.

In plant cell walls, anisotropic fiber deposition is the main controller of longitudinal growth. In our model, this is achieved spontaneously, by applying feedback from the maximal stress direction to the fiber orientation. We show that a stress feedback model is in fact an energy minimization process. This can be considered as an evolutionary motivation for the emergence of a stress feedback mechanism. Then we add continuous growth and cell division to the model and employ the strain signal directing large growth deformations. We show the advantages of strain-based growth model for emergence of plant-like organ shapes as well as for reproducing microtubular dynamics in hypocotyls and roots. We also investigate possibilities for describing microtubular patterns, at root hair outgrowth sites according to stress patterns.

Altogether, the work described in this thesis, provides a new improved growth model for plant tissue, where mechanical properties are handled with appropriate care in the event of growth driven by either molecular or mechanical signals. The model unifies the patterning process for several different plant tissues, from shoot to single root hair cells, where it correctly predict microtubular dynamics and growth patterns. In a long-term perspective, this understanding can propagate to novel technologies for improvement of yield in agriculture and the forest industry.

Key words:
plants, morphodynamics, mechanics, anisotropy, growth, microtubules, microfibrils

Classification system and/or index terms (if any):

Supplementary bibliographical information:		Language English
ISSN and key title:		**ISBN** 978-91-7623-844-8 (print) 978-91-7623-845-5 (pdf)
Recipient's notes	**Number of pages** 175	**Price**
	Security classification	

Distributor
Behruz Bozorg, Department of Astronomy and Theoretical Physics
Sölvegatan 14A, SE–223 62 Lund, Sweden

SAMMANFATTNING

En av de största utmaningarna inom biologin är att förstå hur storleken och formen av olika organ, t ex blad och blommor, regleras. Vi vet att specifika gener påverkar och att tillväxthormoner spelar en stor roll. Samtidigt har det visat sig att fysikaliska egenskaper hos växternas cellväggar är viktigast för att skapa tillväxt i specifika riktningar. När växter växer och nya organ bildas deformeras celler och vävnader vilket innebär att växten kan utsättas för stora fysiska påfrestningar. Det har visats att cellväggen kan förstärkas i vissa riktningar genom att reglera riktningen på cellväggens cellulosafibrer. Det intressanta är att fysiska krafter påverkar fibrerna vilket gör att växten kan hålla emot i de riktningar där påfrestningarna är som störst. Samtidigt leder detta till robust tillväxt i vissa riktningar, vilket gör att en växt till exempel kan växa upp mot ljuset.

Denna avhandling avser att genom datormodellering, pröva några av de hypoteser som ligger till grund för hur mekaniska signaler kan påverka tillväxten av vävnader och nya organ i växter. För att kunna göra detta har vi utvecklat nya mekaniska modeller som inkluderar egenskaper såsom elasticitet, mekanisk anisotropi och tillväxthastigheter som alla tillåts variera i såväl rum som tid. Vi har utgått från Saint-Venants modell, som är en beskrivning av töjningsegenskaper hos ett material, och utökat denna beskrivning så att hänsyn kan tas till att material även kan vara anisotropiska, dvs vara starkare i en specifik riktning. Vi har använt platta element där spänningar går parallellt med planet för att beskriva cellväggen. Denna förenkling har vi validerat genom att jämföra resultaten från vår modell, med resultaten från en finit element modell där skalelement istället för plattor har använts. Vi visar att skillnaderna mellan dessa två modeller är försumbara.

I utkanten av växtskottet så bestäms riktningen av celltillväxten främst av orienteringen av cellulosafibrer. Detta kan i vår modell förklaras genom att låta den maximala spänningsriktningen återkoppla till orienteringen av växtcellens cellolusafibrer. Det kan noteras att graden av anisotropi hos det underliggande materialet, som vi kan justera i vår modell, kan beskriva anisotropin i utläggandet av fibrer i cellväggen.

Vi har även undersökt hur graden och riktningen av anisotropi påverkar mekaniken i en förenklad modell där relationen mellan töjning och spänning följer en klassisk linjär modell, Hookes lag. Vi visar att en sådan

återkoppling mellan töjning och spänning kan ses som en energiminimering. Även om mekanismen bakom återkopplingen mellan töjning och spänning fortfarande inte är helt känd, så kan minimeringen av energi ha varit avgörande i den evolutionära utvecklingen av hur celler påverkas av både spänning och töjning.

Vi har även introducerat kontinuerlig tillväxt i modellen, och vi har visat att resultaten för flera olika rumsliga uppdelningar av modellen alla konvergerar när vi närmar oss mekanisk jämvikt. Vi inkluderar även delning av celler i modellen, där vi minimerar diskontinuiteter hos mekaniska variabler före och efter att en celldelning ägt rum.

Till skillnad från många tidigare modeller där spänning reglerar tillväxt, så har vi undersökt vad som händer när en signal som istället kommer från töjning reglerar tillväxten. Vi har jämfört spännings- med töjnings-baserad tillväxt, och visat att en tillväxt som beror på graden av töjning, tillsammans med en återkoppling från spänning till den mekaniska anisotropin, resulterar i deformationer som kan ge upphov till de former man ser hos växter. Vi visar också hur en sådan modell kan klara av att återskapa cellulosafiberdynamiken som har observerats i flera organ i växter, t ex rötter och hypokotyler i växtfrön.

De olika symmetriska former som finns i växter har inpirerat vetenskapsmän och konstnärer i århundranden. Samtidigt är storleken och formen på växtens organ otroligt viktig för till exempel hur stora frukter och trädstammar som bildas, och en bättre förståelse för hur detta regleras gör att vi kan förbättra produktionen inom jordbruk och skogsindustri.

ACKNOWLEDGEMENTS

I am thankful to all the members of the Department of Astronomy and Theoretical Physics, particularly CBBP. It has been a great pleasure being a part of your team. I can hardly imagine myself, doing science in a better atmosphere, where science, support and friendship meet.

I owe my deepest gratitude to my supervisor, Henrik Jönsson for being a source of knowledge, patience, optimism, inspiration, support and trust. Henrik; I am grateful for working with you.

I had the chance of working with and learning from Pawel Krupinski. I am thankful for all the fruitful discussions and his scientific advices as well as valuable comments on this thesis.

I am grateful to Carsten Peterson for all of the discussions and advices, Anders Irbäck and Mattias Ohlsson for their valuable support and Bo Söderberg for always being ready to tackle a problem with a fresh mind.

I thank all of the members of Jönsson Group in Lund and Cambridge, particularly André Larsson, Niklas Korsbo, Yassin Refahi and Benoit Landrein for helping me in preparation of my thesis.

I am also thankful to my officemates, Karl Fogelmark, Victor Olario and Anna Bille for all of the discussions and nice moments and particularly, Jérémy Gruel for being a true friend.

I am deeply thankful to my family who provided me with endless love and support, without which I could not pave this way.

PUBLICATIONS

The thesis is based on the following publications:

I Behruz Bozorg, Pawel Krupinski and Henrik Jönsson. *Stress and strain provide positional and directional cues in development*. PLoS Computational Biology 10, e1003410 (2014)

II Behruz Bozorg, Pawel Krupinski and Henrik Jönsson. *Morphogenesis can be guided by the dynamic generation of anisotropic wall material optimizing strain energy*. LU TP16-12 (submitted)

III Behruz Bozorg, Pawel Krupinski, Henrik Jönsson. *A continuous growth model for plant tissue*. LU TP16-13 (submitted)

IV Behruz Bozorg and Henrik Jönsson. *Anisotropic growth in plants can result from stress feedback on wall material and strain-regulated growth*. LU TP16-15 (preprint)

V Pawel Krupinski, Behruz Bozorg, André Larsson, Stefano Pietra, Markus Grebe and Henrik Jönsson. *A model analysis of mechanisms for radial microtubular patterns at root hair initiation sites*. LU TP16-14 (submitted)

I have also contributed to the following paper:

Katarina Landberg, Eric R.A. Pederson, Tom Viaene, Behruz Bozorg, Jiri Friml, Henrik Jönsson, Mattias Thelander and Eva Sundberg. *The Moss Physcomitrella patens Reproductive Organ Development Is Highly Organized, Affected by the Two SHI/STY Genes and by the Level of Active Auxin in the SHI/STY Expression Domain*. Plant physiology 162, 1406-1419 (2013)

CONTENTS

To Farideh and Nita

1

INTRODUCTION

Understanding the relation between form and function in biological systems is a challenge [1]. The abundance of data together with the complexity and beauty of problems within this area are attracting experts representing a diverse range of interests. Here, the borderlines between different fields of science, in particular biology, mathematics and physics are becoming blurred. Being facilitated by computers, it is now possible to use the power of mathematics and physics for developing models to reduce the cost and increase the efficiency of cumbersome experimental hypotheses testing. Although it is never possible to replace experiments by purely theoretical analysis, modelling approaches are crucial to understand how such complex systems function and evolve [2, 3].

The extent of parameters and variables that are being identified in biological processes, is the main motivation for *Systems Biology* as an interdisciplinary field [2]. In a systems approach the effort is to decompose a complex network of variables to smaller modules as building blocks of the organism. This systematic simplification allows us to understand the system-wide interactions while low-level details are not confusing the picture [4]. Through multi-scale modelling, systems biologists try to analyse the behaviour of the building blocks at the fine scale and simplify it while keeping its important features. Later, these simplified modules are combined into higher level structures to achieve wider understanding of the system [5].

Biologists often perturb the organisms in experiments. This happens both unintentionally when they perform a measurement and when they test their predictions to support their hypotheses. In both cases modelling provides complementary possibilities, for either analysing the results of the measurements or comparing the results of the experiments with the outputs of the often complicated hypotheses.

The shape is indispensable to the functions of an organism [1]. The specific morphologies arise through targeted growth [6]. In biology, the term

Morphodynamics refers to the evolution of shape in the life span of living systems. The large deformations cannot occur without the mechanics being involved [7]. The elastic and plastic responses of the material to the forces determine the final shape of any tissue. Even if there is no mechanical signal regulating the dynamics of the shape, material properties and underlying laws of mechanics are crucial to understand morphogenesis [8]. The addition of the 4D morphodynamical events transfers Systems Biology to Computational Morphodynamics.

When described as a dynamical system, a living organism has to be characterised by a huge number of variables and parameters [9]. Normally such large degrees of freedom could push a system toward chaotic behaviours [4]. But conversely, life is very robust! This is mainly achieved by tying the enormous degrees of freedom via carefully designed feedbacks. Such mechanisms confine the dynamics of the system to specific domains in their phase space. These domains are related to the specific functions of the system [2, 10]. The connections between different biological components of a system or signalling pathways are often redundant, providing the system with more robustness. During evolution every possibility is used to increase the robustness and adaptability [11]. Mechanics as a fundamental feature of the material is capable to be involved in such processes and should not be disregarded as a fitness factor.

It is not easy to develop mechanical models for a living tissue. Such tissues have almost all the features that are disregarded from simplified classical material models. In general biomaterials are extremely inhomogeneous, composite, anisotropic and dynamically adaptive to the environment. In fact, these complicating factors play some important roles in morphogenesis [7, 12]. The complexity is a reason why despite the long history of continuum mechanics, mechanical models appropriate for simulating finite growth still need to be improved.

The previously developed material models for engineering purposes are described by parameters that are, in many cases, hardly understandable from a biological perspective. A proper material model to be included in a multi modular model in Computational Morphodynamics must be as simple as possible while it still can accurately represent the main features of living tissue such as heterogeneity, anisotropy and growth as well as the dynamics of these features. Furthermore the parameters that such material model is based on, must be biologically understandable. The latter is because finally we need to connect such models to models of other biological modules, e.g. gene regulatory networks. For example, the plant hormone auxin is involved in many growth related processes [13–16]. One can aim at comparing hypotheses based on either auxin softening material or in-

creasing the growth rate. A material model in which these two factors are not explicitly stated can lead to ambiguities. In addition, when extending the models to include more modules, the number of parameters increases which makes computational models costly and complicated. This is why it is crucial to have the lowest possible number of parameters for including the important features of the material when describing morphogenesis.

The main focus of this thesis is to develop a mechanical model for a growing plant tissue. The model framework is developed to evaluate mechanical signals while taking specific features of the plant tissue into account. Such features include material elasticity, compressibility and anisotropy as well as spatial and temporal heterogeneity of the tissue [Papers I-IV]. Some other variables in the system like turgor pressure and shape-related factors like curvature are also of great importance. We try to consider potential feedback mechanisms in two directions. First we investigate the consequences of regulating tissue properties (e.g. orientation of microtubules) by mechanical signals (e.g. maximal stress orientation) [Paper I]. Furthermore we try to consider the possibility of material parameters being regulated by non-mechanical components of the system, e.g. the impact of the plant hormone auxin on elasticity and anisotropy. We investigate the advantages of some already hypothesised feedbacks like stress feedback to the orientation of microtubules from a theoretical perspective and in relation with energy optimization [Paper II]. Later we develop a model for sustainable growth to capture highly anisotropic and large deformations necessary for emergence of patterns and shapes in plant tissues [Paper III]. The growth is parametrized to have the possibility of being regulated by mechanical or non-mechanical signals. As cell division is an inseparable part of the growth process, we take special care to make our model capable of including cell divisions in the growth process. We use different but relevant rules for division while minimising the temporal discontinuity of the mechanical variables [Paper III]. Later we compare stress versus strain as potential growth regulators when the tissue anisotropy is controlled by stress [Paper IV]. We show that regulation of growth by strain while tissue anisotropy is controlled by stress leads to growth patterns and directions similar to those in plants [Paper IV]. Finally, we investigate different possibilities for tissue properties and forces for emergence of specific stress patterns in plant root cells [Paper V].

1.1 BIOLOGICAL BACKGROUND

Here follows a short summary of the key concepts in plant morphogenesis. After a brief description of morphogenetic processes in plants, the main fea-

tures of the plant cell wall, which play a large role in plant patterning, are introduced. Next, the importance of *Cortical Microtubules* (CMT) in relation with cell wall properties and growth is shortly discussed. Finally, in this section, the experimental approaches for quantifying plant deformations and material properties as well as the limitations for achieving the desired accuracy are presented.

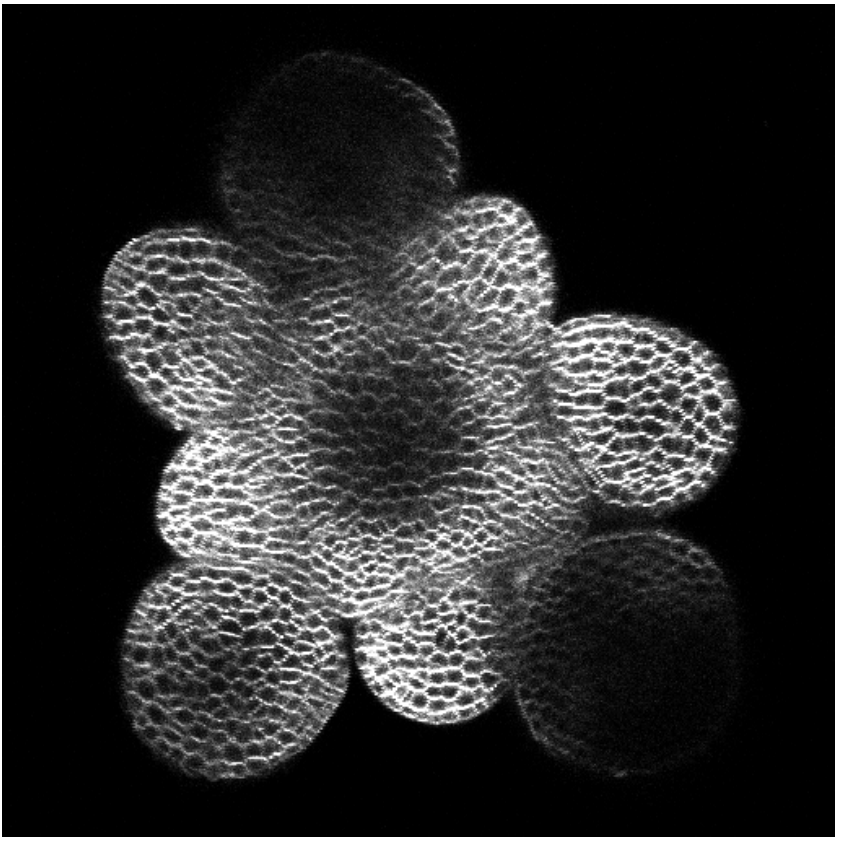

Figure 1.1: **Shoot Apical Meristem**. A confocal microscopy picture of a SAM. The pool of stem cells at the *Central Zone* is surrounded by the *Peripheral Zone* in which cells have higher growth rates [17]. The new organs (*Primordia*) that grow out from periphery form the *Phyllotactic Pattern*. (Courtesy of *Benoit Landerin*, Jönsson Group, Sainsbury Laboratory, University of Cambridge)

1.1.1 *Morphogenesis in plants*

Functionality of biological systems in general and plants in particular depends highly on their shapes. Unlike animals, plants grow and deform throughout their lives. The initiation of organ patterning, e.g. phyllotaxis, in most plants, takes place in a small region of a few hundred micrometers in size at the very tip of the aerial part of the plant. This region is called the *Shoot Apical Meristem* (SAM) [18] (Fig. 1.1). The SAM holds a pool of stem cells, which is maintained at the very center of the shoot, in which two distinct regions in terms of expression of genes are recognized and known as *Central Zone* (CZ) and *Peripheral Zone* (PZ) [18]. Whitin the CZ, in which the tissue is mechanically isotropic, the pool of stem cells is maintained, and the new buds that later will turn into leaves or flowers grow out from the PZ. The growth is highly heterogeneous throughout the SAM and the same is true for material elasticity and anisotropy [17, 19, 20]. Although the SAM is not the only domain in plants that is responsible for patterning, understanding the mechanisms for morphogenesis in the SAM is key to the whole development of shape in a plant tissue. This is mainly due to many similarities that growth-related processes possess in different plant domains.

1.1.2 *The plant cell wall*

Plants are frequently considered as pressure vessels [21]. This is due to the high intracellular turgor pressure which is about about three times the pressure in a car tyre and is mostly held back by the rigid interconnected network of cell walls. Unlike animal cells, plant cells possess a rigid wall adjacent to their plasma membrane [22]. This gives the plant tissue strength to withstand the stresses resulting from environmental factors such as wind and gravity [23], as well as the internal turgor pressure. Furthermore, cell walls are the final mediators of plant growth which is regulated by hormonal signalling and genetic networks [24]. They are also responsible for responding to the environment [25]. The material in the walls is composite with the main components cooperating to facilitate the dynamics in overall material properties needed during growth. Cellulose microfibrils play the most important role in mechanics, providing stiffness and guiding the growth direction [21]. Hemicellulose makes the material extensible and able to grow while a pectin matrix glues all the components to form a composite [26, 27]

The degree of alignment of fibres determines the degree of mechanical anisotropy of the material which can be different both spatially and tempo-

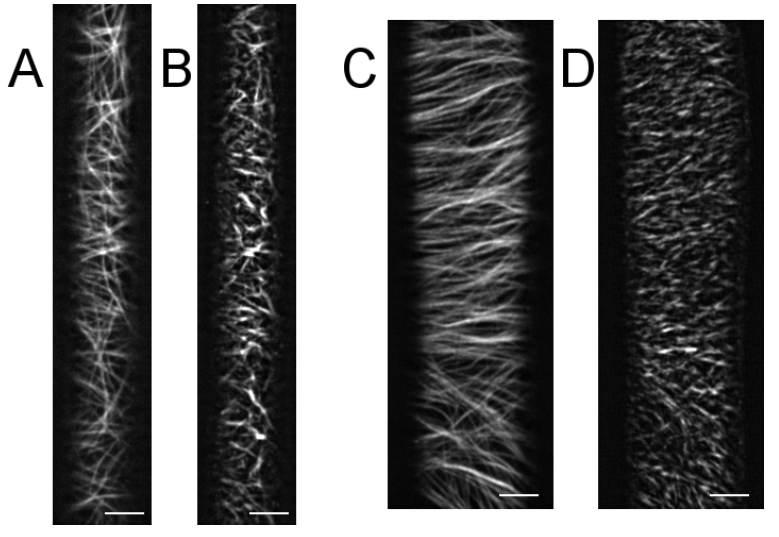

Figure 1.2: **Cortical microtubules and CESA complexes** A,C) Cortical microtubules marked by a GFP reporter where in C the distribution of their orientation is highly anisotropic. B,D) Tracks of cellulose synthesis complexes that are guided by microtubules in the same walls as in A and C respectively which is a proxy for orientation of microfibrils. (Courtesy of *Arun Sampathkumar*, Max Planck Institute of Molecular Plant Physiology, Potsdam, Germany)

rally [6, 22]. From a modelling perspective the cell walls can be considered as planar objects [Paper I]. The average plant cell diameter is about 5-10 μm in the *Arabidopsis* SAM while the average wall thickness is about 100 *nm* inside the plant tissue and they are about 10 times thicker in outer layer of the epidermis [28]. Considering cell walls as planar objects has the advantage of allowing usage of more efficient modelling approaches for evaluating mechanical signals within them.

1.1.3 *Cortical microtubules and cellulose microfibrils*

Microtubules are long polymers which are one of the most important components of the intracellular cytoskeleton [29]. They serve various tasks in all eukaryotic cells including nucleic and cell division as well as intracellular transport. They continuously polymerize from their "plus end" and de-polymerise from their "minus end" giving rise to a dynamical behaviour in their distribution and alignment within the cells. In plant cells, micro-

tubules that are adjacent to the cortex and called "cortical" are able to guide cellulose synthase complexes that deposit fibres on the cell wall on the other side of the plasma membrane [20, 30]. This is the reason why the alignment of microtubules is considered as a proxy for the direction of the latest layer of cellulose microfibrils that are responsible for mechanical properties of the wall [31]. Cellulose fibres are very stiff [32]. The have been regarded as a key factor in anisotropic elongation of the cells [21]. The alignment of microtubules, and consequently fibres, varies throughout the plant tissue. In the SAM, where a complicated growth pattern emerges, directionality of microtubules provides valuable information about anisotropic properties of the tissue. It has been shown that in the central zone of the meristem cortical microtubules show a random alignment whereas they become more aligned in a circumferential direction in the peripheral zone [33]. CMTs become highly aligned at the boundary between central zone and newly grown primordia [33]. The study of these properties in relation to stress fields generated by turgor pressure and shape of the tissue is central to this thesis.

1.1.4 *Experimental data and its limitations*

From a mechanical modelling perspective, the experimental data of plant tissue are highly limited. *Green Florecent Protein* (GFP) that emits green light when exposed to ultraviolet light can be used to mark microtubules [34, 35]. Visualizing microtubules by using confocal microscopy can then give the information about concentration and alignment of microtubules as well as their dynamics. However the quality of the data is decreasing for deeper layers of the tissue, also for those walls that are parallel to the direction of microscopy. Visualizing cellulose fibres is more challenging and needs more manipulation of the tissue as they are inside the cell walls together with many other components of the composite material. This makes the measurements limited to single time points. Quantifying growth rates and deformations has also many difficulties. It is almost impossible to decompose the elastic and plastic deformations directly. Assuming that the elasticity of the material can vary due to different processes comparing the volumes of the cells and/or areas of the cell walls gives only the overall deformation. Even if there is no interaction between their body and the environment, plants move as they grow. Due to these movements, providing time series data where different time points can be directly compared is extremely challenging [36].

Analysing the microscopic data is often done by advanced computational methods that include various optimization methods to reduce noise and

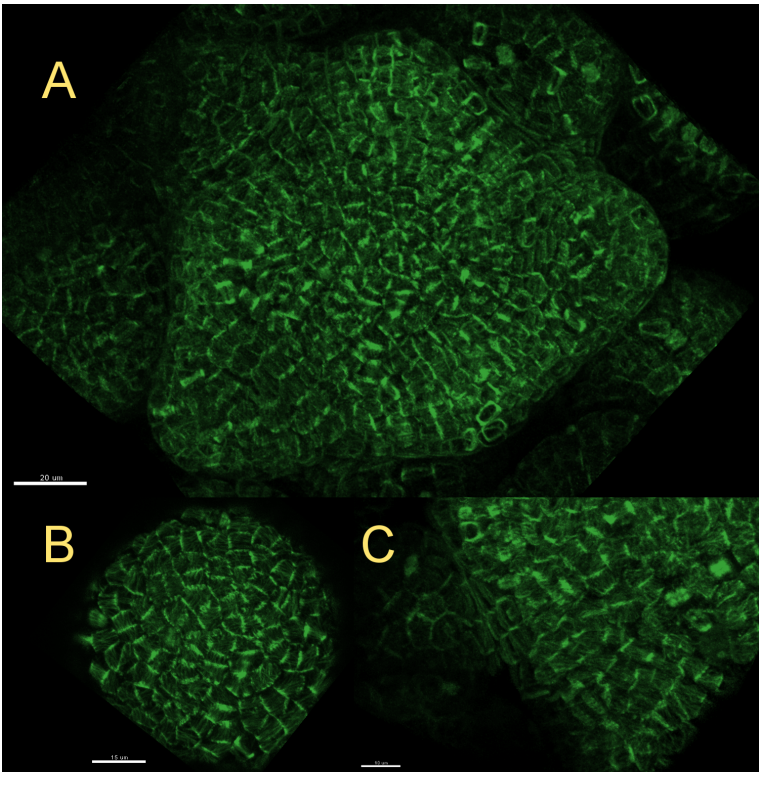

Figure 1.3: **Orientation of microtubules in the meristem** A) Microtubules are marked in the meristem, using a GFP marker. B) The orientation of microtubules is isotropic in the central zone. C) The boundary between meristem and a growing primordium where microtubules are highly organized.(Courtesy of *Neha Bhatia*, Heisler Group, EMBL, Heidelberg, Germany)

extract the most interesting details. *MorphoGraphX* [37] , *MARS* [36] and *COSTANZA* (*http://dev.thep.lu.se/costanza/*) are examples of the tools that are used for extracting plant cells and structures in the Computational Morphodynamics community.

Measuring material properties of the plant tissue is even more challenging. *Atomic Force Microscopy* (AFM) is the main tool that has been used to measure the resistance of the tissue against poking [38–42]. The problem is that such resistance can result from a combination of turgor pressure, tissue elasticity and often highly complex geometry of the tissue [43]. Analysing the AFM data is usually done by combining hypotheses where these com-

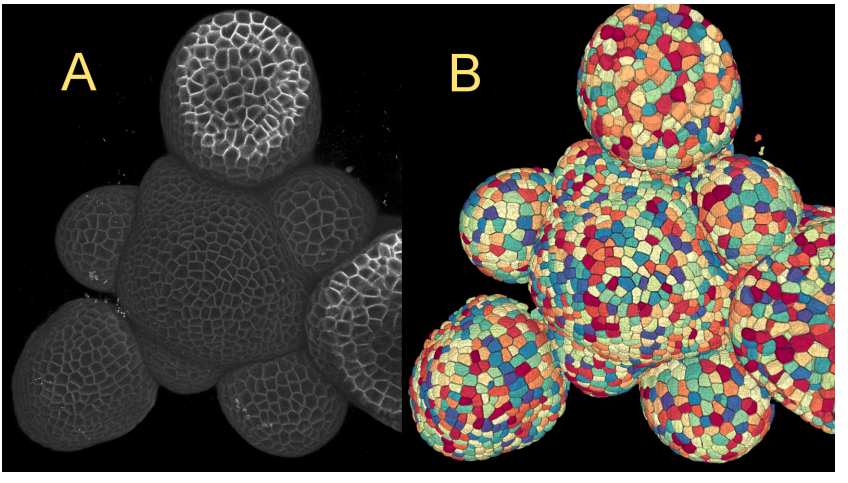

Figure 1.4: **Segmentation of confocal microscopy data by MARS**. (Courtesy of *Yassin Refahi* ,*Weibing Yang* and *Niklas Korsbo*, Jönsson Group, Sainsbury Laboratory, University of Cambridge)

ponents of the overall resistance are combined in models, and the accuracy of such approaches is questionable [43].

Above all, the effects of such experiments on plants can often be so severe that they can not survive or lose their normal functionality. This makes the experimental data ambiguous as it is then hard to access data on healthy plant tissue in its "natural" state with a high level of confidence.

In general, all of these limitations make the experimental data to some degree qualitative rather than quantitative. Still, the latest advances in microscopy and image processing tools as well as methods of perturbations are promising enough to motivate modelling approaches.

1.2 THE QUESTION

In this section, the purpose of the research in this thesis is described. Then, some of the previous efforts on modelling mechanics in plants are briefly introduced.

1.2.1 *The aim*

The most important mechanical variables are stress and strain. They represent the distribution of forces and deformations within a tissue. This thesis

is an investigation, firstly on evaluating these mechanical signals through modelling, and secondly on potential feedbacks between such signals and anisotropic properties of the cell wall material. Later we extend our questions to the potential relation between the elastic deformations and growth patterns in the tissue. We also study the advantages of those feedbacks both from a purely theoretical point of view and for the possibilities that they provide for plants to achieve anisotropic shape changes. For each stage, we first develop a finite element model to test our hypotheses and we make sure that the generated results are consistent with experiments. While we try to keep our model as simple as possible, we include the key features of the plant tissue in our continuous description of the material. Such features include material compressibility and anisotropy, finite elastic deformations, finite growth, spatial and temporal heterogeneity and cell division. As a first step, we try to validate our models by applying them on simple geometries. This is a standard method in FEM which is called *Patch Test Analysis*. Later, we apply our verified models on more complex geometries that are key to understand plant morphogenesis.

1.2.2 *Prior art*

Linear spring models are frequently used in models of plant mechanics [33, 44]. These models cannot be extended to 3D with an accurate representation of the interconnected network of walls as a continuous structure, mainly because the structures built by finite number of simple springs do not effectively resist against shear forces. Another problem is related to defining accurate measures for stress and strain fields. Moreover, mechanical anisotropy with a distinct anisotropy direction for cells may not be well defined via simple springs.

Finite Element Methods (FEM), on the other hand, provide more rigorous approaches for analysing mechanical problems in continua. FEMs are designed for finding the approximate solution to partial differential equations and are very well developed for solid mechanics [45]. They work well for evaluating mechanical signals in an arrangement of cell walls [33, 42, 46]. However, FEM is computationally expensive. For achieving a certain level of accuracy in analysing a multi-modular model, the computational cost of numerical analysis of mechanical variables by FEM is much higher than that of biochemical variables that in general follow much simpler differential equations. This difference becomes larger when important features such as tissue anisotropy, heterogeneity and growth are included in the analysis. The natural way to address this problem is to simplify the FEM

models by adopting them with respect to specific properties of the plant tissue structure.

Some recent mechanical models for plants fit into this description [47–49]. The models developed and used in this thesis also follow a similar approach. The most common simplification is to use planar elements. This is mainly due to the almost planar structure of the plant cell walls. Also, based on the important role of the epidermis, in many models the plant is considered as a pressure vessel. We show that planar elements provide adequate description for the outer faces of epidermal cell layer [Paper I]. In case of mechanics being considered passively, it is only used to maintain the tissue integrity. In such case, growth can be simulated by removing the mechanical fields after each growth-related update of the tissue. This is similar to models based on tissue growth determined by morphogens [47, 50]. However for investigating hypotheses that are based on mechanical feedbacks there is a need for maintaining mechanical signals during growth. This is highly crucial also when cell divisions are taken into account. Due to the need for re-meshing after each cell division there are new degrees of freedom that are added into the system via new elements and nodes. Including such new information in equations with minimum discontinuity in time is a challenge that has most often been disregarded or simplified in models so far.

The existing models can represent many of the complicated but crucial features of the plant tissue. Still, We try to improve modelling capabilities for building and testing hypotheses with all the mentioned aspects included.

1.3 METHODS AND MODELS

In this section follows a summary on the methods that are used in this thesis. The general trend is to use simple assumptions to keep the number of model parameters as low as possible. Alongside simplicity, we include tissue anisotropy, heterogeneity, growth and cell division as well as the possibility of application of feedbacks between mechanical and non-mechanical variables in our model. By including all of these details, we can test hypotheses based on any combination of them.

1.3.1 *Spring model*

Although we have not used simple springs thoroughly in our models, it is possible to combine them with our continuous description of the material. These models are based on Hooke's Law for linear spring elements. The

springs exchange forces between all the "vertices (nodes)" with which the cells are represented. Multiple walls, represented by edges, meet at each vertex [51]. For every two vertex,

$$\mathbf{F}_{ji} = k\frac{\mathbf{u}_{ij}}{|\mathbf{u}_{ij}|}\frac{|\mathbf{u}_{ij}| - L_{ij}}{L_{ij}} \,, \tag{1}$$

where $\mathbf{F}_{ij}$ is the force exerted from node j on node i, k is the spring constant of the unit length, $\mathbf{u}_{ij}$ is the position vector of node j relative to node i and L_{ij} is the resting length of the spring between two nodes. The energy from which such force can be calculated, does not depend on the angles between the directions of the springs, that meet on nodes explicitly, therefore cells lack realistic shear resistance. The direction of forces and deformations can be determined for each spring. However, how such forces and deformations can be used to represent stress and strain fields in the continua, is not well defined and often ambiguous. In these simple models, growth can simply be included by updating the resting length of the springs [44, 52], using e.g.

$$\frac{dL_{ij}}{dt} = k_g\mathcal{R}(\frac{|\mathbf{u}_{ij}| - L_{ij}}{L_{ij}}) \,, \tag{2}$$

where $\mathcal{R}$ is the ramp function and is defined by:

$$\mathcal{R}(x) \quad = \quad \begin{cases} 0 & if \;\; x \leq 0 \,, \\ x & if \;\; x > 0 \,. \end{cases} \tag{3}$$

This is the most basic formulation of growth which is in close relation with the classical growth model for plant cells first proposed by Lockhart in 1965 [53].

1.3.2 *Deformation field and strain measure*

In continuum mechanics, displacement of the material points of a body is expressed by a deformation function, $\mathbf{\Phi}$ [54], as

$$\mathbf{x} = \mathbf{\Phi}(\mathbf{X}, t) \,, \tag{4}$$

where $\mathbf{x}$ represents the current configuration of all the material points and $\mathbf{X}$ is the corresponding configuration in undeformed (material) coordinates.

The derivative of deformation function with respect to $\mathbf{X}$ is called deformation gradient tensor, $\mathbf{F}$, and given by

$$\mathbf{F} = \nabla_{\mathbf{X}} \Phi \, . \tag{5}$$

A commonly used measure for strain is the Green-Lagrange strain tensor, $\mathbf{E}$, which is defined in terms of the deformation gradient tensor

$$\mathbf{E} = \frac{1}{2}(\mathbf{F}^T\mathbf{F} - \mathbf{I}) \, , \tag{6}$$

where T denotes transpose of a second order tensor, and $\mathbf{I}$ is the second order identity tensor. We can note that for calculating strain, we only need information about the reference and deformed states of the material.

1.3.3 *Strain energy and stress*

Mathematically, for *Hyperelastic* materials, the way a material responds to the strain field depends on the strain energy. In fact, all the properties of the material and its expected behaviour must be encoded in the strain energy expression that determines the stress field throughout the material body as a function of a strain field [54]. The second Piola-Kirchhoff stress tensor, $\mathbf{S}$, which is the energy conjugate of the Green-Lagrange strain tensor is introduced by

$$\mathbf{S} = \frac{\partial W}{\partial \mathbf{E}} \, , \tag{7}$$

where W is the energy and $\mathbf{E}$ is the Green-Lagrange strain tensor.

In the continuum mechanics terminology a *Material Model* is a hypothesized expression of energy in terms of strain. There are different models that each describes a specific material. The complexity of the material is mirrored in the corresponding energy expression. The simplest model for linear elastic materials when the deformations are very small is Hooke's Law

$$W = \frac{1}{2}\boldsymbol{\epsilon}^T : \mathbf{C} : \boldsymbol{\epsilon} \, , \tag{8}$$

where $\boldsymbol{\epsilon}$ is the second order infinitesimal strain tensor and $\mathbf{C}$ is the fourth order stiffness tensor, which includes elasticity, compressibility and anisotropy

properties of the material. Eqs. 7 and 8 can be used for driving the expression for the Cauchy stress tensor, **œ**,

$$\boldsymbol{\sigma} = \mathbf{C} : \boldsymbol{\epsilon} \, . \tag{9}$$

When the strain is finite and not very small, the relation between stress and strain can be non-linear. In this thesis we use the often used St. Venant-Kirchoff description for the isotropic material energy density [54], given by

$$W_{iso} = \frac{\lambda}{2}(tr\mathbf{E})^2 + \mu \; tr\mathbf{E}^2 \, . \tag{10}$$

The material is parametrized in terms of λ and μ which are called Lame constants and are related to material elasticity and compressibility by Young's modulus Y and Poisson's ratio ν, respectively. The relations between these parameters are given by

$$\lambda = \frac{Y\nu}{(1+\nu)(1-2\nu)}, \;\; \mu = \frac{Y}{2(1+\nu)} \, . \tag{11}$$

Due to the planar structure of plant cell walls, in plane stresses are dominant and the assumption of a plane stress condition can be used. In such condition, the stresses perpendicular to the plane of the walls are neglected and Eqs. 5 become [54],

$$\lambda = \frac{Y\nu}{1-\nu^2}, \;\; \mu = \frac{Y}{2(1+\nu)} \, . \tag{12}$$

By using Eqs. 10 and 7 again we get an expression for stress

$$\mathbf{S} = \lambda(tr\mathbf{E})\mathbf{I} + 2\mu\mathbf{E} \, , \tag{13}$$

These expressions only represent the isotropic material and need some modifications in the case of material anisotropy. In case of infinitesimal strain this anisotropy can be encoded in the stiffness tensor **C** but for finite strain, the St. Venant-Kirchoff description of energy (Eq.10) must be modified.

1.3.4 *Material anisotropy*

For including anisotropy in the material when the strain is infinitesimal, the classical way is to express the stress strain relation as

$$\begin{pmatrix} \epsilon_1 \\ \epsilon_2 \\ \epsilon_3 \end{pmatrix} = \begin{pmatrix} \frac{1}{Y_m} & -\frac{\nu}{Y} & 0 \\ -\frac{\nu'}{Y_m} & \frac{1}{Y} & 0 \\ 0 & 0 & \frac{1}{2G} \end{pmatrix} \begin{pmatrix} \sigma_1 \\ \sigma_2 \\ \sigma_3 \end{pmatrix} , \tag{14}$$

$$\tag{15}$$

where Y_m and Y are Young moduli of the stiffer and weaker principal directions of the material, ν' and ν are the corresponding Poison ratios and G is the shear modulus [54] . This equation is written in the principal coordinate system of the material. The symbols $\epsilon_{1,2,3}$ and $\sigma_{1,2,3}$ are related to the strain and stress components by

$$\begin{aligned} \epsilon_1 = \epsilon_{xx} , \quad \epsilon_2 = \epsilon_{yy} , \quad \epsilon_3 = \epsilon_{xy} = \epsilon_{yx} \quad , \\ \sigma_1 = \sigma_{xx} , \quad \sigma_2 = \sigma_{yy} , \quad \sigma_3 = \sigma_{xy} = \sigma_{yx} \quad . \end{aligned} \tag{16}$$

As a consequence of the plane stress assumption, stresses in the z direction are neglected. Eq. 15 is a simplified version of Eq. 9 in which many of the elements of $\mathbf{C}$, $\boldsymbol{\epsilon}$ and $\boldsymbol{\sigma}$ are set to zero or neglected due to the symmetries and plane stress condition.

For finite strain Eq. 10 needs to be modified. We do this by penalizing the energy in the specific direction of material anisotropy with higher stiffness [Paper I]. For deriving the amount of penalty, first we partition the isotropic energy in Eq. 10 into parts, each corresponding with one of the principal directions. Then, we derive the general form of the additional energy needed for anisotropy in the direction of a unit vector $\boldsymbol{a}$ as

$$\Delta W_{aniso} = \frac{\Delta\lambda}{2}(\boldsymbol{a}^T\mathbf{E}\boldsymbol{a})tr\mathbf{E} + \Delta\mu(\boldsymbol{a}^T\mathbf{E}^2\boldsymbol{a}) , \tag{17}$$

where

$$\Delta\lambda = \lambda^L - \lambda^T \tag{18}$$

and

$$\Delta\mu = \mu^L - \mu^T , \tag{19}$$

where λ^L, μ^L are *Longitudinal* Lame constants in a given direction $\vec{a}$ and λ^T, μ^T are *Transverse* Lame constants in a plane transverse to $\boldsymbol{a}$. Now the full expression of the energy for anisotropic material becomes

$$W = W_{iso} + \Delta W_{aniso} \ . \tag{20}$$

Again we can derive a correction term for the stress-strain relation, ΔS, in Eq. 13, by using Eqs. 7 and 17, which gives

$$\Delta S = \frac{\Delta\lambda}{2}\left((\boldsymbol{a}^T\mathbf{E}\boldsymbol{a})\mathbf{I} + (tr\mathbf{E})(\boldsymbol{a}\otimes\boldsymbol{a})\right) + \Delta\mu\left(\mathbf{E}(\boldsymbol{a}\otimes\boldsymbol{a}) + (\boldsymbol{a}\otimes\boldsymbol{a})\mathbf{E}\right) \ . \tag{21}$$

We have added this term to the stress tensor wherever the anisotropic material has been considered [Papers I-IV].

1.3.5 *Fundamental balance laws*

The physics behind continuum mechanics can be summarized in terms of balance equations for *Mass*, *Energy*, *Linear* and *Angular Momentum*.

The balance of mass can not be formulated without the knowledge about input and output of mass in the system. Throughout this thesis we have assumed that the mass density of the cell walls in the tissue is constant. This might not be true but considering that we are not aiming at calculating the accelerations (as we will see in the next section), the parameters such as Young moduli and Poison ratios are sufficient to represent the role of the material in the system. Furthermore, in most tissues we are investigating, we have no indication of primary cell walls getting thicker or thinner over the time scales we are interested in. So we always assume

$$\frac{d\rho}{dt} = 0 \ , \tag{22}$$

where ρ is the mass density. Also, for deriving the balance equation for energy we need to include not only all the components of the plant tissue but also the inward and outward flows of energy. In our models we are only focusing on plant cell walls and this is not enough for such derivation. Neglecting the impact of temperature and different forms of energy on material parameters is another major simplification that we apply. These assumptions are commonly used by mechanical models developed for plant tissue. Angular momentum balance is not needed to be explicitly included in the model as it is encoded by the stress tensor symmetry.

The most important balance equation in the system for calculating the stress field is the one for linear momentum which results in Cauchy's first law of motion

$$\rho \frac{d\mathbf{V}}{dt} + \eta \mathbf{V} - \nabla \cdot \mathbf{S} - \rho \mathbf{b} = 0 \,, \tag{23}$$

where $\mathbf{V}$ is the velocity and $\mathbf{b}$ represents the body forces. The term $\nabla \mathbf{S}$ is traction generated by stress divergence and $\eta \mathbf{V}$ is the damping force resulting from viscosity of the medium. As shown in the next section we can use this equation to calculate the equilibrium state of the stress field.

1.3.6 *Quasi-static equilibrium*

Considering the solidity of the plant cell walls the time needed for the forces in the tissue to equilibrate is much shorter that the time interval necessary for noticing the tissue dynamics resulting from growth. This difference in time-scale allows us to neglect the first two terms on the left hand side of Eq. 23. Integration of remaining terms over the domain of the material gives the fundamental equation for balance of forces in continuum mechanics [55],

$$\delta W = \int_{\omega} \mathbf{S} : \delta \mathbf{d} \, dv - \int_{\omega} \mathbf{b} \cdot \delta \mathbf{v} \, dv - \int_{\partial\omega} \boldsymbol{\tau} \cdot \delta \mathbf{v} \, da = 0 \,, \tag{24}$$

where δW is the variation of energy, which should be zero when the stress field $\mathbf{S}$ is equilibrated by the body forces $\mathbf{b}$ and traction forces $\boldsymbol{\tau}$ on the boundary ($\partial\omega$) of the region of interest (ω) within the continuum. After each update in the material we make sure that this equation is satisfied.

1.3.7 *Spatial discretisation*

Generally, FEMs are methods for discretisation of the domains of partial differential equations when numerical solutions are needed [45]. Although these methods share many basic principles, they are highly problem dependent when considering details. Due to the cell wall geometry, using planar elements is a relevant approximation. We have mainly used triangular plates for discreetizing the cell walls in this thesis. The deformation gradient tensor $\mathbf{F}$ can be derived in terms of position of the nodes in the

resting and deformed states of the element [56]. The i'th shape vector $\mathbf{D}_i$ is related to node $\mathbf{P}_i$ in the resting shape (Fig. 1B in Paper I) and

$$\mathbf{D}_i = \frac{1}{A_P}(\mathbf{P}_j - \mathbf{P}_k)^{\perp}; \quad \epsilon_{ijk} = 1 \ , \tag{25}$$

where A_P is the resting area of the element, ϵ_{ijk} is the permutation symbol and $X^{\perp}$ is orthogonal to the vector X. In this case the expression for F becomes [56]

$$\mathbf{F} = \mathbf{Q}_i \otimes \mathbf{D}_i \ , \tag{26}$$

where Q_i is the position vector of the i'th node in the deformed shape. All of the mechanical variables can be expressed in terms of the deformation gradient tensor and by Eq. 26 they can be easily related to the resting and current position vectors of the nodes.

In Paper I, we also compare the simulation results of planar elements with those of standard shell elements. Spatial discretisation by shells is well developed and can be found in standard textbooks [55].

1.3.8 *Modelling growth in continua*

We model growth by updating the resting configuration. The overall deformation, $\mathbf{F}_{eg}$, can then be expressed as a combination of deformations by

$$\mathbf{F}_{eg} = \mathbf{F}_e\mathbf{F}_g(t) \ , \tag{27}$$

where $\mathbf{F}_e$ represents the elastic component of deformation and $\mathbf{F}_g(t)$ is the growth tensor at time t. After an infinitesimal time step δt the resting configuration $\mathbf{X}_0$ is given by

$$\mathbf{X}_0(t + \delta t) - \mathbf{X}_0(t) = \mathbf{f}_g\mathbf{X}_0(t)\delta t \ , \tag{28}$$

where f_g is the differential growth tensor which can be related to the overall growth tensor by

$$\mathbf{F}_g(t) = \exp\left[\int_0^t \mathbf{f}_g(t')dt'\right] . \tag{29}$$

The most general form of the growth tensor that we use in our models (Paper III) is in the form of

$$\begin{aligned}\mathbf{f}_g = &\quad k_{rate}\Sigma_i \mathcal{R}(g_i - g_t)|g_i\rangle\langle g_i| \\ = &\quad k_{rate}|F_e^{\mathcal{T}}F_e|^{-1}\Sigma_i \mathcal{R}(G_i - G_t)F_e^{\mathcal{T}}|G_i\rangle\langle G_i|F_e \ , \end{aligned} \tag{30}$$

where k_{rate} is the growth rate, $\mathcal{R}$ is the ramp function defined by Eq. 3, G_i and $|G_i\rangle$ are the i'th principal value and vector of growth signal and G_t is the growth threshold in the current configuration. The corresponding variables in the resting configuration are g_i, $|g_i\rangle$ and g_t respectively. The growth signal can be hypothesised as stress, strain or a non-mechanical signal, e.g. a morphogen.

1.3.9 *Cell division*

A consequence of large deformations during growth is the need for cell division and re-meshing the tissue description. As the growth field might be incompatible, cell division cannot be performed in the resting configuration. To avoid discontinuity of the strain field when a cell divides we have to estimate the resting configuration of the daughter cell walls with the constraint of maintaining the strain from the mother cell wall. The biological motivation is that cell division is a continuous process in which the material is slowly deposited in a new wall [57]. In the model, this can be done via a reverse calculation of the resting shape, granted that we know the average strain field in the current configuration.

The Eulerian-Almansi finite strain tensor, $\mathbf{e}$, is a measure for strain in the current configuration and can be expressed in terms of the deformation gradient tensor as

$$\mathbf{e} = \frac{1}{2}(\mathbf{I} - \mathbf{F}^{-1}\mathbf{F}^{-T}) \ . \tag{31}$$

In Paper III, we show that the resting length of each element edge can be estimated via

$$L = [\Sigma_i(1 - 2e_i)\langle l|e_i\rangle^2]^{\frac{1}{2}} \ , \tag{32}$$

where e_i and $|e_i>$ are the i'th eigenvalue and eigenvector of the average Almansi strain tensor of the mother cell wall and $|l>$ is the corresponding element edge vector in the current configuration.

This method does not depend on the plane of division. The criteria which determine how the cell division occurs specifies the direction and position of the emerging wall and the necessary re-meshing.

1.3.10 *Feedbacks within mechanics and beyond*

The pressure inside the plant tissue is the main source of stress. In addition, the shape (mainly curvature on epidermis) has a major role on both magnitude and degree of anisotropy of the stress field. On the other hand, the shape itself is the result of the growth field. The material properties including the stiffness as well as degree and direction of material anisotropy determine the resulting strain field via the strain energy expression. The relations between all the mentioned parameters and variables are dictated by the laws of physics.

Models for bridging between mechanical and biological components of the plant tissue, have often included auxin, PIN and cortical microtubules [28, 46, 58]. The plant hormone auxin is supposed to be highly involved in the growth-related processes while a protein family known as PIN (PIN-FORMED) are responsible for cell polarity and active transport of auxin. Also, cortical microtubules are related to tissue anisotropy through their role in guiding the fibre deposition processes in the primary cell walls. Much bulk of the research on plant mechanics, including this thesis, is focused on the relation between stress and tissue anisotropy via CMT organisation [33]. It has been shown in some models that stress can be considered as the main regulator of PIN polarity in cells for generating patterns of auxin concentration via active transport [46]. Also auxin is suggested as a growth regulator due to its role in altering material properties of the cell wall [13–16]. Although the description of main regulators of growth in plant tissues yet needs to be improved, in different models, stress, strain and morphogen-based mechanisms have been assumed to be involved [33, 47–49, 53]. In this thesis we have provided tools to use any of these signals [Paper III] and in particular compared possibilities of the growth being regulated by stress or strain [Paper IV]. The stress feedback to the direction of material anisotropy and also stress anisotropy feedback to the degree of material anisotropy are used in Papers I, II and IV. In Papers III and IV there are examples of regulating the growth based on mechanical signals such as stress or strain and also non-mechanical signals such as auxin.

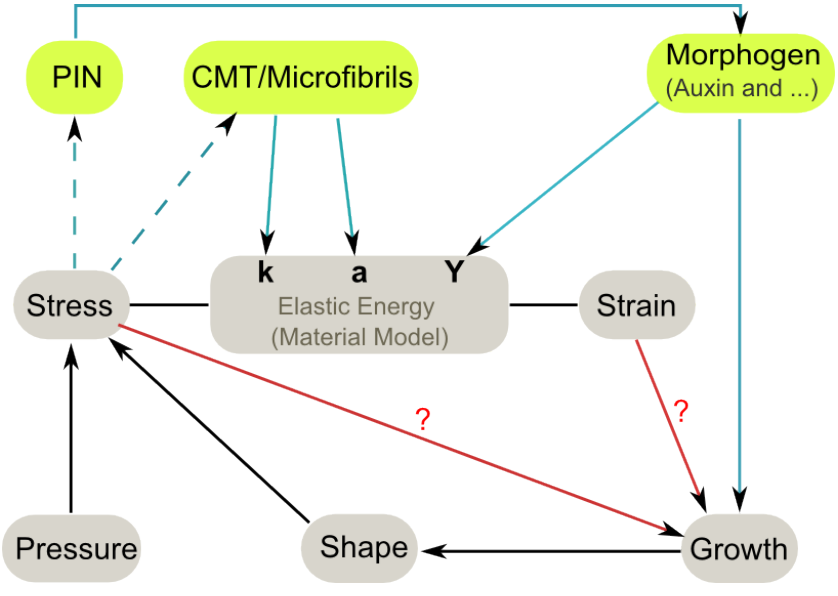

Figure 1.5: **A potential model for feedback network among mechanical and biological parameters and variables in plant tissue**. Y is overall elasticity, k represents mechanical anisotropy and a is the vector of anisotropy direction. CMT is the short term for Cortical Microtubules. The mechanical parameters and variables are in gray boxes and the molecular variables are in green boxes. The arrows and lines in black show physical connections. There are strong experimental evidences for blue arrows. The two dashed arrows in blue are the connections that are currently under investigation. The red arrows are proposed in different growth models (including in this thesis). We have not used PIN dynamics in our models.

1.3.11 *Numerical solvers*

Throughout this thesis we develop mechanical models. The computational cost however is greatly dependent on the solvers that are used. In our multi-modular model, as dynamics of the system in biochemical modules are of high interest, explicit solvers are used. For non-stiff problems we use an adaptive 5th order Runge Kutta Fehlberg method [59]. Occasionally, when we encounter stiff problems with short temporal discontinuity of the parameters we switch to the 4th order Runge Kutta with fixed step size. However in continuum mechanics implicit solvers are more efficient. The development of implicit solvers is a remaining step in our project and should be taken in the near future.

REFERENCES

1. D. W. Thompson, *On Growth and Form*. Cambridge University Press, 1917.
2. U. Alon, *An introduction to systems biology: design principles of biological circuits*. CRC press, 2006.
3. H. Jönsson, J. Gruel, P. Krupinski, and C. Troein, "On evaluating models in computational morphodynamics," *Current Opinion in Plant Biology*, vol. 15, no. 1, pp. 103 – 110, 2012. Growth and development.
4. S. H. Strogatz, *Nonlinear dynamics and chaos*. Addison Wesley, 1994.
5. B. Palsson, *Systems biology*. Cambridge university press, 2015.
6. D. J. Cosgrove, "Growth of the plant cell wall.," *Nature reviews. Molecular cell biology*, vol. 6, pp. 850–61, nov 2005.
7. K. J. Niklas, *Plant biomechanics: an engineering approach to plant form and function*. University of Chicago press, 1992.
8. O. Hamant and J. Traas, "The mechanics behind plant development," *New Phytologist*, vol. 185, no. 2, pp. 369–385, 2010.
9. E. Schrödinger, *What is life?: With mind and matter and autobiographical sketches*. Cambridge University Press, 1992.
10. Y. Lazebnik, "Can a biologist fix a radio?—or, what i learned while studying apoptosis," *Biochemistry (Moscow)*, vol. 69, no. 12, pp. 1403–1406, 2004.
11. J. Gerhart, M. Kirschner, and E. S. Moderbacher, *Cells, embryos, and evolution: Toward a cellular and developmental understanding of phenotypic variation and evolutionary adaptability*. Blackwell Science Malden, 1997.
12. R. Barbucci, *Integrated biomaterials science*. Springer Science & Business Media, 2002.
13. D. L. Rayle and R. E. Cleland, "The Acid Growth Theory of auxin-induced cell elongation is alive and well.," *Plant physiology*, vol. 99, pp. 1271–1274, Aug. 1992.
14. K. Nishitani and Y. Masuda, "Auxin-Induced Changes in the Cell Wall Xyloglucans: Effects of Auxin on the Two Different Subtractions of Xyloglucans in the Epicotyl Cell Wall of Vigna angularis," *Plant & cell physiology*, vol. 24, pp. 345–355, Apr. 1983.
15. S. C. Fry, "Cellulases, hemicelluloses and auxin-stimulated growth: a possible relationship - Fry - 2006 - Physiologia Plantarum - Wiley Online Library," *Physiologia plantarum*, 1989.
16. P. Schopfer, A. Liszkay, M. Bechtold, G. Frahry, and A. Wagner, "Evidence that hydroxyl radicals mediate auxin-induced extension growth.," *Planta*, vol. 214, pp. 821–828, Apr. 2002.

17. D. Kwiatkowska, "Surface growth at the reproductive shoot apex of arabidopsis thaliana pin-formed 1 and wild type.," *Journal of experimental botany*, vol. 55, pp. 1021–32, may 2004.
18. T. A. Steeves and I. M. Sussex, *Patterns in plant development*. Cambridge University Press, 1989.
19. D. Kwiatkowska and J. Dumais, "Growth and morphogenesis at the vegetative shoot apex of anagallis arvensis l," *J Exp Bot*, vol. 54, pp. 1585–95, Jun 2003.
20. A. Endler and S. Persson, "Cellulose synthases and synthesis in arabidopsis," *Molecular Plant*, vol. 4, no. 2, pp. 199 – 211, 2011.
21. P. B. Green, "Mechanism for plant cellular morphogenesis," *Science*, vol. 138, no. 3548, pp. 1404–1405, 1962.
22. T. I. Baskin, "Anisotropic expansion of the plant cell wall," *Annu Rev Cell Dev Biol*, vol. 21, pp. 203–22, Jan 2005.
23. B. Moulia, C. Coutand, and C. Lenne, "Posture control and skeletal mechanical acclimation in terrestrial plants: implications for mechanical modeling of plant architecture," *American Journal of Botany*, vol. 93, no. 10, pp. 1477–1489, 2006.
24. Y. B. Park and D. J. Cosgrove, "Xyloglucan and its interactions with other components of the growing cell wall.," *Plant & cell physiology*, vol. 56, pp. 180–194, Feb. 2015.
25. S. A. Braybrook and H. Jönsson, "Shifting foundations: the mechanical cell wall and development," *Current Opinion in Plant Biology*, vol. 29, pp. 115 – 120, 2016. Growth and development.
26. A. Boudaoud, "An introduction to the mechanics of morphogenesis for plant biologists," *Trends Plant Sci*, vol. 15, pp. 353–60, Jun 2010.
27. V. Mirabet, P. Das, A. Boudaoud, and O. Hamant, "The role of mechanical forces in plant morphogenesis," *Annual review of plant biology*, vol. 62, pp. 365–85, Jun 2011.
28. H. Jönsson, M. G. Heisler, B. E. Shapiro, E. M. Meyerowitz, and E. Mjolsness, "An auxin-driven polarized transport model for phyllotaxis," *Proceedings of the National Academy of Sciences*, vol. 103, no. 5, pp. 1633–1638, 2006.
29. A. Desai and T. J. Mitchison, "Microtubule polymerization dynamics," *Annual review of cell and developmental biology*, vol. 13, no. 1, pp. 83–117, 1997.
30. A. R. Paredez, C. R. Somerville, and D. W. Ehrhardt, "Visualization of cellulose synthase demonstrates functional association with microtubules.," *Science*, vol. 312, pp. 1491–5, jun 2006.
31. T. I. Baskin, "On the alignment of cellulose microfibrils by cortical microtubules: A review and a model," *Protoplasma*, vol. 215, pp. 150–171,

mar 2001.
32. Y. Nishiyama, "Structure and properties of the cellulose microfibril," *Journal of Wood Science*, vol. 55, no. 4, pp. 241–249, 2009.
33. O. Hamant, M. G. Heisler, H. Jönsson, P. Krupinski, M. Uyttewaal, P. Bokov, F. Corson, P. Sahlin, A. Boudaoud, E. M. Meyerowitz, Y. Couder, and J. Traas, "Developmental patterning by mechanical signals in arabidopsis," *Science*, vol. 322, pp. 1650–1655, Dec 2008.
34. S. Sakaguchi, T. Hogetsu, and N. Hara, "Arrangement of cortical microtubules at the surface of the shoot apex invinca major l.: Observations by immunofluorescence microscopy," *The botanical magazine= Shokubutsu-gaku-zasshi*, vol. 101, no. 4, pp. 497–507, 1988.
35. J. M. Selker, "Microtubule patterning in apical epidermal cells ofvinca minor preceding leaf emergence," *Protoplasma*, vol. 158, no. 1-2, pp. 95–108, 1990.
36. R. Fernandez, P. Das, V. Mirabet, E. Moscardi, J. Traas, J.-L. Verdeil, G. Malandain, and C. Godin, "Imaging plant growth in 4d: robust tissue reconstruction and lineaging at cell resolution," *Nat Meth*, vol. 7, pp. 547–553, Jul 2010.
37. P. Barbier de Reuille, A.-L. Routier-Kierzkowska, D. Kierzkowski, G. W. Bassel, T. Schüpbach, G. Tauriello, N. Bajpai, S. Strauss, A. Weber, A. Kiss, A. Burian, H. Hofhuis, A. Sapala, M. Lipowczan, M. B. Heimlicher, S. Robinson, E. M. Bayer, K. Basler, P. Koumoutsakos, A. H. Roeder, T. Aegerter-Wilmsen, N. Nakayama, M. Tsiantis, A. Hay, D. Kwiatkowska, I. Xenarios, C. Kuhlemeier, and R. S. Smith, "Morphographx: A platform for quantifying morphogenesis in 4d," *eLife*, vol. 4, p. e05864, may 2015.
38. A. Peaucelle, S. A. Braybrook, L. Le Guillou, E. Bron, C. Kuhlemeier, and H. Höfte, "Pectin-induced changes in cell wall mechanics underlie organ initiation in Arabidopsis.," *Current biology : CB*, vol. 21, pp. 1720–6, oct 2011.
39. A.-L. Routier-Kierzkowska, A. Weber, P. Kochova, D. Felekis, B. J. Nelson, C. Kuhlemeier, and R. S. Smith, "Cellular force microscopy for in vivo measurements of plant tissue mechanics.," *Plant physiology*, vol. 158, pp. 1514–22, apr 2012.
40. P. Milani, M. Gholamirad, J. Traas, A. Arnéodo, A. Boudaoud, F. Argoul, and O. Hamant, "In vivo analysis of local wall stiffness at the shoot apical meristem in arabidopsis using atomic force microscopy," *The Plant journal : for cell and molecular biology*, vol. 33, May 2011.
41. P. Milani, S. A. Braybrook, and A. Boudaoud, "Shrinking the hammer: micromechanical approaches to morphogenesis," *Journal of experimental botany*, p. ert169, 2013.

42. A. Sampathkumar, P. Krupinski, R. Wightman, P. Milani, A. Berquand, A. Boudaoud, O. Hamant, H. Jönsson, and E. M. Meyerowitz, "Subcellular and supracellular mechanical stress prescribes cytoskeleton behavior in *Arabidopsis* cotyledon pavement cells," *eLife*, vol. 3, p. e01967, apr 2014.
43. S. A. L. Weber, J. I. Kilpatrick, T. M. Brosnan, S. P. Jarvis, and B. J. Rodriguez, "High viscosity environments: an unexpected route to obtain true atomic resolution with atomic force microscopy," *Nanotechnology*, vol. 25, no. 17, p. 175701, 2014.
44. P. Sahlin, O. Hamant, and H. Jönsson, "Statistical properties of cell topology and geometry in a tissue-growth model," *Complex*, vol. LNICST 4, pp. 971–979, 2009.
45. O. C. Zienkiewicz, R. L. Taylor, and J. Zhu, *The Finite Element Method: Its Basis and Fundamentals, Sixth Edition*. Butterworth-Heinemann, 2005.
46. M. G. Heisler, O. Hamant, P. Krupinski, M. Uyttewaal, C. Ohno, H. Jönsson, J. Traas, and E. M. Meyerowitz, "Alignment between pin1 polarity and microtubule orientation in the shoot apical meristem reveals a tight coupling between morphogenesis and auxin transport," *PLoS Biol*, vol. 8, p. e1000516, Jan 2010.
47. R. Kennaway, E. Coen, A. Green, and A. Bangham, "Generation of diverse biological forms through combinatorial interactions between tissue polarity and growth," *PLoS computational biology*, vol. 7, no. 6, p. e1002071, 2011.
48. G. W. Bassel, P. Stamm, G. Mosca, P. Barbier de Reuille, D. J. Gibbs, R. Winter, A. Janka, M. J. Holdsworth, and R. S. Smith, "Mechanical constraints imposed by 3D cellular geometry and arrangement modulate growth patterns in the Arabidopsis embryo," *Proceedings of the National Academy of Sciences of the United States of America*, vol. 111, no. 23, pp. 8685–8690, 2014.
49. F. Boudon, J. Chopard, O. Ali, B. Gilles, O. Hamant, A. Boudaoud, J. Traas, and C. Godin, "A computational framework for 3d mechanical modeling of plant morphogenesis with cellular resolution," *PLoS Comput Biol*, vol. 11, pp. 1–16, 01 2015.
50. N. Hervieux, M. Dumond, A. Sapala, A.-L. Routier-Kierzkowska, D. Kierzkowski, A. H. Roeder, R. S. Smith, A. Boudaoud, and O. Hamant, "A mechanical feedback restricts sepal growth and shape in arabidopsis," *Current Biology*, 2016.
51. P. Sahlin and H. Jönsson, "A modeling study on how cell division affects properties of epithelial tissues under isotropic growth," *PLoS ONE*, vol. 5, p. e11750, Jan 2010.

52. R. M. Merks, M. Guravage, D. Inzé, and G. T. Beemster, "Virtualleaf: an open-source framework for cell-based modeling of plant tissue growth and development," *Plant physiology*, vol. 155, no. 2, pp. 656–666, 2011.
53. J. A. Lockhart, "An analysis of irreversible plant cell elongation," *Journal of Theoretical Biology*, vol. 8, no. 2, pp. 264 – 275, 1965.
54. G. T. Mase, R. E. Smelser, and G. E. Mase, *Continuum Mechanics For Engineers*. CRC Press, 2010.
55. J. Bonet and R. D. Wood, *Nonlinear continuum mechanics for finite element analysis*. Cambridge University Press, 1997.
56. H. Delingette, "Triangular springs for modeling nonlinear membranes," *IEEE Transactions on Visualization and Computer Graphics*, vol. 14, pp. 329–341, mar 2008.
57. L. G. Smith, "Plant cell division: building walls in the right places," *Nat Rev Mol Cell Biol*, vol. 2, pp. 33–9, Jan 2001.
58. S. Stoma, M. Lucas, J. Chopard, M. Schaedel, J. Traas, and C. Godin, "Flux-based transport enhancement as a plausible unifying mechanism for auxin transport in meristem development," *PLoS Comput Biol*, vol. 4, no. 10, p. e1000207, 2008.
59. W. H. Press, *Numerical Recipes with Source Code CD-ROM 3rd Edition: The Art of Scientific Computing*. Cambridge University Press, 2007.

2

OVERVIEW OF THE PAPERS

PAPER I:

Stress and strain provide positional and directional cues in development

Coordinated changes in material properties in the plant tissue is a key to the development of shape in plant organs [1, 2]. A fundamental question is how plants manage to control the cell wall anisotropy and achieve desired deformation patterns. For investigating questions and trying different hypotheses, in Paper I, we first develop a mechanical model based on a finite element method for planar elements [3]. We adopt the model to include dynamical anisotropy of the tissue. Next we validate the anisotropic plate model versus a standard "Shell" finite element method [4] and show that the results agree in the case of tissue pressure simulations of the epidermis. In our model it is possible to tune both direction and degree of anisotropy of the cell walls. This represents anisotropic deposition of fibres. Later we apply feedbacks to the direction of anisotropy of the tissue from stress and perpendicular direction to strain. In the presence of material anisotropy, stress and strain can have different directions and these two scenarios have different impacts on the dynamics of the system. We show that stress-fibre feedback can produce anisotropy patterns similar to what is observed in different domains of the plants. The results are opposite for a strain-fibre feedback, which alters those patterns with anisotropic patterns not agreeing with experiments. Furthermore, we show that the stress-fibre feedback model can generate zones of different mechanical properties in the radial direction of the plant shoot. Such zones are similar to the previously identified regions of specific gene expressions. Also the elastic deformations resulting from stress-fibre feedback are in favour of growth patterns seen in experimental measurements. Such deformations are necessary for

anisotropic growth and a key factor in plant morphogenesis.

My contribution: The initial idea of the project was conceived by H.J. and P.K.. I added more details to the initial plan. I derived the mathematical formulation of the model with inputs from P.K. and extended the software for anisotropic mechanical model of plates. I performed all the simulations for plates and generated all the figures except those of the "Shell" model. I analysed the data together with H.J. and P.K. and contributed to the writing of the manuscript.

PAPER II:

Morphogenesis can be guided by the dynamic generation of anisotropic wall material optimizing strain energy.

In this paper we analysed the stress-fibre feedback model from a theoretical point of view. The dynamics of any system toward its mechanical equilibrium can be derived by minimization of strain energy [5]. In the plant tissue, both the degree of mechanical anisotropy and its direction are dynamical variables. We ask whether the stress-fibre feedback with all of its favourable results for plant morphogenesis, is also in favour of elastic energy minimization. First, we try this idea on a linear elastic material model. We parametrize the energy in terms of the angle between the maximal stress direction with the stiffest direction of the material and the degree of material anisotropy. We assume the constraint of constant overall material stiffness, which is equivalent to constant fibre content in the cell wall. We show that, minimization of elastic energy is equivalent to the alignment of the direction of material with highest stiffness with maximal stress direction. Furthermore, we minimize the energy respect to the degree of material anisotropy and derive an analytical relation between material and stress anisotropies at the minimum energy. The direction and anisotropy of stress on epidermis is prescribed by turgor pressure and curvature of the surface and correlated with orientation of cortical microtubules and fibres in the same domains [6, 7]. Therefore we tried the stress-fibre feedback model, which is developed in Paper I, on a pressurized template with similar curvatures as in the shoot apical meristem while observing the overall elastic energy. We showed while stress-fibre feedback mechanism aligns the directions of material anisotropy with maximal stress, the elastic energy declines. The elastic energy declines further, after applying the stress-fibre feedback for degree of material anisotropy.

My contribution: I conceived the idea of the project with inputs from H.J.. I did the mathematical derivations. I developed the software and performed all of the simulations. I analysed the data together with H.J. and P.K.. I generated all of the figures and contributed to the writing of the manuscript.

PAPER III:

A continuous growth model for plant tissue.

The large deformations leading to organogenesis in plants are generated by residual growth in the cell walls. Analysing growth at such a detailed level needs a continuous description of the tissue. There are models developed for this purpose [8], each based on specific assumptions. Due to the complexity of the growth process and different possibilities for its regulation, we aimed at developing a growth model, in which all the key features of the tissue that potentially can coordinate growth are included. We represent a general form for the continuous growth process. In our description a mechanical signal, e.g. strain or stress, as well as a non-mechanical signal, e.g. a morphogen, can regulate the growth rates and directions. Due to the importance of stability of such model we compare its results when applied on templates of different resolution in spatial discretiation. We show that such results converge by improving the closeness of growth dynamics to the mechanical equilibrium where all the forces in the tissue are balanced. We show how this model is able to use stress or strain as well as a growth field prescribed by a morphogen to coordinate growth. We demonstrate the differences between such results even under the same material properties and stress condition in the tissue. This stresses the importance of a careful comparison between different candidates used as growth regulators. Finally, we introduce an approximate method for implementing cell division and re-meshing. While it is possible to use different cell division rules in our model we always minimize the discontinuity of the mechanical signals between their values before and after cell division. The above mentioned aspects of such model allows us to ask fundamental questions about the potential underlying feedback mechanisms involved in growth-related processes.

My contribution: I conceived the idea of the project with inputs from H.J. and P.K.. I did the mathematical derivations. I developed the software and performed all of the simulations. I analysed the data together with H.J. and

P.K.. I generated all of the figures and wrote the paper together with H.J. and P.K..

PAPER IV:

Anisotropic growth in plants can result from stress feedback on wall material and strain-regulated growth.

Here we combine models developed in Papers I and III. We introduced stress-fibre feedback as a regulator of anisotropy direction of the tissue in Paper I. We showed advantages of such feedback mechanism for generating realistic patterns of anisotropy in plant tissues. By using the growth model introduced in Paper III, we can compare different growth signals working alongside with the stress-fibre feedback mechanism. In this paper we compare stress and strain as growth signals. These two can be decomposed when the material elasticity and stress field are both anisotropic. We show that regardless of tissue anisotropy, a stress signal fails to generate favourable growth patterns for organ formation and development. Conversely, strain provides growth coordination that fits very well in many important domains. According to our results the classic growth model for plant tissue, introduced by James A. Lockhart in 1965 [9], needs to be interpreted correctly. Although, strain based growth is able to work nicely together with stress-fibre feedback mechanism to generate anisotropic pattern on a stem, it is not enough to describe the observed slow growth in the central zone of the shoot meristem. We revisit our previously made assumption about constant overall elasticity throughout the epidermis. We show that if there is a softening factor, e.g. auxin, at the shoot, the shape and curvature are maintained during growth. Next, we show that with such assumption, it is possible to tune the radius of the stem by the rate of morphogen production, which defines the area at the shoot apex with a concentration above a threshold value. Finally, we show that the stress-fibre feedback mechanism together with a strain based growth can describe the transient reversal of the cortical microtubules when growth has a layer dependent rate.

My contribution: I conceived the idea of the project with inputs from H.J. I modified the software and performed all of the simulations. I analysed the data together with H.J.. I generated all of the figures and wrote the paper together with H.J..

PAPER V:

A model analysis of mechanisms for radial microtubular patterns at root hair initiation sites.

This paper is an investigation of the growth process of plant root hairs. The growth of root hairs involve extremely anisotropic shape changes governed by tip growth. Investigating the patterns of material properties as well as stresses in the tissue can reveal information about the initiation process of root hairs. In the experiments we observed a star like arrangement of microtubules which forms before initiation of root hairs. Due to the correlation between microtubules and stress pattern in other domains of the plant tissue, we investigate if these patterns can be generated by stress. We map such stress patterns into patterns of material elasticity as well as forces that can be applied on the tissue. We show that there are two possibilities for the formation of such stress patterns. Local addition of material and increased local tension both can produce such arrangement of stress directions. Also, we implement a molecular model for interactions between ROP and auxin and show that a cell polarity driven by auxin concentration can lead to a patch of activated ROP at the basal side of the epidermal root cell.

My contribution: All of the authors conceived the idea of the project. I did the trial run of mechanical simulations and contributed to analysing the data. I edited the manuscript.

REFERENCES

1. T. I. Baskin, "On the alignment of cellulose microfibrils by cortical microtubules: A review and a model," *Protoplasma*, vol. 215, pp. 150–171, mar 2001.
2. E. T. Gertel and P. B. Green, "Cell growth pattern and wall microfibrillar arrangement: experiments with nitella.," *Plant physiology*, vol. 60, pp. 247–54, aug 1977.
3. H. Delingette, "Triangular springs for modeling nonlinear membranes," *IEEE Transactions on Visualization and Computer Graphics*, vol. 14, pp. 329–341, mar 2008.
4. J. Bonet and R. D. Wood, *Nonlinear continuum mechanics for finite element analysis*. Cambridge University Press, 1997.
5. G. T. Mase, R. E. Smelser, and G. E. Mase, *Continuum Mechanics For Engineers*. CRC Press, 2010.
6. O. Hamant, M. G. Heisler, H. Jönsson, P. Krupinski, M. Uyttewaal, P. Bokov, F. Corson, P. Sahlin, A. Boudaoud, E. M. Meyerowitz, Y. Couder, and J. Traas, "Developmental patterning by mechanical signals in arabidopsis," *Science*, vol. 322, pp. 1650–1655, Dec 2008.
7. A. Sampathkumar, P. Krupinski, R. Wightman, P. Milani, A. Berquand, A. Boudaoud, O. Hamant, H. Jönsson, and E. M. Meyerowitz, "Subcellular and supracellular mechanical stress prescribes cytoskeleton behavior in *Arabidopsis* cotyledon pavement cells," *eLife*, vol. 3, p. e01967, apr 2014.
8. F. Boudon, J. Chopard, O. Ali, B. Gilles, O. Hamant, A. Boudaoud, J. Traas, and C. Godin, "A computational framework for 3d mechanical modeling of plant morphogenesis with cellular resolution," *PLoS Comput Biol*, vol. 11, pp. 1–16, 01 2015.
9. J. A. Lockhart, "An analysis of irreversible plant cell elongation," *Journal of Theoretical Biology*, vol. 8, no. 2, pp. 264 – 275, 1965.

I

STRESS AND STRAIN PROVIDE POSITIONAL AND DIRECTIONAL CUES IN DEVELOPMENT

Behruz Bozorg [1,†], Pawel Krupinski [1,†] and Henrik Jönsson [1,2].

[1] Computational Biology & Biological Physics, Lund University, Sölvegatan 14A, SE 223 62 Lund, Sweden.
[2] Sainsbury Laboratory, Cambridge University, Bateman Street, CB2 1LF Cambridge, United Kingdom

[†] These authors contributed equally to this work.

PLoS Computational Biology, 10, e1003410 (2014)

Morphogenesis of organs necessarily involves mechanical interactions and changes in mechanical properties of a tissue. A long standing question is how such changes are directed and coordinated on cell to tissue scale. Growing evidence suggests that mechanical cues are participating in control of the expansion and growth in development. We introduce a mechanical model for describing dynamical anisotropy in plant cell walls in which both the degree of material anisotropy and anisotropy direction are regulated by stress anisotropy as a model for the deposition of cellulose fibers in primary plant cell walls. We show that the finite element shell model and the more simple triangular biquadratic springs approach using flat two-dimensional elements provide equally adequate descriptions of the cell mechanics in tissue pressure simulations of the epidermis. In the case of a growing organ, where circumferentially organized fibers act as a main controller of longitudinal growth, we show that the fiber direction can be correlated with both maximal stress direction and orthogonal to maximal strain direction. However, when dynamic updates of the fiber direction are introduced, the mechanical stress provides a robust directional cue for the circumferential organization of the fibers, while the strain model leads to an unstable situation where the fibers reorient longitudinally. Our investigation of the more complex shape and growth patterns in the shoot apical meristem where new organs are initiated shows that a stress based feedback on

fiber directions is capable of reproducing main features of known fiber directions, deformations and material properties in different regions of the shoot. Especially, we show that the purely mechanical model can create distinct regions in the radial direction where cells are expanding slowly and isotropically in the central zone and faster and in a radial direction at the periphery, which is a well known behavior in the meristem.

I.1 AUTHOR SUMMARY

Development is dependent on a coordination between cell differentiation and morphogenesis. Plants, that lack cell migration, control directional growth by adjusting cellulose fiber directions to form the organ shapes and it has recently been shown that mechanical cues can guide the fibers. We developed detailed mechanical models to investigate how fiber directions may be listening to mechanical cues and what consequences this have for positional and directional growth patterns. We could show that a model where fibers align to maximal stress dirtections spontaneously generates a radial zonation in the shoot, with the known slowly growing center and faster growing peripheral region. This connects mechanics with the gene expression important for stem cell maintenance, which are expressed in a similar pattern. We also showed that the stress model is robust in defining anisotropically growing organs, which stress the importance of stress in generating correct organ shapes in plants.

I.2 INTRODUCTION

Mechanical forces are integral part of any living system and recent data is confirming their importance as signaling cues in animal and plant development [1–3]. This may be especially important for plants which have to sustain large environmental forces while achieving shape and form which can be advantageous in their habitat [4]. Due to lack of cell migration, plants require changes in mechanical properties of the tissue on the cellular scale for facilitating directional growth of organs.

The mechanical properties of plant tissue can be linked down to the properties of cell walls. The walls are composed of a network of cellulose microfibrils interconnected by polysaccharides and xyloglucans [5–7], which constitute the structurally strong element of plant tissue providing support against turgor pressure and internal tension. From a mechanical point of view, the walls can be considered to be thin visco-elastic elements.

The epidermis of plant tissue is thought to play a special role in morphogenesis [8, 9]. It is generally more mechanically stiff than internal tissues,

which suggest a 'tissue pressure' model where tensional forces in the epidermis are generated by the pressure and growth of the internal cells [8]. Under action of hormones or enzymes the epidermis can experience substantial changes in its mechanical properties [10–12], which is determinant in the outgrowth of plant organs. The prevailing idea of how an isotropic tissue pressure generates anisotropic growth has to do with anisotropy of plant material. The cellulose microfibrils, which have been shown to have highly organized directional pattern in epidermis [13, 14], restrict the elastic expansion of a tissue in direction parallel to them. The organization of the wall fibers is regulated by the cells via deposition of cortical microtubules [15]. This fact has been exploited by experiments which often use microtubule direction as a proxy for fiber direction. While directional fibers can translate the isotropic forces into specific strain directions, additional mechanisms for long-term plastic anisotropic growth are also needed. The data suggests that such growth is the result of a molecular break and slip behavior with new material constantly added to the walls [16, 17], where plastic growth is triggered by the stresses in the wall exceeding yield threshold. When anisotropic material is generated by adding strong fibers, the picture becomes more complex, and the idea how the growth proceeds is that weaker molecules connecting the fibers break and allow for extension in the direction perpendicular to the fiber [17]. While simple models of plant growth have been developed, a model for complete plant tissues compatible with the stress-based growth and anisotropic cell wall material is yet to be defined [18–20].

The composition of the plant cell wall has to be controlled by the genetic program of the cell allowing large degree of adaptivity for the whole plant, existence of specialized tissue types and the wealth of plant forms. However, as recent evidence [3, 21] and previous ideas [22] suggest, it is likely that the reciprocal signaling, linking the mechanical state of the tissue and cell walls to biochemical process takes place too, connecting growth rate and direction with mechanical properties of the plant tissue in a feedback loop. Molecular details of the mechanism of such two way relation between mechanics and cell functions are still elusive and require further investigation [7]. Especially, the organization of the cellulose fibers, leading to a directional growth may be determined by several cues. One suggestion is to align the fibers orthogonally to the maximal strain direction. This has been proposed for anisotropically growing tissues [23, 24]. Another suggestion is to organize the fibers in the maximal stress direction [25], which found support in the patterns observed in the plant meristem [3, 26]. In a situation of isotropic mechanical materials the two ideas would be easy to discriminate among given that maximal principal strain and stress in

such situation point in the same direction. However, in the case of mechanically anisotropic plant walls, maximal strain and stress may very well be orthogonal and it may not be easy to discern between the two rules of fiber alignment. The situation is complicated further by the fact that a change in the fiber direction will lead to a change in stresses and strains resulting from the same external load. This complex feedback loop makes it difficult to predict *a priori* if stress or strain directions can act as stable inputs for shape generation, even if their directions are easily predicted given the material anisotropy. The intricate dynamics of fiber alignment resulting from such feedbacks has yet to be investigated in more detail.

Mechanical strains and stresses in the tissue, are not easily measurable quantities, and reliable mechanical models of biological materials can offer significant help to quantitatively predict both magnitude and direction of the strains and stresses. Within such models, given the material properties and loading forces, one can accurately describe the mechanical response of the tissue and test different scenarios of its coupling to biochemical signals. There exists a large variety of finite element or particle based methods which can be applied when modeling mechanical interactions of different materials [27]. These methods, however, are usually quite computationally intensive and large scale cellular models are not always feasible within them. In addition those methods have not been designed and optimized to cope with dynamic complexity of biological materials and growth of the tissue, which means rapid changes to cellular topology and material composition of the models.

Given the geometry of a plant cell wall, where the thickness is often more than an order of magnitude smaller than its planar extension, finite element method (FEM) shell models provide an adequate description since they are specifically designed for thin curved surfaces and describe tensile and bending behavior (Figure 1A) [28, 29]. More recently, Triangular Biquadratic Spring (TRBS) models have been developed to describe two-dimensional elastic elements [30]. TRBS has the benefit that a model can describe the mechanical variables encoded just in the resting and current lengths of the triangular edges ($\{L_i\}$, $\{l_i\}$ in Figure 1B), and hence provide a simplistic description of two-dimensional mechanical elements. The TRBS implementation has been shown to accurately represent continuum properties of mechanics [30]. However, since bending energy is disregarded, it is less obvious that such models can provide a good description of plant walls that typically consists of curved structures.

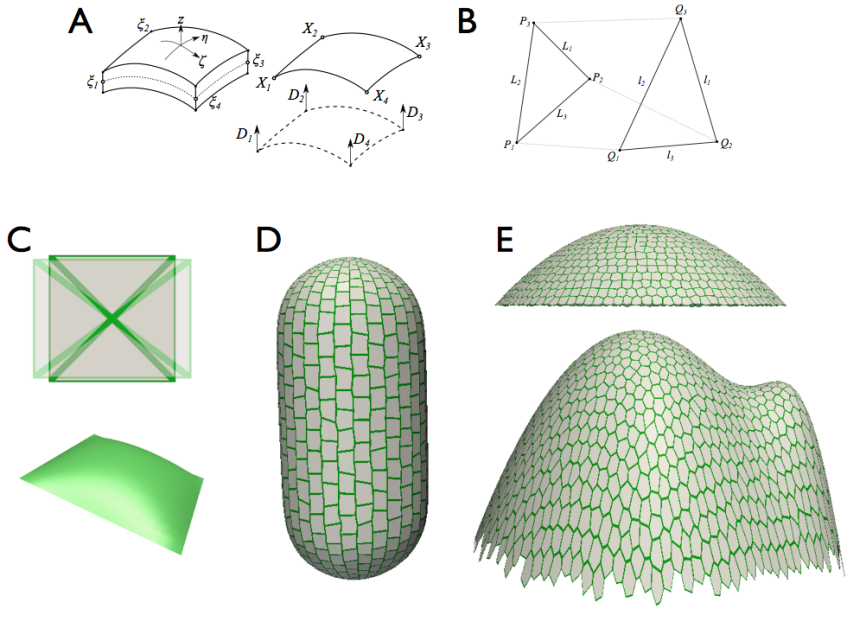

Figure I.1: **Mechanical models and templates.** (A) Geometry of a quadrilateral shell element for the finite element method. The thin three-dimensional surface is parametrized by a two-dimensional shell with implicit thickness and set of director vectors D (Supporting information). (B) An element used in the triangular biquadratic spring model. P_i, Q_i and L_i, l_i represent positions and edge lengths in resting and deformed state, respectively. The strain tensor can be expressed in terms of edges of the element in resting and deformed states. (C) The quadrilateral patch used for comparing triangular biquadratic springs and finite element shell models. (D, E) Different templates representing selected plant-like geometries used in tissue pressure simulations.

In this paper we develop two implementations of a mechanical model for anisotropic plant wall material: a FEM shell model and a TRBS of plates. We compare the models in in-plane loading simulations and in tissue pressure models of the plant epidermis leading to additional bending forces in shells (Figure 1C-E). We analyze the relation between maximal (first principal) stress and strain direction under different loading forces. We use the models to analyze different proposed mechanisms of coupling between mechanical cues and alignment of material anisotropy of cells, based on perception of either maximal stress direction (MSD) or the direction orthogonal to maximal strain (OsD). We apply the models to different geometries representing different tissues in plants in order to evaluate their potential for explaining cellulose fibril patterns and growth patterns observed in epidermal plant tissues (Figure 1D-E).

1.3 RESULTS

1.3.1 *Shell Finite Elements and Triangular Biquadratic Springs offer an adequate description of anisotropic plant wall material*

One of our goals was to establish an efficient computational method and reliable material model that can be used to simulate the behavior of plant walls. Especially, we aimed to investigate whether a Triangular Biquadratic Spring implementation can provide a reliable description, given that it is a two-dimensional representation and that it does not explicitly include any bending behavior. To do this we developed a TRBS model and compared the results with a finite element method shell model (Methods and Supporting information).

To describe the anisotropic wall material, we used a hyperelastic strain energy density formalism applicable to large strain deformations (Supporting information). For the isotropic part we used a St. Venant-Kirchoff description [3, 30], and developed an anisotropic material model penalizing extension in a defined fiber direction (Equations 1,3 and Supporting information).

First, we tested a quadrilateral mechanically isotropic square patch of elements under different loading conditions and different material properties (Figure 1C). When we applied a uniaxial tension, the stress-strain relation completely agreed between both methods (Figure 2A-B). The quantitative agreement was confirmed for a wide range of Young modulus and Poisson ratio configurations when tested on isotropic loading force conditions with a difference less than 0.1 percent between two models (Figure 2C, Figure S1A). Note that the principal stress value is monotonically increasing

function of not only the Young modulus but also of the Poisson ratio for this mechanical model (Figure 2B). We extended the uniaxial tension tests into a large deformation regime to demonstrate the well known deficiency of this material model, where uniaxial loading force can result in infinite stresses and zero volume at finite strains [31]. We found that this deficiency appeared especially when the Poisson ratio is high (Figure 2A-B). In simulations of plant tissues, we do not expect strains to exceed several percent, which corresponds to the typical values 5-10% encountered in experiments [32], and as such the model provides an appropriate description of plant wall material.

Next, we analyzed the behavior of the anisotropic material model for the square patch of elements under biaxial loading forces. Under isotropic loading forces an increased degree of material anisotropy led to an increased difference between the magnitude of principal stresses (Figure S1B), and the maximal stress and strain directions were perpendicular to the fiber direction. When we applied an anisotropic loading force, the behavior depended on the angle between the maximal force direction and the direction of the material anisotropy axis (Figure 2D). When the material anisotropy direction coincided with the dominant loading force direction the maximal principal stress value were lower compared to when those directions were perpendicular. This can have profound implications for plant wall mechanics. Since stresses are responsible for triggering inelastic behavior and breakage of brittle components of a material [33], a plant cell's ability to control the amount of stress in the tissue by adjusting its anisotropy can be a way to direct growth given the stress magnitude's relation to the yield stresses of the wall material [5].

To test how important the lack of a bending resistance is in the TRBS model we compared principal stress pattern, principal strain value and deformation with the FEM shell model for a pressurized quadrilateral plate (Figure 1C, 2E), for different plant-based geometries (Figure 1E, Figure S1C-D), and a saddle-like template (Figure S1E).

The results showed good agreement between the two methods for the pressurized quad suggesting that the deformation in our tissue pressure model is dominated by tensile and not bending behavior (Figure 2E), although we found small quantitative differences. For example, the normalized distribution of equivalent von Mises strain for TRBS model had a slightly higher average (0.052 vs. 0.049) (Figure 2F) indicating the lack of bending energy at the junctions. The similarity held for most geometries tested (Figure S1C-D), although templates where compressive forces generated buckling were an exception (Figure S1E). However, even in this case the general pattern and distribution of stresses was in good agreement

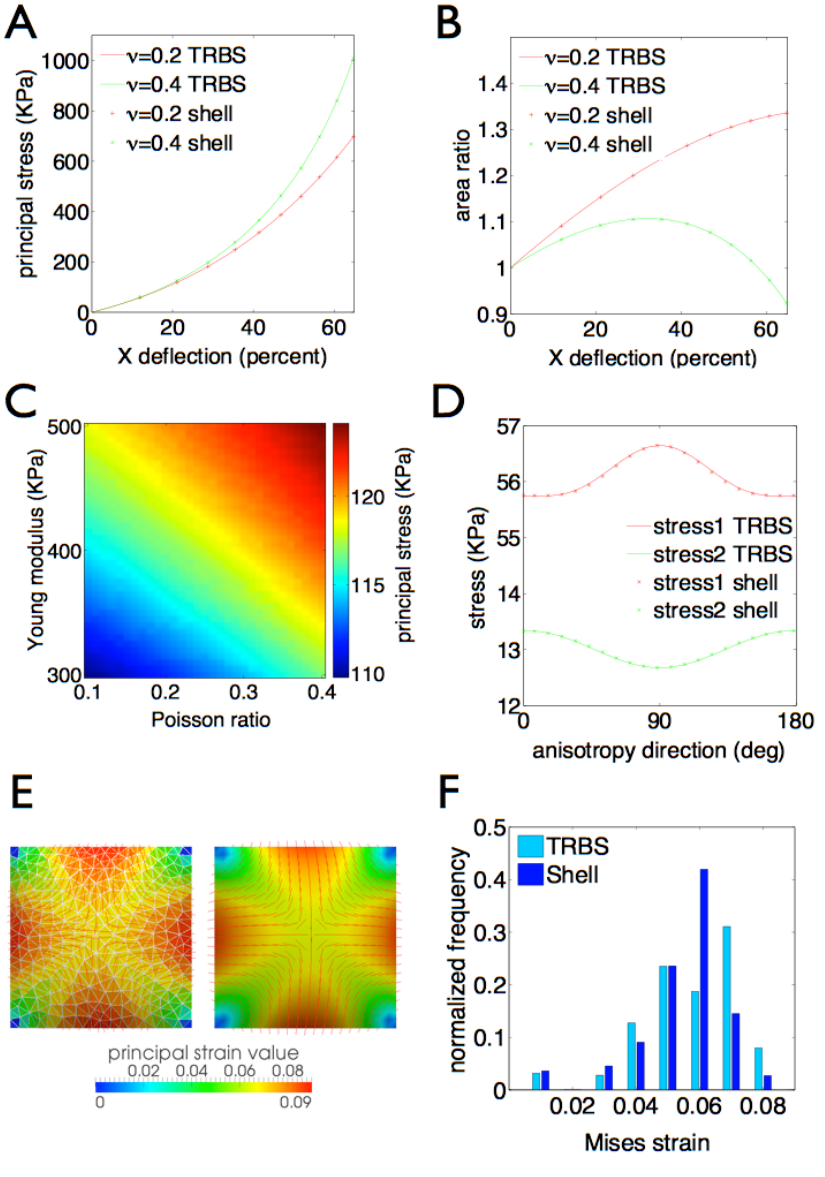

Figure I.2: **Comparing triangular biquadratic springs and finite element shell models.** (A, B) Uniaxial stretching test on a quadrilateral patch shows prefect agreement within numerical accuracy between both methods for principal stress and area ratio versus deflection of top right corner of the quad. Isotropic material (Young modulus = 400 kPa, Poisson ratio = 0.2 and 0.4, thickness = 0.01 m, size = 1 m, force = 8 kN). (A) Principal stress. (B) Area ratio. (C) Principal stress value for isotropically loaded...

Figure I.2: ... patch with 2kN force for the same patch using TRBS method where Young modulus and Poisson ratio were varied. The difference between principal stress value in TRBS method and integrated principal stress over thickness in FEM shell model is less than 0.1% (Figure S1A)(D) First and second principal stress values for the same patch of anisotropic material with transverse and longitudinal Young modulus of 400 and 800 kPa respectively and Poisson ratio of 0.2, under 0.8 kN and 0.2 kN anisotropic loading force. The anisotropy direction was varied between 0 (maximal force direction) and 180 deg. (E, F) bending test results from pressurizing a patch of elements. (E) Principal stress direction and principal strain value for TRBS (left) and shell (right). Material is isotropic with Young modulus 400 kPa and Poisson ratio 0.2. Number of elements is 400 and 250 for shells and TRBS, respectively. (F) Distribution of equivalent Mises strain value over elements. TRBS elements show slightly higher strain value because of the lack of bending energy. Average equivalent Mises strain over elements: 0.0523 and 0.0492 for TRBS and shell, respectively.

between both methods. The similarities of the two methods indicate that tensile forces may dominate over bending forces, but also that although the TRBS approach does not explicitly account for bending energies at individual edges, the triangulated mesh structure may still incorporate a resistance towards bending via stretch and compression of the elements induced by bending.

In conclusion, we have shown that TRBS and shell finite element models agree for describing anisotropic wall material in two dimensions in a wide range of material anisotropy and applied forces. Although quantitative differences appear, the methods also show high degree of similarity in the case where three-dimensional structures are pressurized and where bending forces are induced. We could also see that in a situation of anisotropic loading forces and an anisotropic material, a complex relation between the maximal directions of the load, strains and stresses appear, indicating that plant cells can control these aspects if it is able to control the fiber directions.

I.3.2 *Mechanical strain and stress are not equivalent signals in presence of material anisotropy and loading force anisotropy.*

To analyze the relation between resulting stress and strain directions given different loading forces and fiber directions we first investigated a situation where the direction of maximal applied force coincide with the fiber direction in a simple square shape. The maximal stress direction always followed the maximal loading force direction. Depending on the degree

of anisotropy for the applied force and the material properties used, the resulting maximal direction of strain was either parallel or perpendicular to the maximal stress direction marking distinct regions in the (force-anisotropy, material-anisotropy) parameter space (Figure 3A). As expected, for isotropic materials the maximal principal stress and strain directions coincided with the maximal applied force direction. For anisotropic materials and anisotropic loads we obtained a region where maximal stress and strain directions can be perpendicular (black region in Figure 3A). The extension of this region was dependent on the Poisson ratio of the material (Figure S2A-C). Given a fixed material anisotropy (dashed line in Figure 3A), isotropic loading leads to parallel directions of the maximal principal stress and strain. A higher directional force can be resisted by the stronger component of the material leading to a maximal strain direction perpendicular to the maximal force. However, when the forces are highly anisotropic they overcome the resistance of the stronger component of the material and the maximal strain will follow in the direction of the applied force.

This pinpoints the fact that potential cellulose fibril orienting mechanisms based on the feedback from either stress or strain will behave differently from each other in some parts of a tissue even if in another part they would show consistent behavior. We used the model to analyze the anisotropic growth of shapes resembling plant organs, where the alignment of fibers in epidermal tissues is thought to guide growth. We simulated a cylindrically shaped tissue using the tissue pressure model and mechanical parameters with values from experimental estimates [34–36]. We set the fiber direction to be circumferential to match observed microtubule directions in the epidermis of several plant tissues [3, 37–39]. This led to maximal principal direction of stress in a circumferential and strain in a perpendicular, longitudinal direction (Figure 3B-C). If we use strain as a proxy for growth (see Discussion) the result of this simulation corresponds to the idea that organ growth is perpendicular to the fiber direction, extending the organ along the main axis.

The circumferential fiber direction seems to be explainable equally well by a model where fibers orient perpendicular to the maximal strain (OsD) as by a model where fiber orient in the direction of the maximal stress direction (MSD), both suggested as informative signals for fiber directions in plant tissues [3, 23, 24, 40]. To analyze these potential signaling cues for the fiber directions, we introduced a dynamic description of the wall mechanics, where the deposition of new cellulose fibers leads to changes in magnitude and direction of the mechanical anisotropy of individual plant walls (Methods, Equations 7-9). We assumed a constant addition of fibers

in the walls with the anisotropy of the deposition guided by the anisotropy of the directional signal, i.e if the input signal is isotropic, the material will be isotropic, while an anisotropic input signal will result in an anisotropic material.

Interestingly, the MSD and OsD hypotheses gave very different results, in spite of the fact that maximal strain and stress directions were perpendicular in the fixed fiber direction situation. In case of the stress based feedback, the fiber direction was identical to the fixed anisotropy direction case (Figure 3E-F), whereas in the case of (orthogonal) strain based feedback the initial, circumferential fiber direction became unstable and subsequently reorganized into a longitudinal direction (Figure 3H-K, Movie S1), in contrast to the circumferential orientation of microtubules suggested by experimental data. A more detailed analysis of the influence of material and loading force anisotropy for the MSD and OsD material models showed that the former model results in regions of mutually parallel and orthogonal strain and stress (Figure 3D). The extension of the region with perpendicular stress and strain directions was similar to the static anisotropy direction case (Figure 3A,D), indicating that this configuration represents a stable situation for the MSD dynamical model (Figure 3E, Figure S3). In the OsD model, the region of orthogonality between stress and strain disappeared completely (Figure 3G), indicating that this is an unstable situation for the OsD dynamical model (Figure S3). Independently of the anisotropy of the forces causing elastic deformation, the main principal stress and strain directions always became parallel (Figure 3H-K).

In conclusion, we have shown that in a situation where internal tissue is providing tension to the epidermis, an extension along the maximal axis of the organ can be explained by fibers resisting strain in the circumferential direction. This was clearly seen in a model where static fibers are laid out according to the experimentally suggested pattern which results in the strain orthogonal to the fiber direction. In the situation where fiber directions are allowed to be oriented by mechanical cues, more intricate dynamics was generated. A model where fibers are aligned in the direction of main stress robustly preserved the circumferential directions of the fibers, as seen in experiments. On the contrary, a model where the fiber orientation is aligned perpendicularly to the maximal strain direction led to the initial circumferential fiber pattern becoming unstable and reorienting to the longitudinal direction.

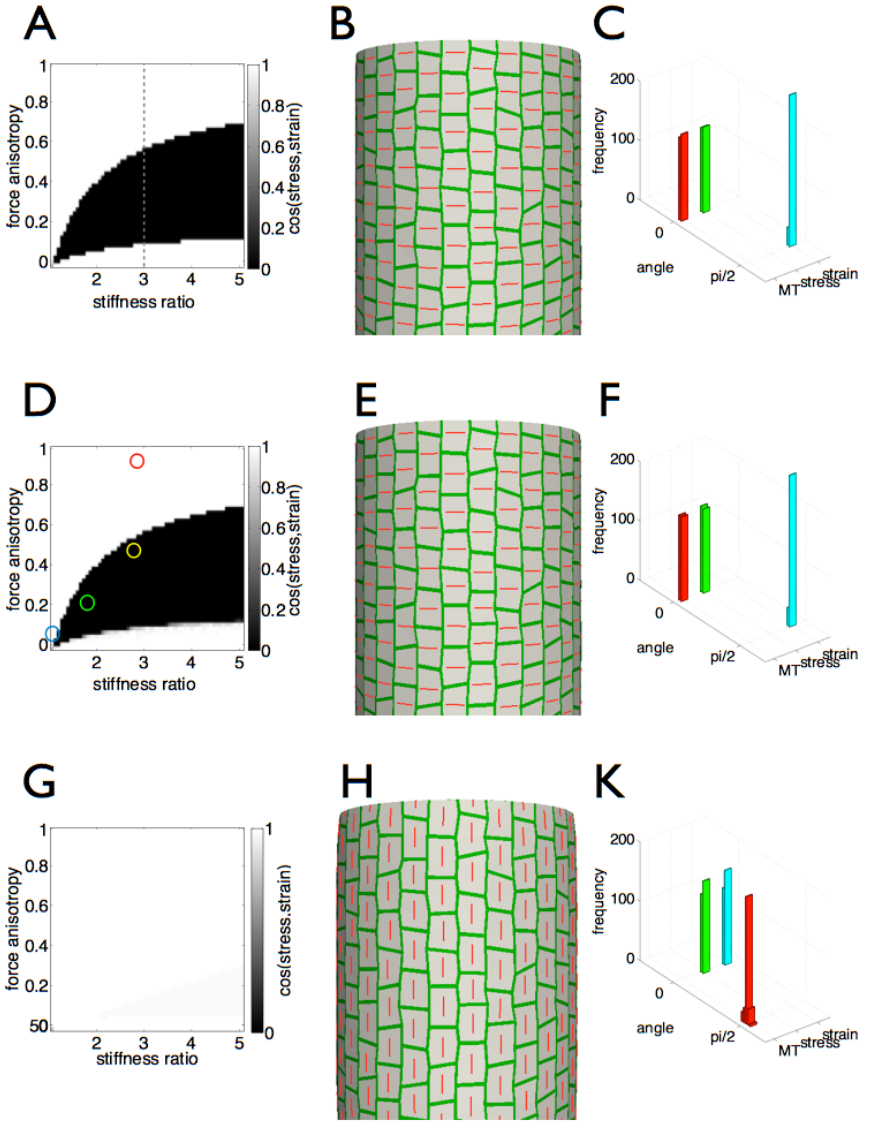

Figure I.3: **Comparison between stress and strain based feedback models.** The results of the three distinct relations between mechanical stress/strain and anisotropy of the material in different loading force situations are analyzed. The first row (A, B, and C) pertains to the predefined and static direction of material anisotropy. The second row (D, C and F) describes the results of stress feedback model and the third row (G, H and K) the orthogonal strain feedback model. The first column (A, D and G)...

Figure I.3: ...presents the results of the simulation of anisotropic biaxial loading of a square patch from Figure 1C. For varied anisotropy of the loading force (vertical axis in the graphs) and the ratio of Young moduli along each of the load directions (horizontal axis in the graphs), the cosine of the angle between maximal stress and strain directions is plotted with the gray-scale map. Force anisotropy and stiffness ratio in A, D and G are calculated by $\frac{F_L - F_T}{F_L}$ and $\frac{Y_L}{Y_T}$, respectively. Force anisotropy 0 corresponds to isotropic loading and stiffness ratio 1 to isotropic material case. The gray dashed line in panel A and circles in panel D are discussed in method section. The second column (B, E and H) shows the equilibrium state of fiber directions (red lines) in the cylindrical part of the tissue pressure model simulation for the template shown in the Figure 1D. The third column (C, F and K) pictures the distributions of the stress, strain and fiber directions in the cells with respect to circumferential (horizontal) direction resulting from the tissue pressure model simulation. (A) For the fixed anisotropy direction we observe distinct regions in the parameter space where maximal stress and strain are either mutually parallel (white) or perpendicular (black). (D) The identity of these regions is maintained by the stress feedback model. The yellow circle in D shows the approximate value for force and material anisotropy on the side of cylinder where anisotropic curvature results in force anisotropy about 0.5. (G) The distinct regions disappear for orthogonal strain feedback and we observe only parallel alignment of maximal stress and strain. (B) The material anisotropy (fiber) direction is set to circumferential. (E) The same, circumferential alignment of the fibers results from stress feedback model. (H) In the orthogonal strain feedback model circumferential alignment of the fibers is not stable and the fibers align in the longitudinal direction. (C) With no feedback mechanism present and the fibers prealigned and set circumferentially the stress becomes parallel to the fiber direction while strain is perpendicular to them. (F) When fibers are dynamically aligned in the direction of the maximal stress the circumferential orientation of them arises spontaneously. The strain is perpendicular to fibers as well. (K) In the case when fibers are dynamically updated to match the direction orthogonal to maximal strain they align longitudinally while both stress and strain are perpendicular to them. The parameters used in the simulation with the pressurized template in Figure 1D were: thickness $h = 1\ \mu m$, cell size 10 to 20 μm, $P = 0.1\ MPa$, $\nu = 0.2$, $Y_{matrix} = 50\ MPa$, $Y_{fiber} = 120\ MPa$, fiber model with $K = 0.4$ and $n = 2$, deformation is between 5% to 10% (B)6%, (E) 6%, (H) 10%).

1.3.3 *A stress feedback model results in a radial zonation and gives an explanation to strain patterns in the shoot apical meristem*

To test the stress feedback together with our fiber material model on a template with regions of varying curvature, we applied the tissue pressure model on a paraboloid template, as a proxy for a bare meristem, in which the curvature is isotropic at the apex and smoothly becomes anisotropic in the periphery (Figure 1E). The dynamical changes of material properties in the cells resulted in a region of isotropic material at the center and anisotropic towards the periphery (Figure 4C), corresponding to isotropic stresses in the center and anisotropic in the periphery (Figure S5B). The dominant fiber direction showed circumferential orientation around the central zone (Figure 4A), as previously reported in experiments and models [3, 40]. Remarkably, the switch from isotropic to anisotropic material (and stresses) in the radial direction was quite rapid, creating a spontaneous zonation of the meristem purely from mechanical interactions. This behavior is the result of the fact that the boundaries between the regions of parallel and perpendicular alignment of maximal stress and strain are very sharp in the parameter space of material and loading force anisotropy (Figure 4A, D, cf. circles in Figure 3D). Therefore, even though these parameters change smoothly in the radial direction of the meristem the material model creates an abrupt transition between the regions. The extension of these regions depended on model parameters, but the switch-like behavior was a robust feature of the stress feedback model (Figure S4).

The meristem has a central zone with slowly growing and dividing cells, and a peripheral zone where cells expand faster [41–43]. The cell expansion rates in the simulations also reflected the zonation (Figure 4B). The model predicted a slower isotropic expansion in the central zone and a higher radially oriented expansion rate in the periphery, correlating well with strain directions reported for meristems [42].

Next, we looked in more detail on the effects of the dynamic update of material anisotropy direction and intensity on a geometry where a primordia appears at the periphery of the meristem with a valley in between (Figure 1E). Previously, we have shown that a tissue pressure model of the epidermis, applied to a meristem shape leads to isotropic stress in the central part while the valley in between the meristem and a primordium develops anisotropic stress. A simple spring model using a stress feedback generated fiber directions comparable to the measured microtubule directions in different areas of the meristem[3]. In the TRBS model, the stress feedback led to similar material fiber patterns (Figure 4D, Movie S2), while the strain feedback model failed to describe these directions (Figure S5E,

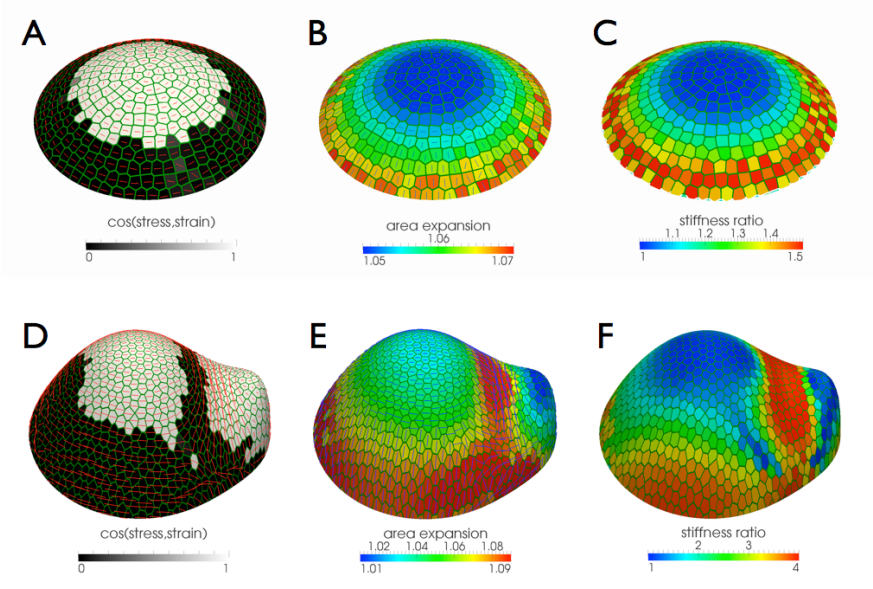

Figure I.4: **Zonation properties of the stress feedback model in meristem-like geometries.** (A) The stress feedback together with fiber model for a paraboloid representing the geometry in the central zone and its close neighborhood results in two distinct zones where maximal stress and strain directions are either parallel (white) or perpendicular (black). The red lines (here and panel D) are showing fiber directions (B, C) Area expansion and material anisotropy (stiffness ratio) show different properties in these two regions. The elastic deformation is larger and radially oriented in PZ and material is anisotropic whereas in the central zone deformation is lower and material becomes more isotropic. The blue lines (in the panels B and E) are showing the maximal strain directions. (D, E, F) The same results as A, B and C respectively for a meristem-like template seen in Figure 1E. Strain and stress are aligned at the apex and valley because of almost isotropic material and anisotropic stress respectively. For the meristem-like template due to the large variability of stress value in different regions the absolute stress anisotropy measure with $S_{max} = 8MPa$ is used. The parameters used for pressurized templates in Figure 1E were: thickness h = 1 μm, cell size about 10 μm, P for paraboloid = 0.05 MPa and for meristem = 0.08 MPa, ν = 0.2 , Y_{matrix} for paraboloid = 40 MPa and for meristem = 50 MPa, Y_{fiber} for paraboloid = 100 MPa and for meristem = 150 MPa, fiber model with K = 0.4 , n = 2. The deformation is within 5% to 7% for paraboloid and within 1% to 9% for meristem.

In summary, we have shown that a stress feedback model is able to explain the microtubular organization seen in experiments. The feedback generates a relatively sharp zonation within the meristem based on the relation between maximal stress and strain directions, providing a purely mechanics-based explanation to strain magnitudes and directions described in experiments, where the central zone has a lower isotropic expansion and the periphery a larger radially directed strain in spite of the circumferential stress direction. The model also predicts that highly anisotropic stresses generated in the boundary between the meristem and a primordium can lead to a maximal strain direction parallel to the main stress direction in this region.

1.3.4 *Stress and strain based feedback mechanisms have different impact on tissue geometry*

Next we analyzed how dynamic properties of wall material effect the elastic deformations locally and at a tissue scale. When anisotropic forces are applied (i.e. when curvature is higher in one direction in our tissue pressure models), the maximal stress feedback model always aligns the fibers parallel to the maximal force. This will resist against the deformation in this direction and procure locally isotropic deformation. Even in the case with strong anisotropy of the loading forces where maximal strain and stress are parallel (Figure 3Bi, cf. boundary region between meristem and primordia) the stress feedback model leads to more isotropic strain compared to an isotropic material of the same total stiffness. Since the strain feedback model is aligning the fibers perpendicular to the loading forces this feedback will tend to increase local strain anisotropies.

To quantify these differences, we tested both material anisotropy feedback mechanisms within the TRBS model where geometries with different degree of shape anisotropy where pressurized (Figure 5). When compared to isotropic material, the stress feedback model resulted in more isotropic strain, and the difference was increasing with the anisotropy of the geometry and hence the loading force (Figure 5C). In contrast, the strain based feedback model led to increased strain anisotropy when compared to an isotropic material (Figure 5C). This local difference had an impact on the resulting global deformation of the structure, where the stress feedback model promoted the maintenance of the geometrical anisotropy while orthogonal strain feedback model led to decreasing of this anisotropy (Figure 5A-B).

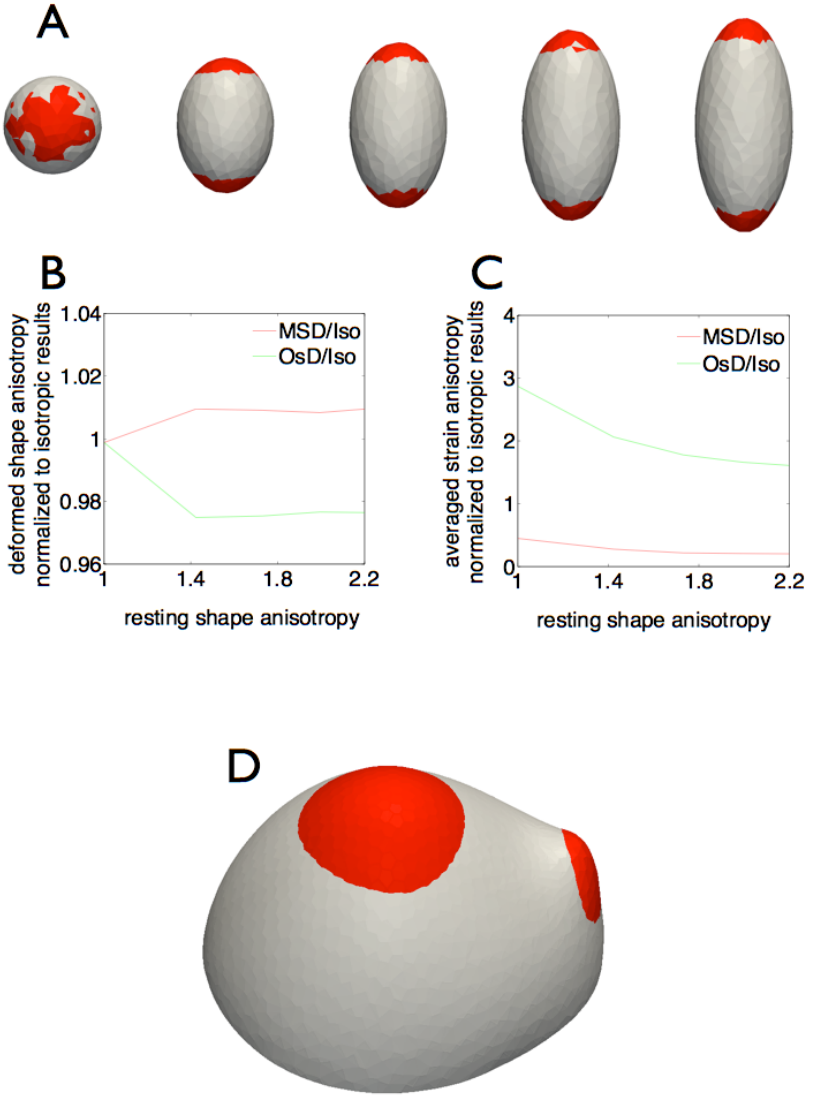

Figure I.5: **Feedback impact on geometry.** (A, B, C) Comparing stress and perpendicular to strain feedback models for a set of templates with different geometric anisotropies which is considered here as the ratio between principal axes. This ratio is 1 for the sphere and increases for more elongated templates. (A) Three different set of simulations are performed for all templates. Isotropic material with Young modulus 8 *GPa* (not shown) and anisotropic material with longitudinal and transverse Young ...

Figure I.5: ... moduli 12 and 4 GPa respectively, with stress feedback (red) and perpendicular to strain feedback (white). Higher anisotropic growth can be seen for the red template in which stress feedback is used. (B) The deformed shape anisotropy versus resting shape anisotropy for different feedback scenarios that are normalized to the same results for isotropic material with the same overall stiffness. The results show that even for a low deformation stress feedback increases shape anisotropy whereas perpendicular to strain feedback decreases this value indicating that strain based feedback pushes the geometry toward symmetry. (C) Averaged strain anisotropy over elements for simulations with the two feedback mechanisms that are normalized to the same value for isotropic template are plotted versus resting shape anisotropy. In case of stress feedback the results are consistently lower than strain feedback. (D) Comparing deformations resulting from different feedback scenarios for the meristem-like pressurized template with the same parameters as Figure 4. More anisotropic growth in the red template (stress feedback) helps the meristem and the primordium to grow outward. The material parameters used in simulation are: $\nu = 0.2$, thickness $h = 0.01\ m$, pressure $P = 1.5\ MPa$. The radius of the sphere is $r\ 1\ m$.

Next we tested the material models on our meristem-like template. The stress feedback model resulted in a more prominent anisotropic shape change at the meristem and primordium apices, promoting the upward movement of the shoot and a more directed shape change of the primordia (Figure 5D). Also, the stress based feedback model resulted in a more pronounced boundary between the meristem and the new organ (Figure 5D, Movie S2). The changes of these features of the meristem have been seen experimentally when comparing wild-type plants and plants treated with oryzalin, a drug that depolymerizes microtubules and is assumed to lead to a more isotropic material [44].

In summary, a stress feedback to fiber directions leads to the ability for plant walls to resist internal forces, which locally generates more isotropic elastic strains, and which at the same time counteracts to the tissue pressure forces acting towards isotropic curvature and hence maintains the shape of anisotropic structures.

I.4 DISCUSSION

The coordination of the changes in mechanical properties across a growing plant tissue is crucial for the creation of the complicated forms and shapes observed in plants [7, 21]. In the shoot apical meristem a connection between the organization of mechanical anisotropy of the tissue and

perception of mechanical stress signals has been suggested [3, 40], while a competing idea that fibers organize perpendicular to the strain direction has emerged given the correlation between growth and fiber directions in anisotropically growing organs [23, 24]. Here we analyzed two models comparing these mechanisms of the feedback between mechanical cues and the orientation of cellulose microfibrils. Our simulations confirm that when looking at the stress and strain patterns in the epidermis on a stem-like geometry, where fibers are fixed to be aligned circumferentially, maximal stress is circumferential and maximal strain is in the longitudinal direction, in accord with both ideas for organizing fiber directions. However, when models of dynamical orientation of mechanical anisotropy of the cell wall material by stress versus strain were compared, we observed drastically different behavior in each of the two models. In the stress based feedback model the circumferential alignment of the fibers as well as perpendicular orientation of maximal stress and strain directions can be robustly maintained (Figure 3E). In contrast, strain based feedback results in longitudinal alignment of the fibers and parallel, circumferential directions of strain and stress, which contradicts the experimentally reported orientation of the cellulose fibrils and microtubules (Figure 3H).

When looking at the more complex shapes appearing around the shoot apical meristem, the strain feedback model again failed to explain the microtubule patterns seen in experiments. The stress feedback model translated the smooth increase of anisotropic curvature in the radial direction to a switching between different material properties in a central and a peripheral zone (Figure 4). It should be noted that even if there is an instant shift of strain and stress directions from mutually parallel to perpendicular, this does not represent a discontinuity in the model since the strain direction is degenerated (isotropic) when crossing these boundaries (Figure S5A,C). A mechanical radial zonation has recently been suggested in experiments and in models [32, 45], but in our material model the different properties of the material in the different areas of the tissue are not dictated by arbitrary specification of the separate regions. These are instead a natural consequence of the stress feedback model reacting to the differences in shape, curvature and stress response and stress anisotropy in different regions of the meristem. Alignment between principal stress and strain directions in the central zone is a consequence of isotropic material in this region. The analogical alignment in the valley between the shoot and a primordium, in spite of anisotropic material, is caused by highly anisotropic stress. The perpendicular stress and strain directions in the periphery are a result of an anisotropic material and anisotropic forces, but where the forces are coun-

teracted enough by the fibers to create a perpendicular strain direction. Such radial growth direction has been reported in experiments [42].

Spontaneously formed mechanical patterns are interesting in relation to the known radial expression patterns in genes regulating differentiation [46]. It has been recently shown that the stem cell regulator WUSCHEL, expressed in the central regions of the shoot, moves between cells and directly represses genes important for differentiation, which is enough to explain their expression in the periphery [47]. Addressing how this molecular network interacts with the mechanical properties will be an interesting question for the future. While there might not be a direct interaction, both models do depend on the shape of the meristem and will hence affect each other via the geometry. Our simulations performed on the templates resembling the shapes of the stem and meristem with outgrowing primordia show that a stress based feedback produces deformations which result in more elongated shapes of outgrowing organs while strain feedback tends to round and level the protrusions of the surface (Figure 5, Movie S2). Interestingly, this is a consequence of the stress based feedback having more isotropic strain locally, compared to an isotropic material or a strain based feedback mechanism.

We have compared the results of simulations using a Triangular Biquadratic Spring description of continuous mechanics with more involved and detailed simulations using a nonlinear shell Finite Element approach. We found that both methods are in agreement in both stretching and bending in tissue pressure simulations that are of interest for models of epidermal plant tissue. This shows that TRBS, despite its simplified treatment of geometry and lack of bending behavior, offers an adequate level of accuracy for the purpose of modeling plant tissue. The simplicity of the TRBS method will prove useful for more complicated three dimensional models involving cell growth and proliferation and thus requiring changes in model topology.

The assumption of modeling the internal cell layers as a simplified tissue pressure contribution leaves room for improvements in future work, which would allow for a more complex interaction between internal layers and the epidermis [9, 11]. Our simulations suggest that this will improve the description mainly in situations with a negative curvature and compressive forces, e.g. in the boundary between the meristem and primordia. Our simulations overestimate the strain rates in these regions and the lack of internal tissue can lead to buckling (Figure S2E).

Another challenge will be to integrate current models with long-term plastic growth of plant cell walls. Plastic growth is described as being triggered by wall stresses above a yield stress, when a break and slip behavior

is induced [48], while we have compared elastic strain in the simulations with the plastic growth in experiments. While this might seem to be a contradiction, as we show that often the stress and strain directions are perpendicular, it would be easy to remedy this difference. Either stresses in the isotropic matrix part of the wall could be used, which is the same as the strain, or the growth direction could follow the maximal stresses, but be oriented perpendicular to the fibers. Interestingly, our model predicts that a matrix stress idea and a stress perpendicular to fibers idea for growth can be discerned by a detailed measuring of growth directions in the boundary between the meristem and the new primordia, since there the fiber and strain directions are parallel. In any scenario, the main stress direction would not provide a good cue for plastic growth, since this would counteract the possibility to generate anisotropically shaped organs.

The development of detailed mechanical models will be integral for understanding morphogenesis in development. It will open up new venues of research for understanding whether mechanical cues are main drivers of the shape changes, but more interestingly will allow the development of integrated models where gene regulation and molecular signaling feed back to each other for describing the combined effects of differentiation and morphogenesis.

I.5 MODELS

I.5.1 *Material models of anisotropic tissue*

There exist many material models which parametrize elastic energy in terms of combination of deformation tensor invariants in different ways and describe behavior of different types of materials. In the simplest isotropic material case the TRBS uses a St. Venant-Kirchoff description, which is an extension of a linear material model. The strain energy, W_{iso}, in this material model becomes

$$W_{iso} = \frac{\lambda}{2}(trE)^2 + \mu trE^2, \tag{1}$$

where λ and μ are Lame coefficients and represent material elasticity and E is Green-Lagrange strain tensor. The advantages of this model are the simple energy form and a clear interpretation of material properties. We assume plane stress condition where Lame constants can be expressed as

$$\lambda = \frac{Y\nu}{1-\nu^2}, \quad \mu = \frac{Y}{2(1+\nu)}. \tag{2}$$

here Y and ν are the Young modulus and Poisson ratio that represent stiffness and incompressibility of the material, respectively.

In order to extend this material model for transversely isotropic materials we considered two sets of Lame constants, one for longitudinal and one for transverse to anisotropy direction [49]. To ensure that the energy expression is not over-penalized in the anisotropy direction we first equipartitioned the energy into three terms each corresponding to one of the principal directions (anisotropy direction and two transverse directions). Then we have penalized only the term corresponding to the anisotropy direction. A procedure which do not take into account equipartitioning of the energy overestimates the contribution of the anisotropic part [49]. The increased energy cost of deformation in direction of the fiber, W_{aniso}, is then described by

$$W_{aniso} = \frac{\Delta\lambda}{2}(\vec{a}^t E\vec{a})trE + \Delta\mu(\vec{a}^t E^2\vec{a}), \tag{3}$$

where the anisotropic part contains invariants of a strain tensor E constructed with a vector in the direction of the fibers $\vec{a}$. The $\Delta\lambda$ and $\Delta\mu$ are the differences between longitudinal and transverse Lame coefficients which are in turn related to Young modulus in longitudinal and transverse directions and Poisson ratio (Supporting information). The total energy, W, including an isotropic term for the matrix and an anisotropic term for the fiber becomes

$$W = W_{iso} + W_{aniso}, \tag{4}$$

which can be used for calculating the stress tensor and forces applied on the nodes of the meshed structure (Supporting information).

1.5.2 *Evaluating strain and stress and their anisotropy*

The expression for St. Venant-Kirchoff energy (Eq. 1) is based on the Green-Lagrange strain tensor, E, which can be expressed in terms of a deformation tensor. The second Piola-Kirchhoff stress tensor, which is the energy conjugate of the Green-Lagrange strain tensor, yields the stress in the resting

shape. For evaluating strain and stress in the deformed shape, which is the current configuration, we calculated Almansi strain and its energy conjugate, Cauchy or true stress tensors, respectively (Supporting information). The stress in case of TRBS was calculated under the assumption of plane stress and in case of shell description we visualized the stress integrated over thickness in order to be comparable to the corresponding values for TRBS.

All of these tensors are two dimensional for TRBS elements and three dimensional for shells. The relative stress (strain) anisotropy measure, a, can be defined as

$$a = \frac{S_1 - S_2}{S_1} \tag{5}$$

where S_1 and S_2 are first and second stress (strain) eigenvalues respectively.

In most simulations the magnitudes of stresses (strains) are of the same order of magnitude and such relative measure is appropriate. However, in the case of our meristem-like template with outgrowing primorium, stress (strain) magnitudes extend over a large range. In such a scenario, a relative value can overestimate an anisotropy measure in regions of low stresses (strains), and it is more appropriate to include the stress (strain) magnitude itself in the measure. In this case we used

$$a = \frac{S_1 - S_2}{S_{max}} \tag{6}$$

where S_{max} is the largest stress (strain) value throughout the template (excluding boundary effects). We have normalized the value of anisotropy measure since we use as an input to the material model an expression assuming the value of this parameter to be between 0 and 1 (see next section). In most cases the anisotropy measures based on both definitions follow the same trend but in more complicated geometries, where strain and stress values are small, there can be significant differences between the two measures (e.g. the primordial apical region in the meristem-like template).

I.5.3 *Fiber model and updating material properties*

Since plant tissue is characterized by different and dynamically changing anisotropic material properties we have devised a model which allows for smooth temporal and spatial changes of anisotropy. The model as-

sumes that stress anisotropy plays a role in defining the degree of material anisotropy while the average elastic strength of the material is maintained. We used a non-linear relation between stress and material anisotropy which saturates when stress anisotropy is maximal (Figure 6A). The relations between longitudinal, Y_L, and transverse, Y_T, Young modulus and anisotropy measure, a, can be written as

$$\begin{aligned} Y_L &= Y_{Matrix} + 0.5(1 + \frac{a^n}{(1-a)^n K^n + a^n}) Y_{Fibre} \\ Y_T &= Y_{Matrix} + 0.5(1 - \frac{a^n}{(1-a)^n K^n + a^n}) Y_{Fibre} \end{aligned} \tag{7}$$

where K and n are model parameters and Y_{Matrix} and Y_{Fibre} are Young moduli of the isotropic matrix and anisotropic fiber part respectively.

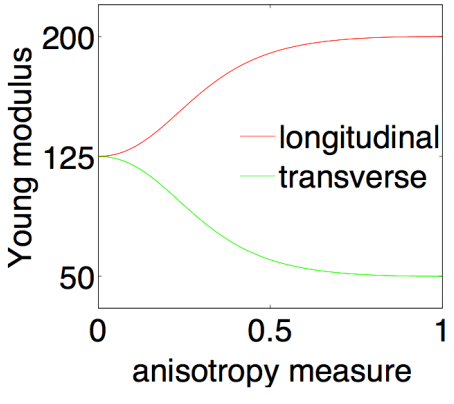

Figure I.6: **The fiber model.** Fibre model adjusts mechanical anisotropy based on anisotropy measure dependent on stress or strain in such way that the overall stiffness of the material is conserved. The plot shows result of using $K = 0.4$, $n = 2$ and a between 0 and 1 in Equation 7. In our simulations model parameters are chosen such that material is close to its maximum anisotropy when stress anisotropy is about 0.5.

We implemented a delay in the update of longitudinal and transverse Young moduli (Fiber model) as well as anisotropy direction of individual cells (stress feedback) to take into account different time scales of propaga-

tion of mechanical and biochemical interactions. Such approach also results in more stable simulations. The Euler steps for updating longitudinal and transverse Young modulus are

$$\Delta Y = K^{Y}_{rate} \Delta t (Y_{new} - Y_{old}). \tag{8}$$

where K^{Y}_{rate} determines the time delay, Δt is the time step, Y_{old} is the current value and Y_{new} is the new values calculated from Equation 7. Similarly the update for anisotropy direction is done based on

$$\vec{\Delta a} = K^{a}_{rate} \Delta t (\vec{S} - \vec{a}) \tag{9}$$

where $\vec{a}$ is the current anisotropy direction vector and $\vec{S}$ is the maximal stress direction vector, and K^{a}_{rate} again sets the time delay.

I.5.4 *Mechanical simulations*

The mechanical simulations have been performed with in house developed software optimized for simulations of cellular structures. Both methods used in our simulations (TRBS and shells) are based on the FEM approach, which relies on the division of the domain of interest into simpler geometrical elements (meshing) and looking for the solution of the continuous mechanics equations in the basis of the functions which are local to each element. In case of FEM simulations we have used quadrilateral shell elements within extensible director formulation [28] (Figure 1A). The implementation of TRBS was based on the explicit procedure used previously in simulation of biological materials [30] (Figure 1B). We triangulated the polygonal cells via adding a vertex at the centroid position. Since we used a single fiber direction in cells, we averaged stress or strain input from the individual triangles. In our simulations both explicit Newark and implicit solvers with Newton- Rapson iteration were used for the shells finite element implementation while explicit forth order and adaptive fifth order Runge–Kutta methods were used for TRBS. The material parameters used in the simulations of plant-like structures (Figures 3 and 4) were matched to the experimental estimates from similar materials [34–36]. We have used Young modulus in range 40 MPa - 50 MPa and 100 MPa - 120 MPa for isotropic and anisotropic part of the material, respectively. Poisson ratio was set to 0.2 and turgor pressure 0.2 MPa. We assumed the thickness of epidermal material of 1 μm and a cell size of order 10 μm to 20 μm. In

the fiber model we have used $K = 0.4 - 0.5$ and $n = 2$. For updating anisotropy directions and material properties using the equations 8 and 9 we used $K^a_{rate} \approx 0.1$ for anisotropy direction update and $K^Y_{rate} \approx 0.01$ for material properties update. As long as small values for update rates were used the results were not sensitive to the exact value of those parameters. We have used smaller update rates for material properties update, assuming the change in material properties is a consequence of microtubular dynamics and should be delayed respect to the anisotropy direction update. These parameters resulted in the deformation of order 5% to 10% in agreement with experimentally reported estimates [32]. We have used fixed (clamped) boundary conditions for our simulations of pressurized templates, which means that there was no deformation on the open boundary edges of the simulated structures. Since such conditions are not exact for real plant organs and can affect the results of simulations close to the boundary we excluded those regions from the analysis. The effects of the boundary conditions can be seen in Movie S2.

AVAILABILITY

The simulation tools are in house implementations and are publicly available upon request.

Operating system(s): Platform independent;
Programming language: C++;
Licence: no licence needed.

AUTHOR CONTRIBUTIONS

Conceived and designed the experiments: BB PK HJ. Performed the experiments: BB PK. Analyzed the data: BB PK HJ. Wrote the paper: BB PK HJ.

ACKNOWLEDGMENTS

This work was supported by grants from the Swedish Research Council, the Crafoord Foundation, and the Gatsby Charitable Foundation.

REFERENCES

1. B. D. Hoffman, C. Grashoff, and M. A. Schwartz, "Dynamic molecular processes mediate cellular mechanotransduction.," *Nature*, vol. 475, pp. 316–23, jul 2011.
2. K. Sherrard, F. Robin, P. Lemaire, and E. Munro, "Sequential activation of apical and basolateral contractility drives ascidian endoderm invagination," *Curr Biol*, vol. 20, pp. 1499–510, 2010.
3. O. Hamant, M. G. Heisler, H. Jönsson, P. Krupinski, M. Uyttewaal, P. Bokov, F. Corson, P. Sahlin, A. Boudaoud, E. M. Meyerowitz, Y. Couder, and J. Traas, "Developmental patterning by mechanical signals in arabidopsis," *Science*, vol. 322, pp. 1650–1655, Dec 2008.
4. J. Read and A. Stokes, "Plant biomechanics in an ecological context.," *American journal of botany*, vol. 93, pp. 1546–65, oct 2006.
5. D. J. Cosgrove and M. C. Jarvis, "Comparative structure and biomechanics of plant primary and secondary cell walls.," *Frontiers in plant science*, vol. 3, p. 204, jan 2012.
6. C. Somerville, S. Bauer, G. Brininstool, M. Facette, T. Hamann, J. Milne, E. Osborne, A. Paredez, S. Persson, T. Raab, S. Vorwerk, and H. Youngs, "Toward a systems approach to understanding plant cell walls.," *Science*, vol. 306, pp. 2206–11, dec 2004.
7. V. Mirabet, P. Das, A. Boudaoud, and O. Hamant, "The role of mechanical forces in plant morphogenesis," *Annual review of plant biology*, vol. 62, pp. 365–85, Jun 2011.
8. U. Kutschera and K. J. Niklas, "The epidermal-growth-control theory of stem elongation: an old and a new perspective.," *Journal of plant physiology*, vol. 164, pp. 1395–409, nov 2007.
9. S. Savaldi-Goldstein, C. Peto, and J. Chory, "The epidermis both drives and restricts plant shoot growth," *Nature*, vol. 446, no. 7132, pp. 199–202, 2007.
10. D. Reinhardt, "Auxin Regulates the Initiation and Radial Position of Plant Lateral Organs," *Plant Cell*, vol. 12, pp. 507–518, apr 2000.
11. A. Peaucelle, S. A. Braybrook, L. Le Guillou, E. Bron, C. Kuhlemeier, and H. Höfte, "Pectin-induced changes in cell wall mechanics underlie organ initiation in Arabidopsis.," *Current biology : CB*, vol. 21, pp. 1720–6, oct 2011.
12. A. J. Fleming, S. McQueen-Mason, T. Mandel, and C. Kuhlemeier, "Induction of Leaf Primordia by the Cell Wall Protein Expansin," *Science*, vol. 276, pp. 1415–1418, may 1997.
13. T. I. Baskin, "On the alignment of cellulose microfibrils by cortical microtubules: A review and a model," *Protoplasma*, vol. 215, pp. 150–171,

mar 2001.
14. E. T. Gertel and P. B. Green, "Cell growth pattern and wall microfibrillar arrangement: experiments with nitella.," *Plant physiology*, vol. 60, pp. 247–54, aug 1977.
15. A. R. Paredez, C. R. Somerville, and D. W. Ehrhardt, "Visualization of cellulose synthase demonstrates functional association with microtubules.," *Science*, vol. 312, pp. 1491–5, jun 2006.
16. T. I. Baskin, "Anisotropic expansion of the plant cell wall," *Annu Rev Cell Dev Biol*, vol. 21, pp. 203–22, Jan 2005.
17. P. Schopfer, "Biomechanics of plant growth.," *American journal of botany*, vol. 93, pp. 1415–25, oct 2006.
18. R. Dyson, L. Band, and O. Jensen, "A model of crosslink kinetics in the expanding plant cell wall: Yield stress and enzyme action," *Journal of Theoretical Biology*, vol. 307, no. 0, pp. 125 – 136, 2012.
19. E. Coen, A.-G. Rolland-Lagan, M. Matthews, J. A. Bangham, and P. Prusinkiewicz, "The genetics of geometry," *Proc Natl Acad Sci USA*, vol. 101, pp. 4728–4735, Apr 2004.
20. R. Kennaway, E. Coen, A. Green, and A. Bangham, "Generation of diverse biological forms through combinatorial interactions between tissue polarity and growth," *PLoS computational biology*, vol. 7, no. 6, p. e1002071, 2011.
21. N. Nakayama, R. S. Smith, T. Mandel, S. Robinson, S. Kimura, A. Boudaoud, and C. Kuhlemeier, "Mechanical regulation of auxin-mediated growth.," *Current biology : CB*, vol. 22, pp. 1468–76, aug 2012.
22. P. B. Green, "Expression of pattern in plants: combining molecular and calculus-based biophysical paradigms.," *American Journal of Botany*, vol. 86, no. 8, pp. 1059–1076, 1999.
23. S. P. Fischer K, "Interaction of auxin, light, and mechanical stress in orienting microtubules in relation to tropic curvature in the epidermis of maize coleoptiles," *Protoplasma*, vol. 196, no. 1-2, pp. 108–116, 1997.
24. N. Holdaway, R. White, and R. Overall, "Is the recovery of microtubule orientation in pea roots dependent on the cell wall?," *Cell Biology International*, vol. 19, no. 11, pp. 913 – 920, 1995.
25. E. Castle, "Membrane tension and orientation of structure in the plant cell wall," *Journal of Cellular and Comparative Physiology*, vol. 10, pp. 113—121, 1937.
26. M. Uyttewaal, A. Burian, K. Alim, B. Landrein, D. Borowska-Wykręt, A. Dedieu, A. Peaucelle, M. Ludynia, J. Traas, A. Boudaoud, D. Kwiatkowska, and O. Hamant, "Mechanical stress acts via katanin to amplify differences in growth rate between adjacent cells in Arabidopsis.," *Cell*, vol. 149, pp. 439–51, apr 2012.

27. S. De, F. Guilak, and M. Mofrad, *Computational Modeling in Biomechanics*. Springer, 2010.
28. J. Simo, "On a stress resultant geometrically exact shell model. Part I: Formulation and optimal parametrization," *Computer Methods in Applied Mechanics and Engineering*, vol. 72, pp. 267–304, mar 1989.
29. O. C. Zienkiewicz, R. L. Taylor, and J. Zhu, *The Finite Element Method: Its Basis and Fundamentals, Sixth Edition*. Butterworth-Heinemann, 2005.
30. H. Delingette, "Triangular springs for modeling nonlinear membranes," *IEEE Transactions on Visualization and Computer Graphics*, vol. 14, pp. 329–341, mar 2008.
31. P. G. Ciarlet, *Mathematical Elasticity: Volume I: Three-Dimensional Elasticity*. Elsevier, 1993.
32. D. Kierzkowski, N. Nakayama, A.-L. Routier-Kierzkowska, A. Weber, E. Bayer, M. Schorderet, D. Reinhardt, C. Kuhlemeier, and R. S. Smith, "Elastic Domains Regulate Growth and Organogenesis in the Plant Shoot Apical Meristem," *Science*, vol. 335, pp. 1096–1099, mar 2012.
33. B. J. Mac Donald, *Practical Stress Analysis With Finite Elements*. Glasnevin Publishing, 2007.
34. P. Ryden, K. Sugimoto-Shirasu, A. C. Smith, K. Findlay, W.-D. Reiter, and M. C. McCann, "Tensile properties of Arabidopsis cell walls depend on both a xyloglucan cross-linked microfibrillar network and rhamnogalacturonan II-borate complexes.," *Plant physiology*, vol. 132, pp. 1033–40, jun 2003.
35. E. Chanliaud, K. M. Burrows, G. Jeronimidis, and M. J. Gidley, "Mechanical properties of primary plant cell wall analogues.," *Planta*, vol. 215, pp. 989–96, oct 2002.
36. I. Burgert, "Exploring the micromechanical design of plant cell walls.," *American journal of botany*, vol. 93, pp. 1391–401, oct 2006.
37. M. Fujita, R. Himmelspach, C. H. Hocart, R. E. Williamson, S. D. Mansfield, and G. O. Wasteneys, "Cortical microtubules optimize cell-wall crystallinity to drive unidirectional growth in Arabidopsis.," *The Plant journal : for cell and molecular biology*, vol. 66, pp. 915–28, jun 2011.
38. E. F. Crowell, H. Timpano, T. Desprez, T. Franssen-Verheijen, A.-M. Emons, H. Höfte, and S. Vernhettes, "Differential regulation of cellulose orientation at the inner and outer face of epidermal cells in the Arabidopsis hypocotyl.," *The Plant cell*, vol. 23, pp. 2592–605, jul 2011.
39. J. Chan, E. Crowell, M. Eder, G. Calder, S. Bunnewell, K. Findlay, S. Vernhettes, H. Höfte, and C. Lloyd, "The rotation of cellulose synthase trajectories is microtubule dependent and influences the texture of epidermal cell walls in Arabidopsis hypocotyls.," *Journal of cell science*, vol. 123, pp. 3490–5, oct 2010.

40. M. G. Heisler, O. Hamant, P. Krupinski, M. Uyttewaal, C. Ohno, H. Jönsson, J. Traas, and E. M. Meyerowitz, "Alignment between pin1 polarity and microtubule orientation in the shoot apical meristem reveals a tight coupling between morphogenesis and auxin transport," *PLoS Biol*, vol. 8, p. e1000516, Jan 2010.
41. G. V. Reddy, M. G. Heisler, D. W. Ehrhardt, and E. M. Meyerowitz, "Real-time lineage analysis reveals oriented cell divisions associated with morphogenesis at the shoot apex of Arabidopsis thaliana.," *Development (Cambridge, England)*, vol. 131, pp. 4225–37, sep 2004.
42. D. Kwiatkowska, "Surface growth at the reproductive shoot apex of arabidopsis thaliana pin-formed 1 and wild type.," *Journal of experimental botany*, vol. 55, pp. 1021–32, may 2004.
43. P. Laufs, O. Grandjean, C. Jonak, K. Kiêu, and J. Traas, "Cellular parameters of the shoot apical meristem in Arabidopsis.," *The Plant cell*, vol. 10, pp. 1375–90, aug 1998.
44. F. Corson, O. Hamant, S. Bohn, J. Traas, A. Boudaoud, and Y. Couder, "Turning a plant tissue into a living cell froth through isotropic growth," *Proc Natl Acad Sci USA*, vol. 106, pp. 8453–8458, May 2009.
45. P. Milani, M. Gholamirad, J. Traas, A. Arnéodo, A. Boudaoud, F. Argoul, and O. Hamant, "In vivo analysis of local wall stiffness at the shoot apical meristem in arabidopsis using atomic force microscopy," *The Plant journal : for cell and molecular biology*, vol. 33, May 2011.
46. R. Sablowski, "Plant stem cell niches: from signalling to execution.," *Current opinion in plant biology*, vol. 14, pp. 4–9, feb 2011.
47. R. K. Yadav, M. Perales, J. Gruel, C. Ohno, M. Heisler, T. Girke, H. Jönsson, and G. V. Reddy, "Plant stem cell maintenance involves direct transcriptional repression of differentiation program," *Molecular Systems Biology*, vol. 9, p. 654, apr 2013.
48. D. J. Cosgrove, "Growth of the plant cell wall.," *Nature reviews. Molecular cell biology*, vol. 6, pp. 850–61, nov 2005.
49. G. Picinbono, J.-C. Lombardo, H. Delingette, and N. Ayache, "Anisotropic elasticity and force extrapolation to improve realism of surgery simulation," *Proceedings 2000 ICRA. Millennium Conference. IEEE International Conference on Robotics and Automation. Symposia Proceedings (Cat. No.00CH37065)*, pp. 596–602, 2001.
50. G. T. Mase, R. E. Smelser, and G. E. Mase, *Continuum Mechanics For Engineers*. CRC Press, 2010.
51. J. Bonet and R. D. Wood, *Nonlinear continuum mechanics for finite element analysis*. Cambridge University Press, 1997.

I.6 SUPPLEMENT FIGURES

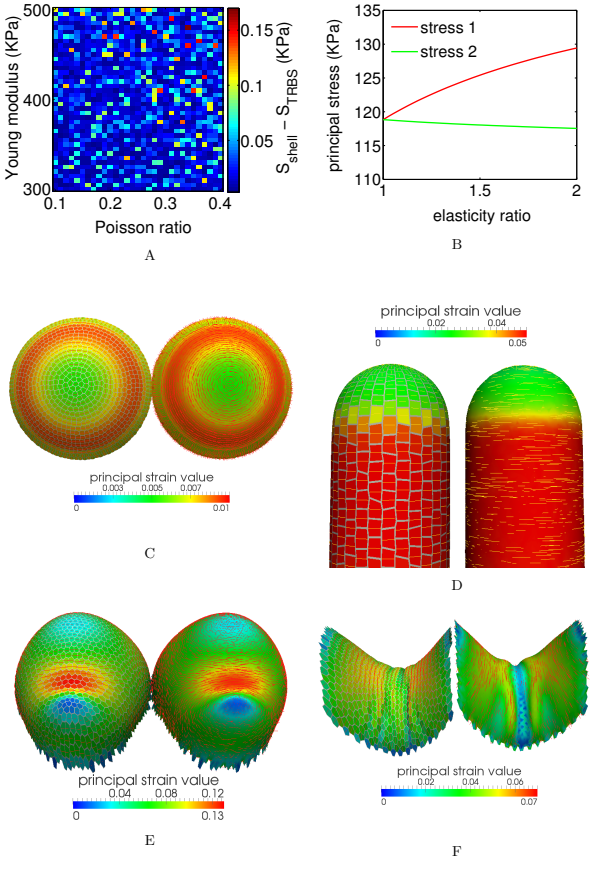

Figure S1: **Comparing triangular biquadratic springs and finite element shell models.** (A) The difference between principal stress value of triangular biquadratic springs model and integrated principal stress over thickness in finite element shell model is subtle (less than 0.1 %) 'Shell' elements for the case of isotropically loaded patch (compare with Fig. 2C, model parameters are the same in two models). (B) The first and second principal stress values for our anisotropic material model become more different as material becomes more anisotropic.The patch was isotropically loaded constantly with 2 KN when material anisotropy was varied by keeping the transverse Young modulus constant ($Y_T = 400kPa$) and changing the fiber Young modulus ($400 < Y_L < 800kPa$) for Poisson ratio(P=0.3). Elasticity ratio is the ratio between longitudinal and transverse Young moduli. (C-E) Comparison between principal stress direction and principal strain value in two models(left: TRBS, right: shell) for different pressurized templates show a major similarity indicating the lack of bending energy in TRBS model is not important when deformation is caused by internal pressure. (C) Isotropic material with Young modulus = 0 MPa, Poisson ratio = 0.2 ,Pressure = 0.01 MPa (D) Isotropic material with Young modulus = 90 MPa, Poisson ratio = 0.2, Pressure = 0.1 MPa (E) Isotropic material with Young modulus = 80 MPa, Poisson ratio = 0.2 ,Pressure = 0.05 MPa(F)for a saddle-like template where the compressive forces become important resulting in buckling, the difference in deformation in two models is obvious.Isotropic material with Young modulus = 40 MPa, Poisson ratio = 0.2 ,Pressure = 0.01 MPa

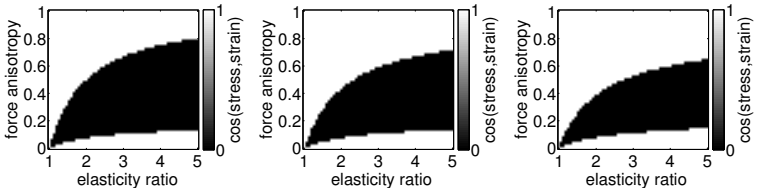

Figure S2: **Poisson ratio analysis** Similar plot as Figure 3A for different values for Poisson ratio (A) $\nu = 0$,(B) $\nu = 0.2$, (C) $\nu = 0.4$. In the force/material anisotropy space the region where principal directions of stress and strain are perpendicular is larger for lower values of Poisson ratio

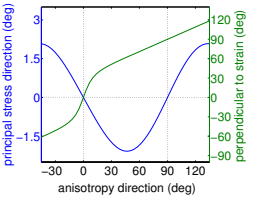

Figure S3: **Fixed points of dynamical stress/strain based feedback updates of anisotropy direction.** For the quadrilateral patch of anisotropic material with constant transverse and longitudinal Young modulus as $Y_T = 400kPa$ and $Y_L = 1200kPa$ respectively and Poisson coefficient = 0.2 under anisotropic loading $F_x = 8kN$ and $F_y = 4kN$ the direction of principal stress and perpendicular to the direction of principal strain are plotted versus the angle of varying anisotropy direction. 0 value for the angles is corresponding with maximal force direction. There is a fixed point at zero for both feedback systems which is stable for stress feedback whereas extremely unstable for the perpendicular to maximal strain feedback.

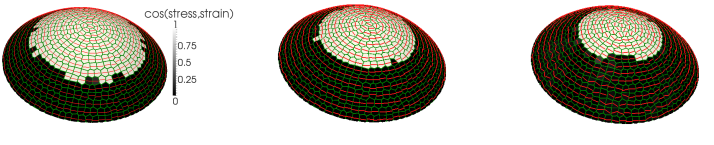

Figure S4: **Different zonation resulting from fiber model with different values for the K parameter.** (A) $K = 0.5$, (B) $K = 0.45$, (C) $K = 0.4$.

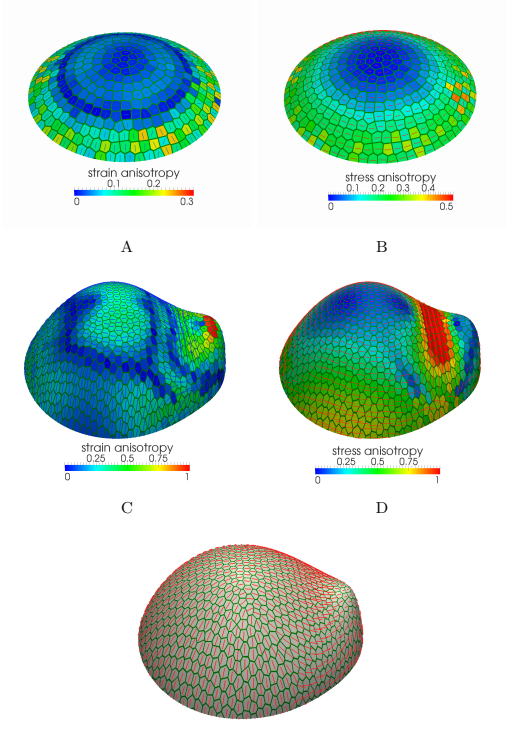

Figure S5: **Additional meristem-like template simulations.** (A-D) Additional information about Figure 4. (E) Anisotropy direction pattern for the same simulation as Figure 4D-F, using perpendicular to strain feedback model and the fiber model with strain anisotropy measure. All of the model parameters are the same except strain constant in Equation 6, $S_{max} = 0.08$

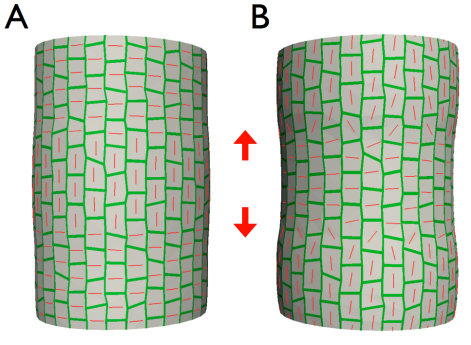

Figure S6: **Effect of axial loading.** Adding regional axial tensile stress (red arrows) to the Tissue Pressure model in different feedback scenarios. Axial stress is applied so that in the region between red arrows maximal stress is axial with stress anisotropy about 0.6-0.7. In other regions maximal stress is circumferential with stress anisotropy about 0.5. (A) Stress feedback. (B) Perpendicular to strain feedback. Material properties and pressure are the same as Figure 3.

I.7 SUPPORTING INFORMATION

I.7.1 *Details of Triangular Biquadratic Springs implementation*

Strain energy formalism

The TRBS model, as most continuous mechanics methods, is based on the minimization of strain energy. In the case of St. Venant-Kirchoff description [30] this energy takes the form

$$W_{TRBS} = \int_{\Omega} w_{TRBS} d\Omega = \int_{\Omega} (\frac{\lambda}{2}(trE)^2 + \mu trE^2) d\Omega, \tag{1}$$

where E is a Green-Lagrange strain tensor and Lame parameters λ and μ are related to Young's modulus Y and Poisson's ratio ν. In case of TRBS, which are two dimensional elements, we assume plane stress condition and relation between those material parameters becomes [50]

$$\lambda = \frac{Y\nu}{1-\nu^2}, \quad \mu = \frac{Y}{2(1+\nu)}. \tag{2}$$

The Green-Lagrange strain tensor can be expressed in terms of Cauchy-Green deformation tensor as

$$E = \frac{1}{2}(C - I). \tag{3}$$

The Cauchy-Green deformation tensor is a function of deformation gradient tensor F

$$C = F^T F. \tag{4}$$

The deformation gradient tensor F is the gradient of the deformation function Φ

$$F = \nabla \Phi \tag{5}$$

It is possible to express Φ in terms of the position vectors of the nodes in resting and deformed states of a triangular element. In this case the expression for F becomes [30]

$$F = Q_i \otimes D_i, \tag{6}$$

where Q_i is the position vector of i'th node in the deformed shape and D_i is the shape vector corresponding with the node P_i in the resting shape (Figure 1B)

$$D_i = \frac{1}{A_P}(P_j - P_k)^{\perp} \quad \epsilon_{ijk} = 1, \tag{7}$$

where A_P is the resting area of the element, ϵ_{ijk} is the permutation symbol and $X^{\perp}$ is orthogonal to the vector X. Using these expressions, the Cauchy-Green deformation tensor becomes

$$C = (D_i \otimes D_j)_{mn}(Q_i.Q_j). \tag{8}$$

In the above equations and through out the text the repeated indices are summed over from 1 to 3, unless stated otherwise (we assume Einstein's summing convention).

The strain energy density is usually expressed in terms of invariants of the strain tensor $I_1 = trE$ and $I_2 = trE^2$

$$w_{TRBS} = \frac{\lambda}{2}I_1^2 + \mu I_2, \tag{9}$$

or equivalently by Cauchy-Green tensor invariants $I_1' = trC$ and $I_2' = trC^2$

$$I_1 = \frac{1}{2}I_1' - 1, \tag{10}$$

$$I_2 = \frac{1}{4}I_2' - \frac{1}{2}I_1' + \frac{1}{2}. \tag{11}$$

These invariants can be calculated in terms of the angles of resting shape α_i, edges of resting and deformed shapes l_i, L_i and areas of resting and deformed shapes A_P, A_Q and the strain energy becomes [30]

$$w_{TRBS}(T_p) = \frac{k_i^{T_P}}{4}(\Delta^2 l_i)^2 + \Sigma_{i\neq j}\frac{c_k^{T_P}}{2}\Delta^2 l_i \Delta^2 l_j, \tag{12}$$

where k and c are tensile and angular stiffness of TRBS:

$$k_i^{T_P} = \frac{2(\lambda + 2\mu)cot^2\alpha_i + 2\mu}{16A_P} = \frac{E(2cot^2\alpha_i + 1 - \nu)}{16(1-\nu^2)A_P}, \tag{13}$$

$$c_k^{T_P} = \frac{2(\lambda + 2\mu)cot\alpha_i cot\alpha_j - 2\mu}{16A_P} = \frac{E(2cot\alpha_i cot\alpha_j - 1 + \nu)}{16(1-\nu^2)A_P}. \tag{14}$$

By taking derivative of W respect to Q_i we can derive an expression for force that is applied on the node i:

$$\begin{aligned} F_i^{TRBS}(T_P) &= -\left(\frac{\partial W(T_P)}{\partial Q_i}\right)^T \\ &= \Sigma_{j\neq i} k_k^{T_P} \Delta^2 l_k (Q_j - Q_i) + \Sigma_{j\neq i}(c_j^{T_P}\Delta^2 l_i + c_i^{T_P}\Delta^2 l_j)(Q_j - Q_i). \end{aligned} \tag{15}$$

This expression provides the force on each node entirely in terms of node positions of triangular element in resting and deformed configurations.

Anisotropic TRBS by equipartition the energy expression

For the isotropic material we wrote strain energy density as:

$$\begin{aligned} w_{iso} &= w_x + w_y + w_z \\ &= \frac{\lambda}{2}(e_1^t E e_1) trE + \mu(e_1^t E^2 e_1) \\ &+ \frac{\lambda}{2}(e_2^t E e_2) trE + \mu(e_2^t E^2 e_2) \\ &+ \frac{\lambda}{2}(e_3^t E e_3) trE + \mu(e_3^t E^2 e_3), \end{aligned} \tag{16}$$

where the e_i, for $i = 1...3$ are versors of Cartesian coordinate system and three terms present the equal parts corresponding to each of the x, y and z directions. Analogically the energy corresponding with arbitrary direction represented by the vector a we expressed as

$$w_a = \frac{\lambda}{2}(\vec{a}^T E \vec{a}) trE + \mu(\vec{a}^T E^2 \vec{a}). \tag{17}$$

Now if we consider transversely isotropic material, which has different mechanical properties in a single direction we can define

$$\Delta\lambda = \lambda^L - \lambda^T \tag{18}$$

and

$$\Delta\mu = \mu^L - \mu^T, \tag{19}$$

where λ^L, μ^L are *Longitudinal* Lame constants in a given direction $\vec{a}$ and λ^T, μ^T are *Transverse* Lame constants in plane transverse to $\vec{a}$. These can be related to the longitudinal Y_L and transverse Y_T Young modulus by the use of the equation 2. With these definitions we introduced the term which has to be added to isotropic strain energy to account for anisotropic material having different mechanical properties in the given direction $\vec{a}$ as

$$\Delta w_a = \frac{\Delta\lambda}{2} I_1 I_4 + \Delta\mu I_5, \tag{20}$$

where $I_1 = trE$, $I_4 = \vec{a}^T E \vec{a}$ and $I_5 = \vec{a}^T E^2 \vec{a}$ are invariants of strain tensor constructed with vector $\vec{a}$. These invariants are easily expressed in terms of analogical invariants of Cauchy deformation tensor C, $I_1' = trC$, $I_4' = \vec{a}^T C \vec{a}$ and $I_5' = \vec{a}^T C^2 \vec{a}$

$$I_1 = \frac{1}{2}(trC - trI) = \frac{1}{2} I_1' - 1, \tag{21}$$

$$I_2 = tr\left(\frac{1}{4}(C^2 - 2C + I)\right) = \frac{1}{4} I_2' - \frac{1}{2} I_1' + \frac{1}{2}, \tag{22}$$

$$I_4 = \frac{1}{2}\vec{a}^T (C - I)\vec{a} = \frac{1}{2} I_4' - \frac{1}{2}, \tag{23}$$

$$I_5 = \frac{1}{4}\vec{a}^T (C^2 - 2C + I)\vec{a} = \frac{1}{4} I_5' - \frac{1}{2} I_4' + \frac{1}{2}, \tag{24}$$

which in terms of position vectors Q_i and shape vectors D_i become

$$I_1' = (Q_i.Q_j)(D_i.D_j), \tag{25}$$

$$I_2' = (Q_m.Q_n)(Q_r.Q_s)(D_n.D_r)(D_m.D_s), \tag{26}$$

$$I_4' = (Q_m.Q_n)(\vec{a}.D_m)(\vec{a}.D_n), \tag{27}$$

$$I_5' = (Q_m.Q_n)(Q_r.Q_s)(D_n.D_r)(\vec{a}.D_m)(\vec{a}.D_s), \tag{28}$$

where we continue using Einstein's summing convention.

The anisotropic correction term for the TRBS force can be derived from our definition of Δw_a (Equation 20) as

$$\Delta F_i = -A_P \frac{\partial \Delta w_a}{\partial Q_i} = -A_P \left[\frac{\Delta\lambda}{2} \left(I_4 \frac{\partial I_1}{\partial Q_i} + I_1 \frac{\partial I_4}{\partial Q_i} \right) + \Delta\mu \frac{\partial I_5}{\partial Q_i} \right]. \tag{29}$$

Strain and Stress in TRBS

The strain is a local measure of deformation. There exist different strain measures comparing the changes of relative material point positions between undeformed and deformed (current) configurations in different ways. If we describe a motion of the particle as

$$\mathbf{x} = \mathbf{\Phi}(\mathbf{X}, t), \tag{30}$$

where $\mathbf{x}$ is a position vector of particle in current configuration and $\mathbf{X}$ its position in undeformed (material) coordinates, we can define a deformation tensor

$$F_{ij} = \frac{\partial \Phi_i}{\partial X_j}. \tag{31}$$

We use two strain measures: Green-Lagrange strain $\mathbf{E}$, which operates o n undeformed (material) coordinates and Euler-Almansi strain $\mathbf{e}$ relating quantities in deformed (current) coordinates. These strains are defined by:

$$\begin{aligned} E &= \frac{1}{2}(F^T F - I) = \frac{1}{2}(C - I), \\ e &= \frac{1}{2}(I - F^{-T} F^{-1}) = \frac{1}{2}(I - b^{-1}), \end{aligned} \tag{32}$$

where we introduced right $C = F^T F$ and left $b = F F^T$ Cauchy–Green deformation tensor. The strain tensors are energy conjugates of appropriate stress measures. The second Piola–Kirchhoff stress tensor $\mathbf{S}$ is an energy conjugate of Green-Lagrange strain $\mathbf{E}$.

$$S = \frac{\partial W}{\partial E} \tag{33}$$

The Euler-Almansi strain **e** is a energy conjugate of the Cauchy stress tensor **œ** which is related to second Piola–Kirchhoff stress by

$$\sigma = \frac{1}{det(F)} FSF^T. \tag{34}$$

In case of St.Venant-Kirchhoff material (1) these become:

$$S = \lambda(trE)I + 2\mu E \tag{35}$$

and

$$\begin{aligned} \sigma &= \frac{A_P}{A_Q}[FF^T(\lambda trE) + 2\mu F\frac{1}{2}(C - I)F^T] \\ &= \frac{A_P}{A_Q}\left[(\lambda trE - \mu)b + \mu b^2\right], \end{aligned} \tag{36}$$

where we used the fact that for TRBS $det(F) = \frac{A_Q}{A_P}$, A_P and A_Q are the areas of resting and deformed triangular element respectively. Analogically the correction energy term from material anisotropy will give rise to stress correction terms

$$\begin{aligned} \Delta S &= \frac{\partial \Delta W}{\partial E}, \\ \Delta\sigma &= \frac{1}{det(F)} F\Delta SF^T. \end{aligned} \tag{37}$$

Direct calculation from anisotropic energy (20) gives

$$\begin{aligned} \Delta S &= \frac{\Delta\lambda}{2}(I_4\frac{\partial I_1}{\partial E} + I_1\frac{\partial I_4}{\partial E}) + \Delta\mu\frac{\partial I_5}{\partial E} \\ &= \frac{\Delta\lambda}{2}((a^TEa)I + (trE)(a\otimes a)) + \Delta\mu(E(a\otimes a) + (a\otimes a)E). \end{aligned} \tag{38}$$

Finally the expression for the Cauchy's stress including effects of anisotropy becomes

$$\sigma = \frac{A_P}{A_Q} F[S + \Delta S]F^T. \tag{39}$$

The forces on the nodes of each element can be calculated alternatively using the total second Piola-Kirchhoff stress

$$F_i = -A_P F(S + \Delta S)D_i. \tag{40}$$

I.7.2 *Nonlinear Finite Element Method*

The Finite Element Method is based on the weak formulation of elasticity equations - the principle of virtual work. The variation of the work due to the virtual rate of deformation tensor $\delta\mathbf{d}$ and velocities $\delta\mathbf{v}$ can be written as [51]

$$\delta W = \int_{\omega} \boldsymbol{\text{œ}} : \delta\mathbf{d}\, dv - \int_{\omega} \mathbf{f} \cdot \delta\mathbf{v}\, dv - \int_{\partial\omega} \mathbf{t} \cdot \delta\mathbf{v}\, da = 0, \tag{41}$$

where $\boldsymbol{\text{œ}}$ is Cauchy's stress tensor, $\mathbf{f}$ and $\mathbf{t}$ are body forces and tractions respectively. The standard procedure of solving this problem is linearization and iterative steps with respect to trial deformation solution φ_k eg. by use of the Newton-Raphson method. The equilibrium equations linearized in the direction of increment $\mathbf{u}$ in φ_k can be written as:

$$D\delta W(\varphi, \delta v)[\mathbf{u}] = D\delta W_{int}(\varphi, \delta v)[\mathbf{u}] - D\delta W_{ext}(\varphi, \delta v)[\mathbf{u}], \tag{42}$$

where

$$\delta W_{int}(\varphi, \delta v)[\mathbf{u}] = \int_{\omega} \boldsymbol{\text{œ}} : \delta\mathbf{d}\, dv \tag{43}$$

$$\delta W_{ext}(\varphi, \delta v)[\mathbf{u}] = \int_{\omega} \mathbf{f} \cdot \delta\mathbf{v}\, dv + \int_{\partial\omega} \mathbf{t} \cdot \delta\mathbf{v}\, da, \tag{44}$$

are describing internal and external work components. A careful derivation shows that linearization of the internal work can be expressed as:

$$D\delta W_{int}(\varphi, \delta v)[\mathbf{u}] = \int_{\omega} \delta\mathbf{d} : c : \mathbf{ffl}\, dv + \int_{\omega} \boldsymbol{\text{œ}} : [(\nabla\mathbf{u})^T \nabla\delta\mathbf{v}]\, dv. \tag{45}$$

Discretization of this equation will yield a stiffness matrix which because of apparent symmetry of above equation in $\mathbf{u}$ and $\delta\mathbf{v}$ will be symmetric too. The discretization of $\mathbf{u}$ and $\delta\mathbf{v}$ is performed with respect to the shape vectors which provide a local support basis for the problem and which specific form depends on the choice of the finite element discretization.

Shell kinematics

The shell description is essentially three-dimensional elasticity with specific kinematic and mechanical assumptions built in into the theory. Here we will in short present extensible director formulation of shell element kinematics which has been used for quadrilateral shell in the simulations

[28]. The undeformed geometry of shell is described with respect to its reference surface with the following relations:

$$\mathbf{X}(\xi_i) = \bar{\mathbf{X}}(\xi_\alpha) + \mathbf{D}(\xi_i) \tag{46}$$

$$\bar{\mathbf{X}}(\xi_\alpha) = \sum_{a=1}^{n} N_a(\xi_\alpha)\bar{\mathbf{X}}_a \tag{47}$$

$$\mathbf{D}(\xi_i) = \sum_{a=1}^{n} N_a(\xi_\alpha) z_a(\xi_3)\bar{\mathbf{D}}_a \tag{48}$$

$$z_a(\xi_3) = N_+(\xi_3)z_a^+ + N_-(\xi_3)z_a^- \tag{49}$$

$$N_+(\xi_3) = \frac{1}{2}(1+\xi_3), \quad N_-(\xi_3) = \frac{1}{2}(1-\xi_3), \tag{50}$$

where Latin and Greek indices are assumed to span from 1 to 3 and from 1 to 2 respectively. The unit vector $\mathbf{D}$ is called the director and it describes position of the body particle with respect to the point on the reference surface $\bar{\mathbf{X}}$. This point in turn is described by the two dimensional shape functions N_a and nodal points of the element $\bar{\mathbf{X}}_a$. The function z_a describes the thickness of the element in terms of the distance from the reference surface to the bottom and top surfaces. The similar interpolation is used to describe the current configuration of the shell element and in consequence the displacement vectors. The director vector in deformed configuration is no longer required to be of unit length which takes into account thickness changes.

II

MORPHOGENESIS CAN BE GUIDED BY THE DYNAMIC GENERATION OF ANISOTROPIC WALL MATERIAL OPTIMIZING STRAIN ENERGY

Behruz Bozorg [1], Pawel Krupinski [1] and Henrik Jönsson [1,2,3].

[1] Computational Biology & Biological Physics, Lund University, Sölvegatan 14A, SE 223 62 Lund, Sweden.
[2] Sainsbury Laboratory, Cambridge University, Bateman Street, CB2 1LF Cambridge, United Kingdom.
[3] Department of Applied Mathematics and Theoretical Physics (DAMTP), University of Cambridge, Cambridge, United Kingdom.

LU TP16-12 (submitted)

A mechanistic understanding of the regulation of morphogenesis is a main challenge in life science. In plants, physical forces generated by high intracellular pressure and anisotropic mechanical properties of cell walls contribute to the growth and generation of shape of the tissue. Plants transform isotropic pressure-driven forces into anisotropic shapes by strengthening the walls in directions specified by controlled synthesis of cellulose fibers. Recently, mechanical stresses have been suggested as an important input signal for regulating growth directions and morphogenesis. We show that it is energetically optimal to lay down the fibers in the direction of maximal loading forces, and that there is a well defined strain energy minimum with respect to the degree of anisotropy of the wall material given internal and external forces acting on the cell wall. Finally we show that the fiber anisotropy patterns predicted by minimizing the strain energy match fiber patterns appearing in the epidermis of various plant organs and we estimate the strain energy gain versus alternative wall compositions of similar strength.

II.1 INTRODUCTION

Plants come in highly diverse forms, often with characteristic anisotropically shaped organs arranged in symmetric patterns [1]. Since plant cells are tightly joined by their walls and cell migration is not present these shapes are acquired by inhomogeneous growth and deformation [2, 3]. Cellular growth is driven by high internal turgor pressure, and growth rate and direction are guided by heterogeneous and anisotropic composition of the cell walls [3]. The primary cell wall consists of a composite material built from cellulose fibers connected via hemicellulose linkages and embedded in a pectin matrix [4]. The regulation of mechanical properties of the cell wall via its components is complex and combines genetic, hormonal and environmental inputs [5]. The importance of mechanics for pattern formation in plant development has been highlighted in seminal work by Paul Green [6] and others [7–9]. Moreover physical forces can feed back as spatial cues for gene regulation and spatial regulation of molecules within cells [10–12]. Several models have explored these possibilities and combined molecular and mechanical regulation of pattern formation in plants [10, 13].

Cell walls can have highly anisotropic mechanical stiffness properties, mainly guided via the synthesis of cellulose fibers in specific directions [2, 3]. The fiber synthesis is directed by cortical microtubules (MTs) forming supra- and sub-cellular patterns [14, 15]. The idea that the cellulose fibers align along maximal stress directions has recently been explored in detail in epidermal tissue [7, 14–17]. The epidermis is a key in regulating tissue growth [18, 19]. Generally its walls are thicker than in internal tissue and internal growth and pressure lead to tensional forces along the epidermal surface. In such scenario cell and tissue surface curvatures prescribe the stress directions, which have been shown to correlate with MT and cellulose fiber directions (Fig. II.1) [14, 15]. A dynamic feedback from stress directions to cell wall material anisotropy directions has been shown to be sufficient to robustly guide anisotropic growth in several plant tissues[17]. In contrast to the situation in animal cells [20, 21], in plants the molecular details for sensing strains and stresses remain unclear [22], even though genetic perturbations have been shown to diminish the response to mechanical perturbations [15, 23].

In this Letter we report that an alignment of cellulose fibers along maximal principal stress directions is minimizing the mechanical strain energy under the constraint of constant total material stiffness and with a constant force distribution acting on the cell wall. In addition, we find that the degree of material anisotropy also has a distinct energy minimum, i.e. for specific anisotropic force load on a wall there exist an optimal anisotropic

distribution of fibers. We also confirm that such an energy minimizing principle can predict fiber orientations reported in the epidermis of different plant structures.

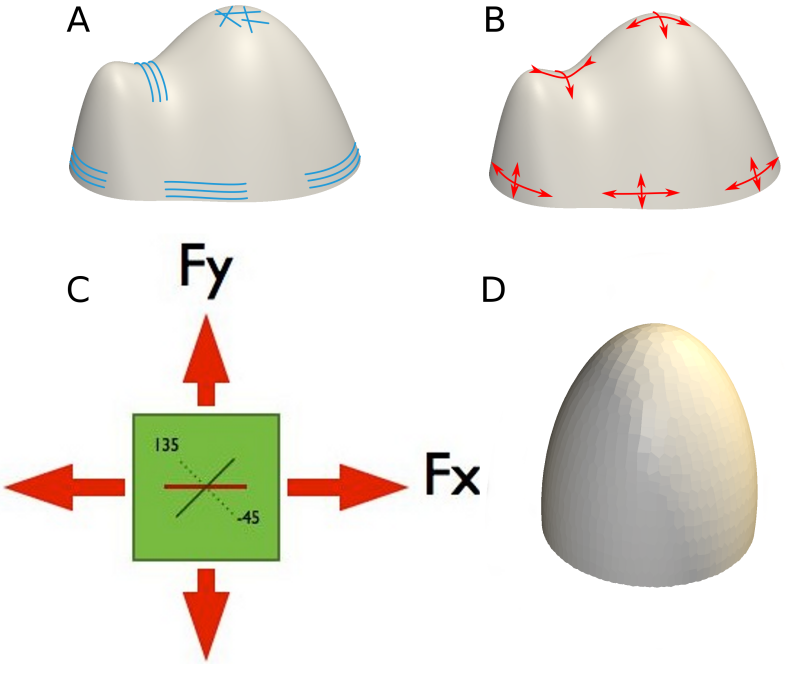

Figure II.1: A) The distribution of expected stresses (red arrows) and observed microtubular directions (blue lines) on the shape resembling the plant meristem with emerging primordium. Observe the alignment of microtubules and first principal direction of stress. B)The set up for a patch test. A square patch of elements under varying load. Forces are applied in x-y plane varying from anisotropic (uni-axial) to isotropic ($F_x = F_y$). Red line shows maximal stress direction which is constant due to constant maximal force direction. Green line depicts anisotropy direction which is varied in $[-45°, 135°]$. C) The template with similar geometrical properties to SAM.

II.2 RESULTS

II.2.1 *A dynamic alignment of fibers in the direction of maximal loading forces minimizes mechanical strain energy*

To simulate different force load distributions appearing in the plant epidermal wall tissue (cf. Fig. II.1 A) we use a simplified square patch description in which the the response of the different materials to varying bi-axial loads can be analyzed (Fig. II.1 C). We employ a linear (Hook's law) model, where the strain energy, W, is given in terms of stress, σ, and strain, ϵ, by $W = \frac{1}{2}\sigma_{ij}\epsilon_{ij}$. Since the thickness of plant walls is small compared to the extension in other dimensions we adopt a plane stress approximation. Strongly aligned cellulose fibers in the walls can result in a large amount of mechanical anisotropy, and hence we consider here a two dimensional ortotropic material for which the constitutive equation in the compliance form and Voigt notation can be written as [24]

$$\begin{pmatrix} \epsilon_1 \\ \epsilon_2 \\ \epsilon_3 \end{pmatrix} = \begin{pmatrix} \frac{1}{E_m} & -\frac{\nu}{E} & 0 \\ -\frac{\nu'}{E_m} & \frac{1}{E} & 0 \\ 0 & 0 & \frac{1}{2G} \end{pmatrix} \begin{pmatrix} \sigma_1 \\ \sigma_2 \\ \sigma_3 \end{pmatrix}, \tag{1}$$

where E, E_m and ν, ν' are Young moduli and Poisson ratios in two orthogonal directions (here we assume $E_m > E$). The required symmetry of the compliance matrix restricts these parameters to satisfy the relation $E_m/\nu' = E/\nu$ and the expression for strain energy can be defined in terms of material parameters and components of the stress tensor

$$W = \frac{1}{2}\left(\frac{\sigma_1^2}{E_m} + \frac{\sigma_2^2}{E} - \frac{2V\sigma_1\sigma_2}{\sqrt{EE_m}} + \frac{\sigma_3^2}{G}\right). \tag{2}$$

In Eq. 2 we introduced $V = \sqrt{\nu\nu'}$ which is the geometric average of ν and ν' and is assumed constant in our analysis (a thermodynamic constraint on ν and ν' implies $\nu\nu' < 1$ [24]). G is the shear modulus. We are interested in studying variations of the strain energy with respect to change of material properties including elasticity parameters and principal directions of the material anisotropy. We consider time scales where turgor and tissue pressure acting on the cell wall are not changing significantly, and hence assume a constant stress field contribution to the strain energy. Firstly we aim to analyze the impact of changing the angle, θ, between the largest

principal stress direction and material anisotropy direction. In terms of this angle and eigenvalues of the stress field, $\Sigma + 2\delta$ and Σ, the strain energy can be rewritten as

$$W(\theta) = \frac{1}{2}[\frac{(\Sigma + \delta + \delta\cos 2\theta)^2}{E_m} + \frac{(\Sigma + \delta - \delta\cos 2\theta)^2}{E} \\ -\frac{2V}{\sqrt{EE_m}}(\Sigma + \delta + \delta\cos 2\theta)(\Sigma + \delta - \delta\cos 2\theta) + \frac{\delta^2 \sin^2 2\theta}{G}] \tag{3}$$

Now we can take derivative of energy with respect to θ. This derivative is a quantity analogical to a "force", which can help us understanding the behavior of the material where the angle θ is a degree of freedom. The derivative is given by

$$\frac{\partial W}{\partial \theta} = \frac{2\delta^2}{E}[(1 - \frac{E}{E_m})(\frac{\Sigma}{\delta} + 1) - (1 - \sqrt{\frac{E}{E_m}})^2 \cos 2\theta] \sin 2\theta. \tag{4}$$

where we substituted G by $\frac{\sqrt{EE_m}}{2(1+\sqrt{\nu\nu'})}$. This expression is based on the analogy with isotropic material, where the shear modulus G is restricted to be $\frac{E}{2(1+\nu)}$ due to invariance of the stiffness tensor with respect to an arbitrary rotation. For the anisotropic case we assume that G is bounded between $G_{min} = \frac{E}{2(1+\nu)}$ and $G_{max} = \frac{E_m}{2(1+\nu')}$ and we replace it with the geometric average of G_{min} and G_{max}. This expression clearly shows the existence of a minimum of the energy when the applied stress and material anisotropy principal directions are aligned, $\theta = 0$ (Fig. II.2A). A maximum appears for $\theta = 90\,\text{deg}$ and the energy difference between the minimum and maximum increases with increased stress anisotropy as measured by the stress anisotropy coefficient, $\alpha = 1 - \Sigma/(\Sigma + 2\delta)$, defined in range from zero for an isotropic load to one for an infinitely anisotropic load. Hence if a plant follows an energy minimizing principle when dynamically adjusting the synthesis or reorganisation of cellulose fibers, it is predicted that walls with isotropic tension should have unstable fiber orientation while walls with highly anisotropic tension should robustly generate a specific fiber orientation along the maximal stress direction. This behavior is also confirmed in simulations which use Saint Venant-Kirchhoff nonlinear strain energy and thus extend beyond linear materials (Fig. II.2B).

II.2.2 *There is an optimal degree of mechanical anisotropy in terms of mechanical strain energy*

Given that a plant can adjust not only the direction of cellulose fibers but also the amount of these load bearing structures, we aim to understand also how the degree of anisotropy influences the minimum of the strain energy. Thus we introduce a material anisotropy coefficient, $\kappa = 1 - E/E_m$, similar to the previously defined stress anisotropy coefficient (α), ranging from zero for an isotropic material to one for a material with highly anisotropic material properties. The strain and hence the strain energy obviously decreases with decrease of loading forces or with increase of total material stiffness. To avoid these effects, we assume overall stiffness of the material and the total loading to be constant, i.e. $E_m + E = C$ and $\Sigma + \Sigma + 2\delta = F$, where C and F are constants. The constant overall material stiffness represents the amount of deposited cellulose fibers to stay roughly the same in all plant walls of interest. The anisotropy of the material, in turn, is controlled by the organization and alignment of these fibers. The constant overall loading would represent roughly constant turgor and tissue pressure in the epidermal tissue. With the above assumptions we can write the strain energy, Eq. 4, for a material where the principal material and stress directions align ($\Theta = 0$) as

$$W = \frac{F^2}{2C}\frac{2-\kappa}{(2-\alpha)^2}\left[1 + \frac{(1-\alpha)^2}{1-\kappa} - \frac{2V(1-\alpha)}{\sqrt{1-\kappa}}\right]. \tag{5}$$

Taking the derivative of above equation with respect to the material anisotropy coefficient, κ gives

$$\frac{\partial W}{\partial \kappa} = \frac{F^2}{2C(2-\alpha)^2}\left[-1 + \frac{(1-\alpha)^2}{(1-\kappa)^2} - V\frac{(1-\alpha)\kappa}{(1-\kappa)^{\frac{3}{2}}}\right]. \tag{6}$$

For a specific value of $\kappa \in [0:1]$, there is a unique value for $\alpha \in [0:1]$ where $\frac{\partial W}{\partial \kappa} = 0$, which represents an energy minimum. Hence, if the majority of cellulose fibers are aligned to the principal stress direction, an energetically optimal configuration of number of aligned fibers exists. If there is no contribution of the Poisson ratios ($V = 0$), Eq. 6 simplifies and results in the strain energy with a minimum when material anisotropy is equal to stress anisotropy $\kappa = \alpha$ (Fig. II.2C). The existence of a unique material anisotropy coefficient corresponding to a strain energy minimum holds also beyond the assumptions of constant material stiffness and linear material, which led us to the simple analytic expressions (Eqs. 5-6), as confirmed in numerical simulations using Saint Venant-Kirchhoff nonlinear strain energy

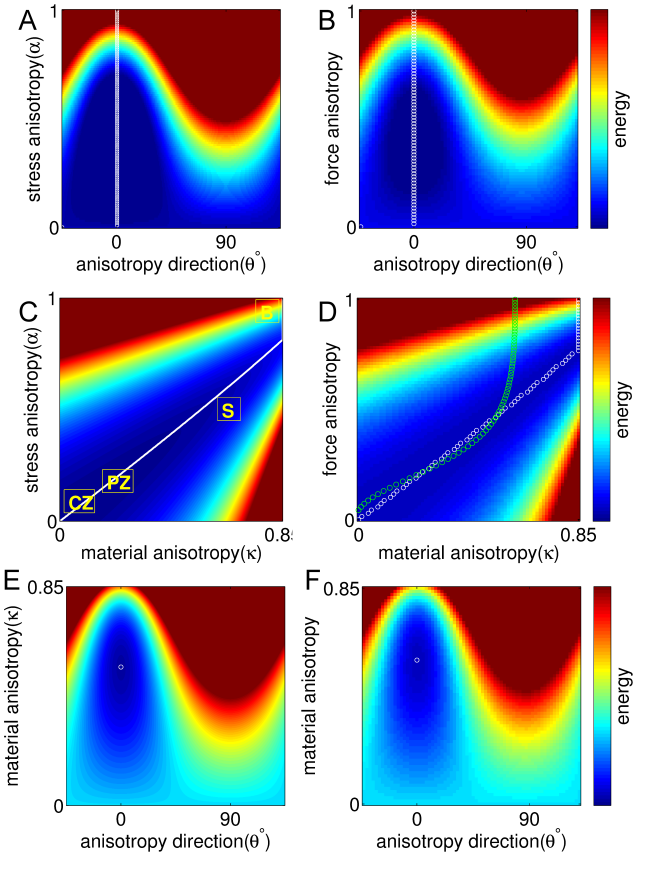

Figure II.2: A) Energy landscape with respect to varied anisotropy direction and stress anisotropy from equation 4. Material anisotropy is constant ($\kappa = 0.5$, see equation 5). White line shows that minimum energy for different values of α is at $\theta = 0$. B) Energy landscape with the same values as in A) for all the parameters resulted from simulations on the patch shown in (Fig. II.1B) at mechanical equilibrium. C) Energy landscape as a function of material anisotropy(κ) and stress anisotropy(α). White line presents the minimum energy for each value of κ. Different regions in SAM are marked as CZ (central zone), PZ (peripheral zone), S (stem) and V (the valley between the meristem and growing primordia) D) Result analogical to C) using Saint Venant-Kirchhoff energy model for a patch shown in (Fig. II.1B). E) Combined angle/kappa plot. For a given value for κ there is a single set of values for anisotropy direction and material anisotropy with minimum mechanical energy(white circle). F) Result analogical to E coming from simulations using Saint Venant-Kirchhoff energy model for a patch shown in (Fig. II.1B).

(Fig. II.2D).

Plant cells have the ability to alter the directions of the cellulose fibers by adjusting the directions of the cortical microtubules as well as the amount of fibers layed out by regulating number and rates of cellulose production of CESA complexes synthesizing the fibers [25, 26]. Hence, the angle between the principal directions of stress and material anisotropies, Θ, as well as the material anisotropy coefficient, κ, are allowed to be altered simultaneously. Strikingly, our results show that a unique minimum exists in the Θ, κ space given a constant anisotropic load (Fig. II.2E and F), and the strain energy forms a continuous landscape with maximal derivatives (Forces) in directions not always parallel to the Θ, κ coordinates.

II.2.3 *Several domains in plants produce mechanical anisotropy patterns correlating with the energy minimization principle*

Having described the strain energy behavior across ranges in material and stress anisotropies we next set out to map different regions in plant epidermal tissues according to their strain energy. The loading forces in a plant epidermis under tension depend highly on the curvature, both at tissue and subcellular resolution (Fig. II.1B) [7, 14, 15]. At the shoot apex, referred to as the central zone (CZ), the curvature is isotropic, and at the side of the shoot, the peripheral zone (PZ), and further down the stem (S), the curvature becomes increasingly anisotropic, where the stem shape can be approximated as a cylinder with a predicted stress anisotropy $\alpha = 0.5$. Even larger stress anisotropy is expected at the boundary (B) between the shoot meristem and developing organ buds (primordia) where the surface along the direction of the valley is convex and in the perpendicular direction is concave. Tracing the strain energy minima when the stress anisotropy range from zero to 0.5 we can identify the CZ as having isotropic material and PZ and stem as having an increasingly higher anisotropic material (Fig. II.2C). This correlates well with the assumed cellulose fiber anisotropy in these tissues, as measured either by the fibers directly or by the direction of the cortical microtubules (Fig. II.1A) [7, 14]. Similarly, a correlation between principal stress directions and fiber/microtubule patterns in various tissue domains implies that the angle between material anisotropy and maximal stress direction is close to zero. Again, following the model behavior on a path from isotropic (CZ) to highly anisotropic (S/B) shows that the energy difference for different angles increases with the anisotropy (Fig. refp2:fig2A and B, Fig. II.3D), and hence an energy minimizing model predicts the alignment directions of fibers/microtubules seen in different epidermal tissue regions

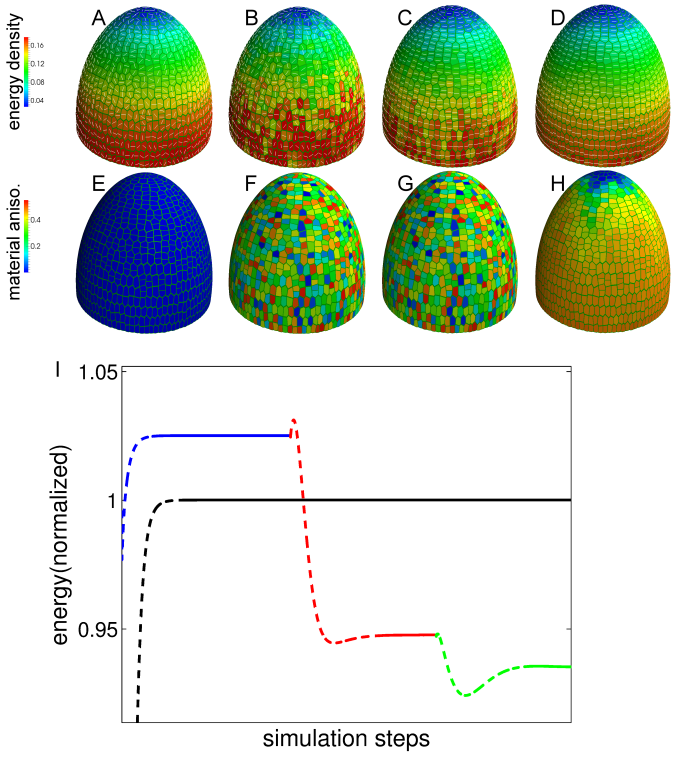

Figure II.3: The evolution of mechanical energy stored in the template shown in (Fig. II.1D). Material anisotropy and stress feedback both on the direction and degree of anisotropy are introduced to the material (A-D). A) Isotropic material B) Material is anisotropic. The degree of material anisotropy and anisotropy direction both randomly vary from cell to cell when the overall young modulus was kept constant. C) The material is similar to B but a feedback from maximal stress direction is applied to the anisotropy direction in each cell. D) Starting from final result from C a feedback from stress anisotropy was applied to the degree of material anisotropy. The results are close to mechanical equilibrium(see methods). E-H) The material anisotropy of individual cells in A-D respectively. I) The overall mechanical energy of the tissue during the simulations regarding the figures A-D. Dashed lines show the transient results before equilibrium. Solid lines show the results that were approved by our equilibrium criteria. Black line shows the base line resulted from isotropic material (A) Blue, red and green lines are showing the overall energy of the figures B, C and D respectively.

and that that the correlation is stronger in regions of highly anisotropic forces [14, 27, 28].

Next, we aimed at getting a quantitative estimation of the strain energy gains possible by adopting direction and magnitude of material anisotropy in plant-like structures. To do this we compared an isotropic material model with anisotropic materials and directions (Fig II.3). Isotropic material results in a smooth increase of strain energy on our meristem template from the apex to the periphery, i.e. from isotropic to anisotropic stresses (Fig. II.3A). Introducing anisotropic material with random directions in individual cells brings noise in the energy density and increases the total energy by about 2% (Figs. II.3B, F and I). Allowing the adaptation of the anisotropy directions in cells to the directions corresponding with optimal strain energy (i.e. maximal stress direction) leads to a drop in strain energy of about 7%, comparing to the previous case of random material anisotropy (Figs. II.3C and G). Finally, adjusting the magnitude of the anisotropy in the material according to the stress anisotropy leads to further reduction in strain energy, about 2% comparing to previous case, and to smoothing of the strain energy density in radial direction of the template (Figs. II.3 D and H). Comparing an isotropic material and a material adapting to minimal strain energy in both direction and magnitude, reveals that the energy gain is in the order of 7% and that the gain is mainly in the regions of anisotropic stresses. This shows that feedback mechanism adjusting material anisotropy direction and magnitude based on direction and value of principal stress leads to favorable configuration for mechanical structure of the plant.

II.3 DISCUSSIONS

Geometrical shape of organs is important feature for the plants allowing them to survive or gain advantage in diverse environmental conditions. This shape is generated by growth driven by intracellular pressure and adjusting mechanical properties of the cell walls [28, 29]. In procurement anisotropic shapes, the alignment of cellulose fibers creating wall material anisotropy plays an important role. Several intrinsic and extrinsic signals have been proposed to alter fiber orientations in plant cells [14, 30, 31]. We show that the previously proposed stress-based feedback is directly corresponding to the strain energy minimizing mechanism. Potentially this can play an important evolutionary role by optimizing the amount and constituents of wall material to generate optimal fitness in terms of growth and mechanical strength. The suggested energy decrease of 7% could represent appropriately less wall material which has to be used in building a

structure which is still able to sustain forces from the same turgor pressure. The energy minimizing mechanism in an epidermis under tension leads to aligning fibers in direction of highest curvature. Interestingly, single cell bacteria have been shown to add wall material in directions defined by the the curvature [32–34], which again might be explained by an energy minimizing mechanism in these highly pressurized cells, potentially extending our results beyond the domain of plants. Finally, the suggested mechanism of strengthening the wall material in specific directions and weakening in others to optimally cope with loading forces resembles the engineering approach of topology optimization [35], where material properties are adjusted to optimally solve constraints of e.g. geometry and weight. In the case of plants, the adaptation needs to be permanently adjusting given the morphological changes, and our results show that the strain energy minimization provides a dynamic and adaptable mechanism for generating optimal shapes via growth.

ACKNOWLEDGMENTS

This work was supported by the Swedish Research Council (VR2013:4632), the Gatsby Charitable Foundation (GAT3395/PR4), and Knut and Alice Wallenberg Foundation via project ShapeSystems (KAW2012.0050).

REFERENCES

1. R. V. Jean and D. Barabe, *Symmetry in Plants*. World Scientific, 1998.
2. T. I. Baskin, "Anisotropic expansion of the plant cell wall," *Annu Rev Cell Dev Biol*, vol. 21, pp. 203–22, Jan 2005.
3. D. J. Cosgrove, "Growth of the plant cell wall.," *Nature reviews. Molecular cell biology*, vol. 6, pp. 850–61, nov 2005.
4. D. J. Cosgrove and M. C. Jarvis, "Comparative structure and biomechanics of plant primary and secondary cell walls.," *Frontiers in plant science*, vol. 3, p. 204, jan 2012.
5. S. Braybrook and H. Jönsson, "Shifting foundations: the mechanical cell wall and development," *Curr Opin Plant Biol*, vol. 29, pp. 115–120, Jan 2016.
6. P. B. Green, "Mechanism for plant cellular morphogenesis," *Science*, vol. 138, pp. 1404–1405, 1962.
7. Z. Hejnowicz, A. Rusin, and T. Rusin, "Tensile tissue stress affects the orientation of cortical microtubules in the epidermis of sunflower hypocotyl," *J PLant Growth Regul*, vol. 19, pp. 31–44, 2000.

8. J. Dumais and C. R. Steele, "New evidence for the role of mechanical forces in the shoot apical meristem," *J PLant Growth Regul*, vol. 19, pp. 7–18, Feb 2000.
9. P. D. Shipman and A. C. Newell, "Phyllotactic patterns on plants," *Phys Rev Lett*, vol. 92, p. 168102, Apr 2004.
10. M. G. Heisler, O. Hamant, P. Krupinski, M. Uyttewaal, C. Ohno, H. Jönsson, J. Traas, and E. M. Meyerowitz, "Alignment between pin1 polarity and microtubule orientation in the shoot apical meristem reveals a tight coupling between morphogenesis and auxin transport," *PLoS Biol*, vol. 8, p. e1000516, Jan 2010.
11. N. Nakayama, R. S. Smith, T. Mandel, S. Robinson, S. Kimura, A. Boudaoud, and C. Kuhlemeier, "Mechanical regulation of auxin-mediated growth.," *Current biology : CB*, vol. 22, pp. 1468–76, aug 2012.
12. B. Landrein, A. Kiss, M. Sassi, A. Chauvet, P. Das, M. Cortizo, P. Laufs, S. Takeda, M. Aida, J. Traas, T. Vernoux, A. Boudaoud, and O. Hamant, "Mechanical stress contributes to the expression of the stm homeobox gene in arabidopsis shoot meristems," *eLife*, vol. 4, p. e07811, 2015.
13. A. C. Newell, P. D. Shipman, and Z. Sun, "Phyllotaxis: cooperation and competition between mechanical and biochemical processes," *J Theor Biol*, vol. 251, pp. 421–439, Apr 2008.
14. O. Hamant, M. G. Heisler, H. Jönsson, P. Krupinski, M. Uyttewaal, P. Bokov, F. Corson, P. Sahlin, A. Boudaoud, E. M. Meyerowitz, Y. Couder, and J. Traas, "Developmental patterning by mechanical signals in arabidopsis," *Science*, vol. 322, pp. 1650–1655, Dec 2008.
15. A. Sampathkumar, P. Krupinski, R. Wightman, P. Malini, A. Berquand, A. Boudaoud, O. Hamant, H. Jönsson, and E. M. Meyerowitz, "Subcellular and supracellular mechanical stress prescribes cytoskeleton behavior in arabidopsis cotyledon pavement cells," *eLife*, vol. 3, p. e01967, 2014.
16. E. Castle, "Membrane tension and orientation of structure in the plant cell wall," *Journal of Cellular and Comparative Physiology*, vol. 10, pp. 113—121, 1937.
17. B. Bozorg, P. Krupinski, and H. Jönsson, "Stress and strain provide positional and directional cues in development," *PLoS Comp Biol*, vol. 10, p. e1003410, 2014.
18. U. Kutschera and K. J. Niklas, "The epidermal-growth-control theory of stem elongation: an old and a new perspective.," *Journal of plant physiology*, vol. 164, pp. 1395–409, nov 2007.
19. S. Savaldi-Goldstein, C. Peto, and J. Chory, "The epidermis both drives and restricts plant shoot growth," *Nature*, vol. 446, no. 7132, pp. 199–202, 2007.

20. D. E. Dischler, P. Janmey, and Y. li Wang, "Tissue cells feel and respond to the stiffness of their substrate," *Science*, vol. 310, pp. 1139–1143, 2005.
21. A. Bershadsky, M. Kozlov, and B. Geiger, "Adhesion-mediated mechanosensitivity: a time to experiment, and a time to theorize," *Curr Opin Cell Biol*, vol. 18, pp. 472–481, 2006.
22. B. Landrein and O. Hamant, "How mechanical stress controls microtubule behavior and morphogenesis in plants: history, experiments and revisited theories," *PLant J*, vol. 75, pp. 324–338, 2013.
23. M. Uyttewaal, A. Burian, K. Alim, B. Landrein, D. Borowska-Wykręt, A. Dedieu, A. Peaucelle, M. Ludynia, J. Traas, A. Boudaoud, D. Kwiatkowska, and O. Hamant, "Mechanical stress acts via katanin to amplify differences in growth rate between adjacent cells in Arabidopsis.," *Cell*, vol. 149, pp. 439–51, apr 2012.
24. P. G. Ciarlet, *Mathematical Elasticity: Volume I: Three-Dimensional Elasticity*. Elsevier, 1993.
25. A. R. Paredez, C. R. Somerville, and D. W. Ehrhardt, "Visualization of cellulose synthase demonstrates functional association with microtubules.," *Science*, vol. 312, pp. 1491–5, jun 2006.
26. A. Endler and S. Persson, "Cellulose synthases and synthesis in arabidopsis," *Mol Plant*, vol. 4, pp. 199–211, 2011.
27. J. Chan, G. Calder, S. Fox, and C. Lloyd, "Cortical microtubule arrays undergo rotary movements in Arabidopsis hypocotyl epidermal cells.," *Nature cell biology*, vol. 9, pp. 171–5, feb 2007.
28. D. B. Szymanski and D. J. Cosgrove, "Dynamic coordination of cytoskeletal and cell wall systems during plant cell morphogenesis," *Current Biology*, vol. 19, no. 17, pp. R800 – R811, 2009.
29. A. Geitmann and J. K. E. Ortega, "Mechanics and modeling of plant cell growth.," *Trends in plant science*, vol. 14, pp. 467–78, sep 2009.
30. T. M. Lynch and P. M. Lintilhac, "Mechanical signals in plant development: a new method for single cell studies.," *Developmental biology*, vol. 181, pp. 246–56, jan 1997.
31. V. Mirabet, P. Das, A. Boudaoud, and O. Hamant, "The role of mechanical forces in plant morphogenesis," *Annual review of plant biology*, vol. 62, pp. 365–85, Jun 2011.
32. J. Dominguez-Escobar, A. Chastanet, A. H. Crevenna, V. Fromion, R. Wedlich-Soldner, and R. Carballido-Lopez, "Processive movement of mreb-associated cell wall biosynthetic complexes in bacteria," *Science*, vol. 333, pp. 225–228, 2011.
33. E. C. Garner, R. Bernard, W. Wang, X. Zhuang, D. Z. Rudner, and T. Mitchison, "Coupled, circumferential motions of the cell wall synthesis machinery and mreb filaments in b. subtilis," *Science*, vol. 333,

pp. 222–225, 2011.

34. S. van Teffelen, S. Wang, L. Furchtgott, H. K. C., N. S. Wingreen, J. W. Shaevitz, and Z. Gitai, "The bacterial actin mreb rotates, and rotation depends on cell-wall assembly," *Proc Natl Acad Sci USA*, vol. 108, pp. 15822–15827, 2011.
35. M. P. Bendsoe and O. Sigmund, *Topology OptimizationL Theory, Methods and Applications*. Springer-Verlag, Berlin Heidelberg, 2003.

III

A CONTINUOUS GROWTH MODEL FOR PLANT TISSUE

Behruz Bozorg [1], Pawel Krupinski [1] and Henrik Jönsson [1,2,3].

[1] Computational Biology & Biological Physics, Lund University, Sölvegatan 14A, SE 223 62 Lund, Sweden.
[2] Sainsbury Laboratory, Cambridge University, Bateman Street, CB2 1LF Cambridge, United Kingdom.
[3] Department of Applied Mathematics and Theoretical Physics (DAMTP), University of Cambridge, Cambridge, United Kingdom.

LU TP 16-13 (submitted 2016)

Morphogenesis in plants and animals involves large irreversible deformations. In plants, the response of the cell wall material to internal and external forces is determined by its mechanical properties. An appropriate model for plant tissue growth must include key features such as anisotropic and heterogeneous elasticity and cell dependent evaluation of mechanical signals such as osmotic pressure, stress and strain. In addition, a growth model needs to cope with cell divisions as a necessary part of the growth process. Here we develop such a growth model, which is capable of employing not only mechanical signals but also morphogen dependent signals for regulating growth. The model is based on a continuous equation for updating the resting configuration of the tissue. Simultaneously, material properties can be updated at a different time scale. We test the stability of our model by measuring convergence of growth results for a tissue under the same mechanical and material conditions but with different spatial discretizations. The model is able to maintain a strain field in the tissue during re-meshing, which is of particular importance for modelling cell division. We confirm the accuracy of our estimations in two and three dimensional simulations. The approach results in a model implementation that can be used to compare different growth hypotheses, while keeping residual stresses and other mechanical variables updated and available for feeding back to the growth and material properties.

III.1 INTRODUCTION

Most of higher plants acquire their shape as a result of growth since cell migration and apoptosis are not present and as such are not contributing to morphogenesis. The plant cells are surrounded by rigid and tightly connected cell walls and thus the changes in cell neighborhood topology are mainly the result of the cell proliferation. High internal pressure in the cells is the driving force of growth while heterogeneous and anisotropic mechanical properties of the cell walls are instrumental in shape formation [1, 2]. A classic growth model, introduced by James A. Lockhart in 1965, suggest that cell extension is appearing when cells walls are under tension, generated by cell pressure above a threshold value [3]. Long term growth is, next to elastic and plastic deformation, a fundamental process of plant tissue morphogenesis leading to organ formation. On a microscopic level it is a complicated and carefully balanced process of mass deposition, stress relaxation and geometrical expansion [4]. The plant cell walls are seen as main mediators of this process, where their composite material plays an important role. The primary cell walls consists of strong load bearing cellulose fibers connected by xyloglucan molecules and residing in a matrix of pectin molecules [5]. The plant cells can guide the synthesis of the cellulose fibers in directions following cortical microtubules (MTs) and thereby they can regulate the anisotropy of their wall material [6]. The exact microscopic description of the plant cell wall growth is still a subject of active research, but a simplistic illustration of process is given by the breakage of the xyloglucan molecules, leading to slippage between the cellulose fibers and then addition of new material in between [2]. The more recent work has introduced the idea of non-homogeneous growth at hotspots [7]. Furthermore, the importance of regulation of the pectin molecular state for growth initiation has been investigated [8–10]. In addition to the physical description of the growth, it is well studied that molecular signals are important for initiating the process. An example is auxin, a growth hormone suggested to alter cell wall properties by different mechanisms to induce growth [11–14]. Also involvement of other hormonal and genetic factors in the growth process has been confirmed by altering the cell wall composition [15, 16]. It is not yet fully understood which quantity is most important for generating growth response in different plant tissues. Stress, strain ,strain energy or morphogen field can be equally well considered as cues for growth and it is probable that different combinations of them play roles in different growth processes.

Plant growth has been modeled at a variety of resolutions, from discrete and continuum descriptions at organ level down to microscopic scales of

single cell walls. At the tissue and whole plant scale models are mainly descriptive in nature, where for example L-systems has been used to build models of plant structures [17, 18]. Growth models are often phenomenological in connecting growth to variables such s water uptake, nutrients or environmental factors [19]. Tissue models where morphogen-driven growth has been combined with mechanics have been used to describe growth of leafs and flowers [20, 21]. The mechanical contribution in these models, however, has been limited to maintenance of the integrity of the tissue, while residual stresses have been disregarded by removal at each update step [22]. At the microscopic scale, interactions between molecular components have been hypothesized, resulting in predictions of larger scale mechanical behavior [23, 24], but experimental verifications at this resolution is still lacking. More recently, models at the cellular level, including molecular signals and continuum descriptions of mechanical properties of the cell walls, have been developed [25, 26]. Tensional stress has been suggested as an input to guide the direction of cortical microtubules, and finite element models were essential to connect the predicted stress directions to the measured MT directions [27, 28]. The stress feedback model was further shown to lead to robust initiation of anisotropic shape via anisotropic material properties [29], while the need for isotropic wall mechanics at the initiation of new organs was supported with another model [30]. The use of atomic force microscopy for measuring mechanical properties of cell walls in vivo has been useful for confirmation of predictions of such models [28, 30]. Also, a 3D finite element model was used to show that the molecular input to growth is transformed to neighboring cells by variable mechanical response of differently sized cells [26], and 3D mechanical stress models have been used to feed back to subcellular molecular behavior within cells [25].

With few exceptions [26, 31], the models at the cellular level have been dealing with small elastic deformations. Thus a reliable mathematical description of growth in terms of continuous mechanics and practical implementation of such description are crucial for relating these mechanical quantities to growth. Here we present a model of finite growth and its regulation by different signals in a plant tissue. The model is based on separation of growth and elastic deformation processes by introduction of growth dependent zero stress configuration [32] as time dependent reference point for constitutive equations. Our growth model can be used with any material model and discretization. Here, due to the almost planar shape of plant cell walls, we use the already developed material model for anisotropic planar elements based on Saint Venant-Kirchhoff strain energy [27–29]. We test different mechanical signals e.g. strain or stress, which can

be evaluated directly from the mechanical variables, as well as mechanically independent signals e.g. morphogens, as inputs to our growth model. When mechanical signals are used their principal directions and values are hypothesized to regulate the direction and rate of the growth.

III.2 METHODS

Plant tissue, as a mechanical system, is restricted by relatively stiff walls with a particularly rapid elastic response to any changes in forces and material properties. This is necessity for the plants considering that they have to keep the the cell walls intact under high stresses generated by turgor pressure driving the growth [1, 2]. On the other hand, due to the relatively long time which takes for molecular processes to produce macroscopic changes, growth is a considerably slower then elastic response. We will take advantage of this difference in time scales and assume that at each time step of the growth the stress field is statically balanced. In this section we first discuss the fundamental force balance laws and derive the quasi static equation of motion. Next we introduce the continuous growth equation and test its stability by comparing its performance over different spatial discretizations. Then we present equations explicitly including parameters by which different signals can regulate principal directions and rates of the growth. Special care is taken for describing cell division and the related re-meshing process. Although our model does not depend on a specific strain energy description, we derive the strain energy for an anisotropic material that is used in our simulations based on a discretization of the tissue into triangular planar elements.

III.2.1 *Balance laws and the quasi static equation of motion*

Deriving the balance laws of mass and energy is challenging since these are not conserved quantities during growth. Energy is constantly provided to a living tissue, and mass is added into the growing tissue continuously. However, given that primary plant cell walls often grow in a plane with thickness of the walls staying constant we assume that the density, ρ, of the tissue is constant during growth

$$\frac{d\rho}{dt} = 0. \tag{1}$$

The balance of angular momentum is satisfied by stress tensor symmetry

$$T_{ij} = T_{ji}, \tag{2}$$

and the balance of linear momentum gives Cauchy's first law of motion

$$\rho \frac{dV}{dt} + \eta V - \nabla.T - \rho b = 0, \tag{3}$$

where V is the velocity, T is the stress tensor and b represents the body forces. The term ∇T gives traction generated by stress divergence and ηV is the damping force resulting from viscosity of the medium. Deposition of new material to a plant cell wall is much slower than the elastic response of the material that moves the material points toward their equilibrium position. This difference is large enough to let us assume that the material points are always in their mechanical equilibrium in which the forces are balanced

$$\nabla.T + \rho b = 0. \tag{4}$$

Since we are interested in finding the equilibrium configuration and not the dynamics of it we use over-damped, Langevin dynamics in which the acceleration term is negligible and the velocity field of the material points is determined by the yet unbalanced traction and body forces

$$\eta V = \nabla.T + \rho b, \tag{5}$$

or

$$\frac{dX}{d\tau} = \nabla.T + \rho b, \tag{6}$$

where $\tau = t/\eta$ is time during which the material configuration X moves towards its equilibrium X_{eq}. The viscosity of the media η is for our purpose the parameter controlling the speed of convergence and does not have a physical meaning. Our final result does not depend on this parameter as we do not take the dynamics into account in the quasi-static case. The equilibrium can be described by the integral

$$X_{eq} = X(\tau = 0) + \int_0^\infty [\nabla.T + \rho b]\, d\tau \Big|_{X_0}, \tag{7}$$

where X_0 is the material resting configuration and is stated here to emphasize the dependency of the integral upon this configuration. Ideally, the

integral in Eq. 7 should be evaluated until Eq. 4 is satisfied. $X(\tau = 0)$ is the configuration from which we start the integration and is equivalent to neither X_0 nor X_{eq}. Generally the uniqueness of equilibrium configuration is not guaranteed and specifically for complicated configurations it is likely to have several of them. However, if the distance between $X(\tau = 0)$ and X_{eq} in phase space is small enough, it is not likely to encounter more than a single equilibrium configuration during the integration. We can reduce the size of the growth-related time step such that this uniqueness is achieved throughout the integration interval, as will be described below. This interval connects two closely related equilibrium configurations in two consecutive time-points, where in each of the configurations Eq. 4 is satisfied. In practice, Eq. 7 can be used to set a numerical recipe for deriving an approximate equilibrium configuration. This leads to the iterative update equation

$$X_{n+1} = X_n + [\nabla.T(X_n) + \rho b(X_n)]\,\delta\tau, \tag{8}$$

where X_n is the material configuration at iteration n. This update should be iterated until

$$\nabla.T(X_n) + \rho b(X_n) < v_c, \tag{9}$$

where v_c is an equilibrium velocity threshold. The stopping criteria 9 assures closeness of the final configuration to the equilibrium state, which we assume is unique within the neighborhood of integration.

III.2.2 *The growth tensor*

The next step is to add growth, implemented as a deformation of the resting configuration X_0. The mapping between the resting and current configurations, given as elastic deformation, is provided by the deformation gradient tensor, F_e, defined by

$$F_e = \frac{\partial X}{\partial X_0}. \tag{10}$$

where X and X_0 are current and resting configurations, respectively. The subscript e is there to emphasis that this mapping describes only the elastic deformation. We define growth as a continuous update of the resting configuration that is assumed to be stress free but not necessarily compatible. A source of incompatibility is the non-uniform growth field under which adjacent elements can have different principal growth directions and rates.

The overall mapping between initial resting configuration and current configuration, F_{eg}, is given by the product of growth and deformation gradient tensors

$$F_{eg} = F_e F_g(t) \tag{11}$$

where $F_g(t)$ is the finite growth tensor at time t.

We introduce growth as an update of the resting configuration after an infinitesimal time step, δt, as

$$\begin{aligned} X_0(t) \;\rightarrow\; X_0(t+\delta t) &= F_g(t+\delta t) X_0(0) && (12)\\ &= X_0(t) + \delta X_0 && (13)\\ &= \left[I + f_g(\delta t)\right] X_0(t)\,, && (14) \end{aligned}$$

where $X_0(0)$ is the initial resting configuration, which is constant, and f_g is the differential growth tensor. The relation between F_g and f_g is given by

$$\frac{\partial F_g}{\partial t} = f_g F_g, \tag{15}$$

which in integral form becomes

$$F_g(t) = \exp\left[\int_0^t f_g(t')dt'\right]. \tag{16}$$

The evolving resting shape and its growth dynamics is described by the difference equation

$$X_0(t+\delta t) - X_0(t) = f_g X_0(t)\delta t, \tag{17}$$

leading to the differential equation

$$\frac{\partial X_0}{\partial t} = f_g X_0(t), \tag{18}$$

with the solution

$$X_0(t) = F_g(t) X_0(0). \tag{19}$$

The differential growth tensor f_g generally depends on time and growth signals. In these cases Eq. 16 becomes more complicated, but in the numerical update via Eq. 17 we need to only update f_g at each time step.

The rest configuration X_0 is piecewise compatible, i.e. each element is compatible within itself. Incompatibility exists at the junctions between elements. In the case of planar elements these junctions are the edges of elements whereas for three dimensional elements, e.g. tetrahedrons, junctions are given by faces. In practice, elements are connected via common nodes at the corners. This by itself constrains all elements in the tissue to stay intact in the current configuration. However, each element in the resting configuration is allowed to be disconnected and stress free.

III.2.3 *Continuous growth*

The current equilibrium configuration, $X_{eq} = X_{eq}(F_g, M)$, is a function of the growth tensor and a vector of all material parameters, M, and its time derivative can be expressed as

$$\frac{\partial X_{eq}}{\partial t} = \frac{\partial X_{eq}}{\partial F_g}\frac{\partial F_g}{\partial t} + \frac{\partial X_{eq}}{\partial M}\frac{\partial M}{\partial t}, \tag{20}$$

where the subscript eq is to stress that the derivative should be evaluated when all the material points are at equilibrium. Assuming that the source of growth comes solely from evolution of the resting shape we keep only the first term on the right hand side and by using Eq. 15 we have

$$\frac{dX_{eq}}{dt} = \frac{\partial X_{eq}}{\partial F_g} f_g F_g. \tag{21}$$

This is the growth equation of a slow process compared to the elastic deformation in which the material properties do not change.

III.2.4 *Time discretization of growth*

In a numerical algorithm we must make sure that the current shape is at the mechanical equilibrium at each time step. For a small step in time, δt, from Eq. 21 we get

$$X_{eq}(t + \delta t) - X_{eq}(t) = \frac{\partial X_{eq}}{\partial F_g} f_g \delta t, \tag{22}$$

or

$$X_{eq}(t + \delta t) = X_{eq}(F_g) + \frac{\partial X_{eq}}{\partial F_g}\delta F_g = X_{eq}(F_g + \delta F_g), \tag{23}$$

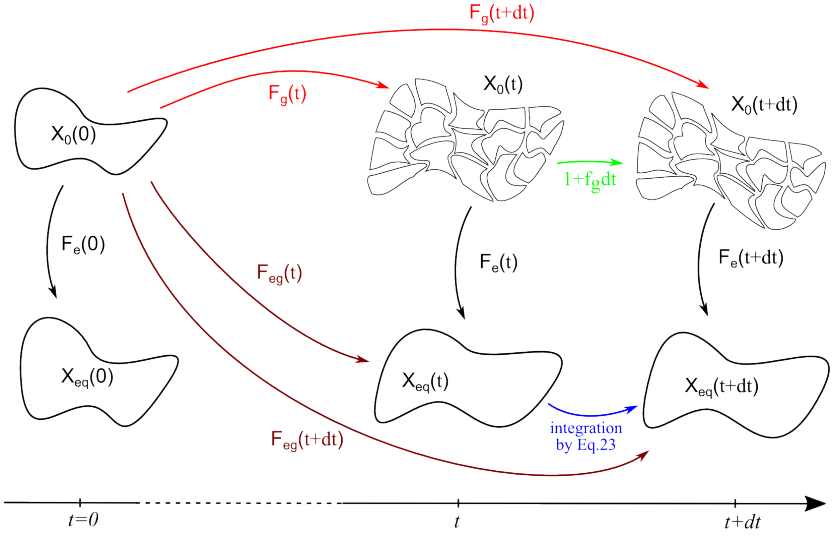

Figure III.1: **Illustration of the growth process**. The resting configuration might be compatible at growth-time zero but can become incompatible later, while the current configuration stays compatible. The integration takes place between two consecutive growth times. All variable notation is defined in the main text.

which from Eqs. 7 and 17 can be rewritten as

$$X_{eq}(t+\delta t) = X_{eq}(t) + \int_0^\infty [\nabla.T + \rho b] d\tau \Big|_{(I+f_g \delta t) X_0(t)}, \tag{24}$$

or

$$X_{eq}^{n+1} = X_{eq}^{n} + \int_0^\infty [\nabla.T + \rho b] d\tau \Big|_{(I+f_g \delta t) X_0^n}. \tag{25}$$

In Fig. III.1 the update of the equilibrium configuration between two consecutive time points is illustrated by the blue arrow. The integral on the right hand side of Eq. 25 can be evaluated more easily if the consecutive equilibrium configurations are close to each other. This is equivalent to choosing a small step size for the growth.

III.2.5 *The growth signal*

A possibility for applying various inputs that connect the growth process with mechanical or biochemical signals is required given the complexity of the growth process. Assuming that the growth field generally can be inhomogeneous and anisotropic, the growth tensor can be defined as

$$f_g = \Sigma_i \mathcal{F}(g_i)|g_i\rangle\langle g_i|, \tag{26}$$

where g_i and $|g_i\rangle$ are the i^{th} principal value and vector of growth signal in the resting configuration. $\mathcal{F}(g_i)$ is a function of the growth signal. This function, due to the potentially complex processes in growth, can be non-linear and possibly very complicated. Here, as an example, we assume a simple piecewise linear relation between growth signal and rate given by

$$\mathcal{F}(g_i) = k_{rate}\mathcal{R}(g_i - g_t). \tag{27}$$

g_t is the growth signal threshold above which growth occurs, k_{rate} is the rate and $\mathcal{R}$ is the ramp function

$$\mathcal{R}(x) \quad = \quad \begin{cases} 0 & if \;\; x \leq 0\,, \\ x & if \;\; x > 0\,. \end{cases} \tag{28}$$

Finally we formulate the general growth tensor as

$$\begin{aligned} f_g \quad &= \quad k_{rate}\Sigma_i \mathcal{R}(g_i - g_t)|g_i\rangle\langle g_i| \\ &= \quad k_{rate}|F_e^{\mathcal{T}}F_e|^{-1}\Sigma_i \mathcal{R}(G_i - G_t)F_e^{\mathcal{T}}|G_i\rangle\langle G_i|F_e\,. \end{aligned} \tag{29}$$

where G_i and $|G_i\rangle$ are the i^{th} principal value and vector of growth signal and G_t is the growth threshold, all given in the current configuration. Similarly, g_i, $|g_i\rangle$ and g_t are the corresponding values and vectors in the resting configuration. F_e is the elastic deformation gradient tensor. For stress or strain-based growth the growth tensor, can be defined as

$$f_g = k_{rate}\Sigma_i \mathcal{R}(S_i - S_t)|S_i\rangle\langle S_i| \tag{30}$$

where S_i and $|S_i\rangle$ are the i^{th} principal value and vector of strain or stress in the resting configuration. S_t is the strain or stress threshold for growth. This is more general than the growth equation, $f_g = k_{rate}\bar{\mathcal{R}}(\mathbf{S} - \mathbf{S_t})$ used in other models [31], where $\mathbf{S}$ and $\mathbf{S_t}$ are tensors of strain or stress and corresponding threshold, respectively, and $\bar{\mathcal{R}}$ is a tensor ramp function.

Unlike the above equation, Eq 26 is invariant under rotation and remains unchanged in different coordinate systems.

In our model the growth signal can be stress, strain or any mechanics-independent factor, e.g. a morphogen concentration. It is also possible to have a growth scenario in which a combination of different factors regulates the growth.

III.2.6 *Growing the elements in practice*

Application of Eq. 18 on the resting configuration for each of its elements after using Eq. 29 means that the growth equation corresponding with each element edge is needed. The growth rate of each element edge should be proportional to its resting length and a monotonic function of the difference between principal strain values and the threshold above which growth occurs, i.e. given by

$$\begin{aligned} \frac{\partial |l\rangle}{\partial t} &= f_g |l\rangle \\ &= k_{rate} \Sigma_i \mathcal{R}(g_i - g_t) |g_i\rangle \langle g_i | l\rangle . \end{aligned} \tag{31}$$

For the i^{th} component of the edge element

$$\frac{\partial l_i}{\partial t} = k_{rate} \mathcal{R}(g_i - g_t) l_i. \tag{32}$$

Here we have assumed that the growth rates of the components of the element edges are proportional to their size and strength of the growth signal in the corresponding direction.

III.2.7 *Residual stresses*

In case of incompatible growth process we expect arising of residual stresses i.e. stresses which are remaining in the tissue after loading forces are removed. Then the stress, T, in Eqs. 3-9 includes both residual, T_r, and loading, T_l, stresses

$$T = T_l + T_r. \tag{33}$$

Note that residual stresses are divergence free. This follows from the assumption that there are no external forces in the reference configuration [33].

Eqs. 3-9 are also true for net stresses, i.e.

$$\nabla.T_l + \rho b = 0, \tag{34}$$

and

$$\nabla.T_r = 0. \tag{35}$$

The superposition principle allows us to add up the above equations and Eq. 35 provides a recipe for evaluating the residual stresses by

$$X_{eq} = \int_0^{\infty} [\nabla.T] d\tau \Big|_{X_0(T_{tot})}, \tag{36}$$

where T_{tot} is the total growth time and

$$X_0(T_{tot}) = F_g(T_{tot}) X_0 = \left[\int_0^{T_{tot}} \exp(f_g t) dt \right] X_0. \tag{37}$$

Note that the tissue always experiences the overall stress field. Decomposing the stress into loading and residual components needs global information, which is not available to the cells. However, this decomposition can be of great importance when a stress field needs to be evaluated from the shape of the current configuration. When residual stresses exist, the geometrical information is not enough for the evaluation of the overall stress field. Eq. 37 can be used after each stage in the growth process to evaluate residual stresses. When this is done iteratively, the appearance and evolution of the residual stress field can be investigated.

III.2.8 *Cell division*

Growth often involves large deformations in which cells divide multiple times. Although a cell division includes various processes, e.g. mitosis and microtubular bundle formation, in a mechanical view it can be simplified to adding a new wall connected to existing walls. For the existing walls this leads to addition of new degrees of freedom to the tissue without changing the material properties or mechanical variables such as stress and strain fields (Fig. III.2). At each cell division, a domain of the tissue that belongs to the cell wall to be subdivided is replaced by new domains connected to the new daughter cells. The positioning of a new wall by the cell it thought to follow specific rules [34, 35]. Generally, the new wall created at division connects to the old walls at the points that do not respect the arrangement of the elements in existing mesh.

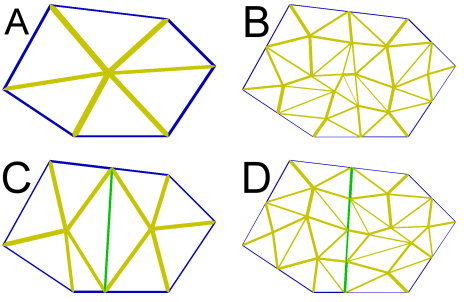

Figure III.2: **Cell division and remeshing.** Main walls are in blue. The new main wall resulted from division is in green. All the walls in yellow are the internal walls which are the interface between triangular elements and their resting lengths must be estimated after re-meshing.

Assuming each cell wall is meshed with some elements (Fig. III.2), the new wall will divide connecting cell walls regardless of its mesh and the arrangement of the elements. This will require re-meshing after each cell division such that the new elements appear solely in walls connected to one of the daughter cells. Consequently the dimensions, strains and stresses for the new elements must be recalculated, and here we provide a recipe for minimizing the difference in strains before and after the division in individual cell walls.

Strain maintenance

We could perform the division in the resting configuration of the cell wall if the elements are compatible, but this is not true after an incompatible growth process. Still it is possible to divide the mother cell wall and re-mesh the daughter cell walls in the compatible current configuration. As the resting configuration is essential for evaluating the strain energy, we then need to estimate this for each element based on the average strain field of the daughter cell walls, which has to be inherited from the mother cell wall. In such way we make sure that the strain field in a wall does not go through an discontinuous change when a cell divides. If the average Almansi strain tensor of the cell wall is known, it is possible to estimate the resting edges of elements from their edge vectors and eigenvalues and eigenvectors of the strain tensor. The Almansi strain in one dimension, ϵ_E, is defined by

$$\epsilon_E = \frac{1}{2}\left(\frac{l^2 - L^2}{l^2}\right), \tag{38}$$

where l and L are the current and resting lengths, respectively. We can invert this relation to calculate the resting length in terms of strain and current length

$$L = [(1 - 2\epsilon_E)l^2]^{\frac{1}{2}}. \tag{39}$$

Similarly the Eulerian-Almansi finite strain tensor, $\mathcal{S}$, is defined by

$$\mathcal{S} = \frac{1}{2}(I - F^{-\mathcal{T}}F^{-1}) \tag{40}$$

where F^{-1} is the inverse and $F^{-\mathcal{T}}$ is the inverse of the transpose of F. Inspired by Eq. 39, the resting length of each element edge is estimated by

$$L = [\Sigma_i(1 - 2\mathcal{S}_i) \langle l|\mathcal{S}_i \rangle^2]^{\frac{1}{2}} \tag{41}$$

where $\mathcal{S}_i$ and $|\mathcal{S}_i \rangle$ are the i^{th} eigenvalue and eigenvector of the average Almansi tensor of the mother cell wall and $|l \rangle$ is the corresponding element edge vector in the current configuration.

Eq. 41 is equivalent to a transformation under the inverse of the average stretch component of the deformation gradient tensors of all elements of a cell wall.

III.2.9 *Saint Venant-Kirchhoff strain energy for anisotropic material and planar triangular elements*

We use the strain energy based on the well known Saint Venant-Kirchhoff description

$$W_{iso} = \frac{\lambda}{2}(trE)^2 + \mu trE^2, \tag{42}$$

where E is the Green-Lagrange strain tensor and λ and μ are the Lame coefficients of the material. We assume plane stress condition where the Lame constants can be expressed as

$$\lambda = \frac{Y\nu}{1 - \nu^2}, \quad \mu = \frac{Y}{2(1 + \nu)}. \tag{43}$$

Here Y and ν are the Young modulus and Poisson ratio that represent stiffness and incompressibility of the material, respectively. The modified

version of Saint Venant-Kirchhoff model for anisotropic material is given by

$$W = W_{iso} + W_{aniso}, \tag{44}$$

where

$$W_{aniso} = \frac{\Delta\lambda}{2} \langle a|E|a \rangle trE + \Delta\mu \langle a|E^2|a \rangle, \tag{45}$$

$|a\rangle$ is the anisotropy vector which shows the direction in the material with the largest elasticity constant. The $\Delta\lambda$ and $\Delta\mu$ are the differences between longitudinal and transverse Lame coefficients which are in turn related to Young modulus in longitudinal and transverse directions and Poisson ratio.

Elements are triangular plates under plane stress condition. It has been shown that such a description is appropriate for describing the main mechanical features of different plant tissues domains in an epidermal pressure model[29].

III.3 RESULTS

To test the proposed growth model we perform simulations using a square patch of material, a Saint Venant-Kirchhoff strain energy model allowing for anisotropic material properties and triangular plate elements in the mesh. Material parameters and stresses are chosen such that the elastic deformation is about 8 to 12 %. This value has been reported to be a relevant elastic deformation in plants [36].

III.3.1 *The growth model can be made highly independent on spatial discretization*

The continuity of the growth model can be tested via comparing the resulting deformations for the same mechanical conditions but using different spatial discretizations where the degrees of freedom of the tissue varies. First, we investigate the convergence properties of the area expansion on grown templates with different discretization resolution.

A template with isotropic material and discretized at three different resolutions from coarse to fine is used (Fig. III.3A). Forces are applied to grow the template to about double the size. In the test cases we applied isotropic loading forces (Fig. III.3B), uniaxial loading forces (Fig. III.3C), or forces generated by applying a pressure from one side (Fig. III.3D).

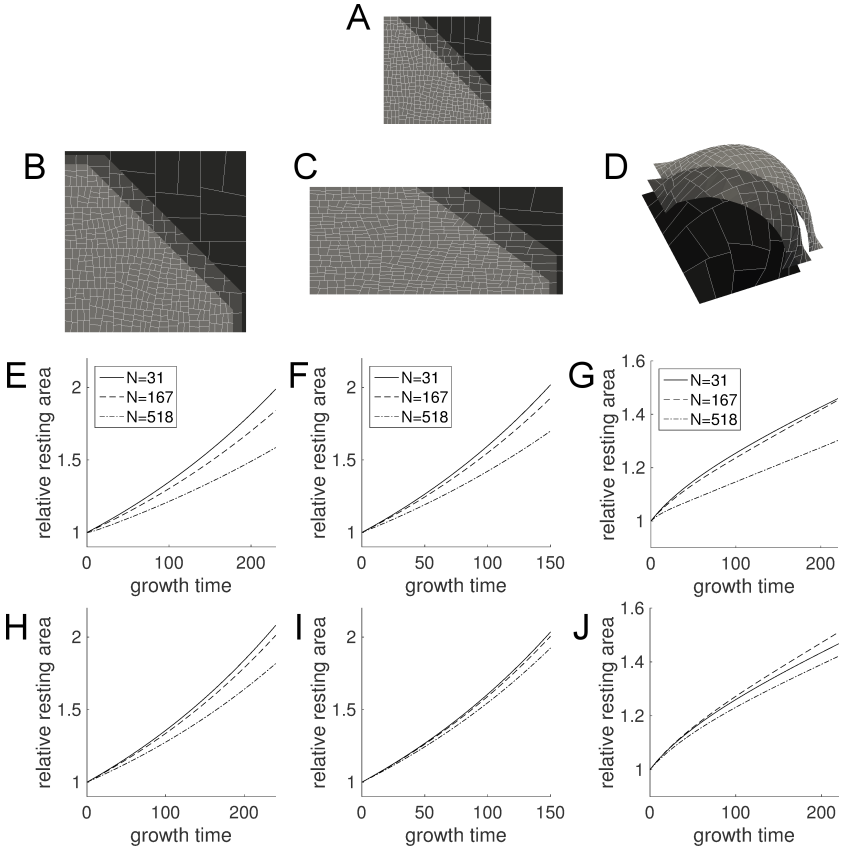

Figure III.3: **Growth and different spatial discretizations.** (A) A square template meshed in three different sizes is used as initial configuration. (B, E, H) The template is grown isotropically (C, F, I) The template is grown uniaxially. (D, G, J) The template is grown in three dimensions by inflating it by applying pressure on one side. (B, C, D) The deformed templates after growth. (E-J) Relative resting areas versus growth time (different than simulation time) are presented for two different equilibrium thresholds, v_c. The equilibrium threshold value is 0.01 for E and F, 0.003 for H and I, 0.001 for G and 0.0004 for J. Elastic deformation $\approx$ 10% for A and B, $\approx$ 0 *to* 15% for C.

Since growth is applied on the resting shape, we compared the area of the resting shape as a function of time of growth for different discretization resolutions (Figs. III.3E-J). As described in the Methods section (Eq. 9), numerical simulations use an equilibrium threshold value (v_c) to estimate when the tissues is close enough to an elastic equilibrium between each growth updates. Lowering this value leads to a convergence of the resting shape areas for the different meshes (cf. Figs. III.3E-G with Figs. III.3H-J where the value of v_c has been lowered less than one third in H and I and less than halved in J. This is particularly evident in the 2D simulations, where it is possible to reduce the growth error by decreasing v_c, at the cost of longer simulation times. For example, when comparing the difference between meshes with more than one order of magnitude difference in number of elements (N=31 vs N=518), the difference decreases from 20% and 15% (Figs. III.3E and F) to 12% and 5% (Figs. III.3H and I) after the area of the coarser mesh has been doubled when v_c is less than one third. For the pressurized template (Figs. III.3D, G and J) it becomes more complicated and the area convergence is not monotonic or might not happen at all. In case of applying pressure load to the template, not only is the tissue growing, but it is also changing the shape and curvature. Such shape changes are mesh dependent in our description using (planar) plate elements and the fine meshing will always be preferable if high resolution details of shape is to be investigated.

While it is possible to tune the difference in growth between different mesh resolutions, a finer mesh results in slower growth in general (using the same v_c). This is because after growing the elements, strain drops to lower values and it takes a while for the template to regain its quasi-equilibrium strain field, and this time is longer when using a fine mesh. Consequently, principal growth values in Eq. 26 will be lower for the same equilibrium threshold (v_c).

In summary, we showed that continuous growth can be described using our framework, and that it is important to make sure the system is close to its elastic equilibrium for a mesh-independent error in describing the growth of the tissue.

III.3.2 *Different input signals for growth can lead to heterogeneous residual stresses*

Our approach allow for regulating growth by using mechanical or other signals (Eqs. 26 and 29). It is of interest to compare the situations where growth is controlled by stress or strain signals since these can differ in the presence of material anisotropy in a tissue under anisotropic loading forces. Anisotropic forces are expected in plant (epidermal) tissue and is a

result from growth in neighboring tissue as well as the curvature of the tissue. The anisotropic alignment of cellulose fibers in key tissue domains in plants highlights the importance of such comparison, and although we will disregard dynamical material anisotropy changes in our simulations, feedback between stresses and material anisotropy can be of great importance for explaining robust material patterning in cells and tissues [28, 29].

To investigate the difference between strain and stress-based growth we simulate an anisotropic patch of material loaded such that the stress is anisotropic (Figs. III.4A and B). The material anisotropy and the stress anisotropy and their directions are chosen to give the maximal strain direction in the vertical direction and perpendicular to the horizontal maximal stress. Growing the tissue using Eq. 26 with either strain or stress as growth promoting signals results in different growth fields and completely different shapes (Fig. III.4 D and E). This provides an illustrative example of how alternating the growth signal under the same mechanical conditions can produce different growth patterns and ultimately shapes. In particular it is important to discern between stress and strain as signals for growth [29].

An alternative is to regulate growth by mechanically independent signals, e.g via morphogens or morphogen gradients. To test such a case we assume a growth field exists within the tissue (white bars in III.4C), and that it is independent of strain and stress signals. The material is isotropic and loaded isotropically by application of a constant internal pressure (in 2D). Here, the growth is regulated by the growth tensor (f_g in Eq. 29). The combined vertical and horizontal maximal growth signals in the left and right parts of the tissue generate an heterogeneous deformation (Fig. III.4F), where the elasticity of the material still keeps it continuous. A consequence is that a heterogeneous distribution in tissue stresses is generated (Fig. III.4F), in stark contrast to the strain and stress based growth examples (Figs. III.4 D and E), which generate uniform but different stress and strain fields. If the stress and strain fields are not uniform, due to non-uniformity of body forces and/or material properties, a heterogeneous growth field can be produced also by mechanical signals. However, if the body forces and material properties are uniform, stress and strain based growth has the built-in feature to reduce residual stresses.

In our approach it is possible to evaluate residual stresses if they exist (Eqs. 33-37). After finite growth (Figs. III.4E-F), the body forces can be removed and the tissue can be relaxed following Eq. 37. The remaining stress field is a divergence free field [33]. While the examples using stress and strain based growth lead to zero residual stresses (Figs. III.4 G and H), the non-uniform growth signal results in tensile and compressive stresses in

different domains of the tissue that arise from keeping the tissue compatible and connected (Fig. III.4I).

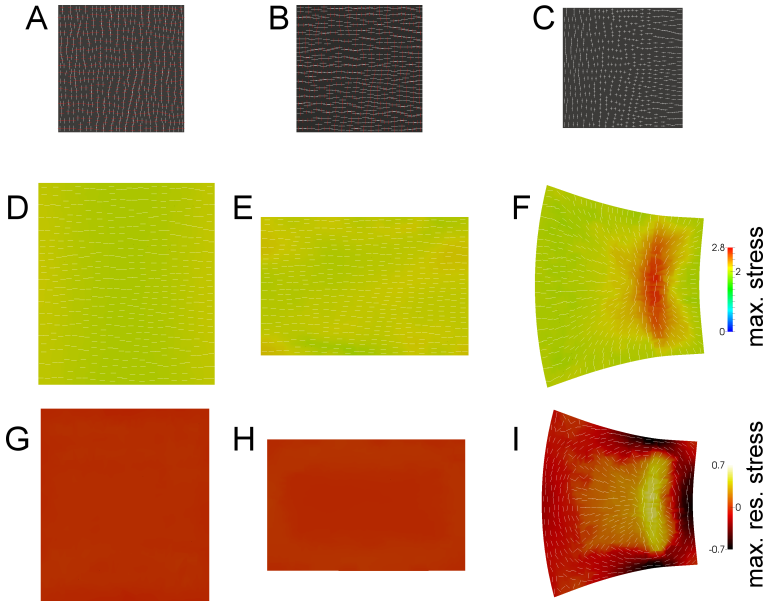

Figure III.4: **Shape changes, overall and residual stress fields under different growth rules.** (A,B) A patch of anisotropic material is loaded by anisotropic stress so that the principal stress and strains are perpendicular. (C) The same patch with isotropic material and isotropic stress can be grown under a predefined non-uniform growth field (white lines). Growth is given by Eq. 29. (D) Strain based growth results in vertical growth. (E) Stress based growth generates horizontal growth. (F) The result of the predefined non-uniform growth. (D,E,F) The color shows maximal principal value of the overall stress field resulting from body forces and residual stresses. (G,H,I) The maximal principal value of the residual stress field, measured after removing the body forces and letting the tissues relax.

We have shown the capabilities of the proposed model to employ different growth signals and demonstrated how this impacts the morphogenesis in some simple examples. We explain how the shapes can be generated by stress and strain signals and using non-mechanical inputs in the model. In particular, we evaluated how growth patterns relate to stress distributions, including how complex residual stresses can result when non-uniform growth is applied.

III.3.3 *The strain field is maintained during growth and cell division*

The difference between the resting and deformed configurations is given by the strain. Normally, by having the information about resting and current configurations the strain field can be calculated. However, as discussed in the Methods section, when cells divide new degrees of freedom need to be introduced, e.g. new nodes and edges for the resting configuration. This is done by interpolating the variables of the resting configuration in a finite element discretization. As we average the strain tensor over each cell wall, this tensor together with the values of the variables in the current configuration can be used to perform the necessary interpolation (Eq. 41).

For validating how well the method is able to predict a resting shape, we estimate the already known resting variables (here resting edges of triangular elements) from the average strain tensor of each cell wall and the current values of those variables. To do this we use elements of a collection of cells in a strained tissue and compare them with the corresponding exact values for a strained template in two and three dimensions (Fig. III.5). For the 2D strain, the estimation is very accurate with an error (normalized mean square error) of about 0.055, which is expected since the triangular elements building up the cell wall experience quite homogeneous forces in a single plane (Fig. III.5)C). In the 3D pressurized template, the error is slightly larger (0.058), as a result of some cell walls becoming curved. The errors in 3D are in general not high and the larger values come from curved cell surfaces, that are mainly located at the boundary where the cells are connecting the tissue to an infinitely stiff boundary in this simulation.

Next, growth is added to the template using an isotropic material where the growth is regulated by a strain signal and where cells are allowed to divide according to a shortest path rule after reaching a threshold size [34]. The accuracy of cell division performance is evaluated by comparing the principal values of the average strain tensor of daughter cells with each other and those of their mother cell before and after cell division. Differences are very low (Fig. III.6), and strikingly, even lower than in the non-growing situation (cf. Fig. III.5). The reason for that is that when a cell divides there is an update of the estimate of the resting edge connected to a division plane, which decreases the error in further estimations. The error is generally small and smaller in the 2D simulation (Fig. III.6D) then in the 3D simulation (Fig. III.6E). The outliers in the 3D case are again coming from the divisions that happen adjacent to the stiff boundary where non-planar cell walls appear.

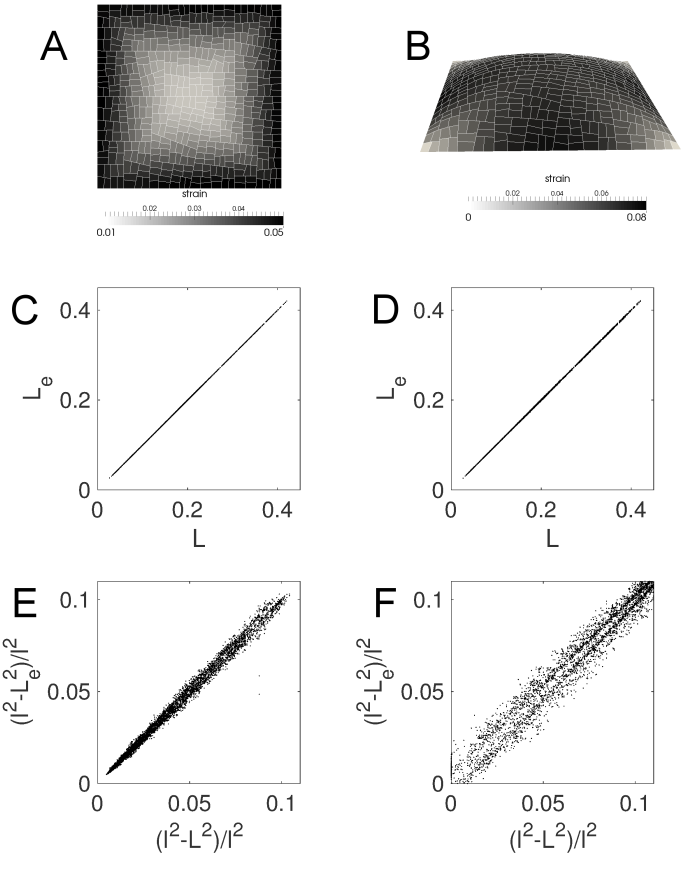

Figure III.5: **Resting shape estimation.** (A,C,E) A tissue strained by an in-plane isotropic stress. (B,D,F) A tissue strained into 3D by a pressure force from one side. (A,B) The maximal strain is visualized on the current shape. (C,D) The estimated, L_e resting lengths of all edges are compared with the known resting lengths, L. (E,F) The strain calculated from the estimated resting lengths vs the train calculated from the known resting lengths.

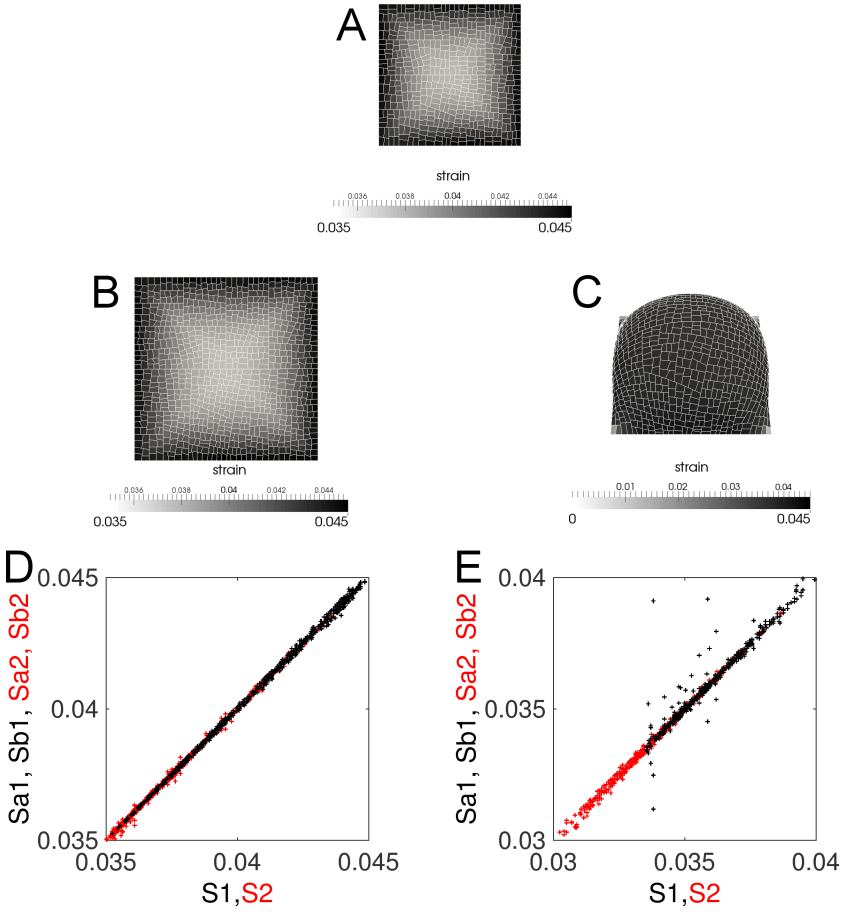

Figure III.6: **Growth and cell division.** (A) Initial tissue. (B) The grown tissue with cell division in 2D by isotropic forces applied. (C) The tissue grown using a pressure force from below. (D) Normalized mean square error (NMSE) is 0.002 (E) Error(NMSE) is 0.02 (including the outliers) (D-E) S1,S2 are the first and second principal values of strain in the mother cell before division, S1a and S2a are the principal values of strain in one of the daughter cells labeled with "a" after division and similarly S1b and S2b are the same values in the other daughter cell that is labeled with "b".

We have shown that the error in estimating the resting state from the strain field and current configuration is quite low in our approach, including in the case with growth and cell division that leads to re-meshing of the wall discretization. Errors are increased close to the boundary, which can easily be mediated by adding additional tissue between the boundary and the region of interest or alternatively define more advanced boundary conditions.

III.4 DISCUSSION AND CONCLUSIONS

We have presented a way by which the processes of cell growth and division can be incorporated in finite element simulations of a biological tissue with particular focus on plant cell wall growth. The proposed formulation allows for simulating biomechanical events for a prolonged period of time and analyzing dynamic phenomena that extend over large periods of time. This includes all morphogenetic events that can now be approached with proper amount of mechanical details on cellular scale, and where feedback from gene regulatory, hormonal, mechanical and environmental cues can be incorporated at levels of material properties as well as for growth rates and thresholds.

Inclusion of both growth and cell division causes several complications, which have to be carefully taken care of in order for a model to present consistent results. In particular, we show that our description of growth, when implemented using Saint Venant-Kirchhoff strain energy on triangular plates, provides a mesh-independent growth (Fig. III.3). Importantly, this includes the remeshing appearing at cell division, where we show how to preserve the strain field in dynamics remeshing (Fig. III.6). Further, we show how a variety of growth signals, including stress, strain or morphogens can be applied by altering mechanical properties of the cell walls, and how the residual stresses that result from different inputs can be identified. In particular we show how strain and stress based growth leads to less residual stresses, while a morphogen-based growth can lead to both tensional and compressing residual stresses even if the tissue is pressurized and only contain tensional stresses driving the growth (Fig. III.4). We have used a simplistic linear growth rate, inspired by the Lockhart model of growth [3], but our description allows for nonlinear inputs to growth rates and other parameters leading to growth. The current formalism would for example allow for adding growth in a consistent way to nonlinear changes of material properties from molecular or stress inputs, as previously has been applied in non-growth simulations where there was a nonlinear feedback from the plant hormone auxin on Young modulus [25], or a nonlinear

feedback on material anisotropy from principal stress directions [27, 29]. Also, the use of a specific strain energy formalism and triangular springs in our simulations is to exemplify possible applications, while the derivations presented in the Methods section are more generally applicable. While we have used examples of surfaces in two and three dimensions, there is nothing preventing the construction of tissues of 3D cells surrounded by 2D wall elements. Notably, we use two edges to connect two cell walls in our current description, and the 3D extension will need to adopt to connecting several cells by multiple edges and using two faces per mesh element to connect neighboring cells.

Our approach has similarities with some recent efforts of modeling plant cell wall growth [22, 26, 27, 31, 34, 37]. In several of these examples, 2D tissues or surfaces in 3D were described [27, 34, 37], where the walls were represented by 1D edge elements which cannot represent the material complexity described using our 2D descriptions of cell wall mechanics. An extension to this was to use proper 2D descriptions of the cell wall mechanics, but still apply the growth on edges of the mesh independently [26]. Such growth description will fail to be mesh-independent and will not be able to properly take into account anisotropies in material variables or in stresses. Most similar to our approach is the 2D element growth described in [31], where strain was applied as growth signal. The main difference is our reference system invariant description, more easily handling properties such as the growth threshold, and hence a more general methodology to add growth signals from strains, stresses, morphogens or other signals.

The need for detailed mechanical models is increasingly apparent for growth models in biology. Our work provides a rigorous way to include growth in such simulations, and its generality in terms of possibilities to include various input signals provides an important step towards models of plant morphogenesis over long time scales. The connection to the cells make it possible to connect the mechanical and growth description to 4D cellular data generated for example by confocal microscopy. As such, our description represents an essential model development within Computational Morphodynamics.

AUTHOR CONTRIBUTIONS

Conceived and designed the experiments: BB HJ. Performed the experiments: BB. Analyzed the data: BB PK HJ. Wrote the paper: BB PK HJ.

ACKNOWLEDGMENTS

This work was supported by the Swedish Research Council (VR2013:4632), the Gatsby Charitable Foundation (GAT3395/PR4), and the Knut and Alice Wallenberg Foundation via project ShapeSystems (KAW2012.0050).

REFERENCES

1. T. I. Baskin, "Anisotropic expansion of the plant cell wall," *Annu Rev Cell Dev Biol*, vol. 21, pp. 203–22, Jan 2005.
2. D. J. Cosgrove, "Growth of the plant cell wall.," *Nature reviews. Molecular cell biology*, vol. 6, pp. 850–61, nov 2005.
3. J. A. Lockhart, "An analysis of irreversible plant cell elongation," *Journal of theoretical biology*, vol. 8, pp. 264–275, Mar. 1965.
4. S. Braybrook and H. Jönsson, "Shifting foundations: the mechanical cell wall and development," *Curr Opin Plant Biol*, vol. 29, pp. 115–120, Jan 2016.
5. Y. B. Park and D. J. Cosgrove, "Xyloglucan and its interactions with other components of the growing cell wall.," *Plant & cell physiology*, vol. 56, pp. 180–194, Feb. 2015.
6. C. Somerville, "Cellulose Synthesis in Higher Plants," *Annu. Rev Cell Dev Biol*, vol. 22, p. 53–78, Oct. 2006.
7. T. Zhang, Y. Zheng, and D. J. Cosgrove, "Spatial organization of cellulose microfibrils and matrix polysaccharides in primary plant cell walls as imaged by multichannel atomic force microscopy - Zhang - 2016 - The Plant Journal - Wiley Online Library," *The Plant Journal*, 2016.
8. A. Peaucelle, S. A. Braybrook, L. Le Guillou, E. Bron, C. Kuhlemeier, and H. Höfte, "Pectin-induced changes in cell wall mechanics underlie organ initiation in Arabidopsis.," *Current biology*, vol. 21, pp. 1720–1726, Oct. 2011.
9. S. A. Braybrook and A. Peaucelle, "Mechano-chemical aspects of organ formation in Arabidopsis thaliana: the relationship between auxin and pectin.," *PloS one*, vol. 8, no. 3, p. e57813, 2013.
10. A. Peaucelle, R. Wightman, and H. Höfte, "The Control of Growth Symmetry Breaking in the Arabidopsis Hypocotyl.," *Current biology : CB*, vol. 25, pp. 1746–1752, June 2015.
11. D. L. Rayle and R. E. Cleland, "The Acid Growth Theory of auxin-induced cell elongation is alive and well.," *Plant physiology*, vol. 99, pp. 1271–1274, Aug. 1992.
12. K. Nishitani and Y. Masuda, "Auxin-Induced Changes in the Cell Wall Xyloglucans: Effects of Auxin on the Two Different Subtractions of Xy-

loglucans in the Epicotyl Cell Wall of Vigna angularis," *Plant & cell physiology*, vol. 24, pp. 345–355, Apr. 1983.
13. S. C. Fry, "Cellulases, hemicelluloses and auxin-stimulated growth: a possible relationship - Fry - 2006 - Physiologia Plantarum - Wiley Online Library," *Physiologia plantarum*, 1989.
14. P. Schopfer, A. Liszkay, M. Bechtold, G. Frahry, and A. Wagner, "Evidence that hydroxyl radicals mediate auxin-induced extension growth.," *Planta*, vol. 214, pp. 821–828, Apr. 2002.
15. D. J. Cosgrove, "Plant cell wall extensibility: connecting plant cell growth with cell wall structure, mechanics, and the action of wall-modifying enzymes.," *Journal of experimental botany*, vol. 67, pp. 463–476, Jan. 2016.
16. P. Marowa, A. Ding, and Y. Kong, "Expansins: roles in plant growth and potential applications in crop improvement.," *Plant cell reports*, vol. 35, pp. 949–965, May 2016.
17. P. Prusinkiewicz and A. Lindenmeyer, *Algorithmic Beauty of Plants*. Springer, New York, 1990.
18. F. Boudon, C. Pradal, T. Cokelaer, P. Prusinkiewicz, and C. Godin, "L-py: an L-system simulation framework for modeling plant architecture development based on a dynamic language.," *Frontiers in plant science*, vol. 3, p. 76, 2012.
19. R. Sievänen, C. Godin, T. M. DeJong, and E. Nikinmaa, "Functional-structural plant models: a growing paradigm for plant studies.," *Annals of botany*, vol. 114, pp. 599–603, Sept. 2014.
20. E. E. Kuchen, S. Fox, P. B. De Reuille, R. Kennaway, S. Bensmihen, J. Avondo, G. M. Calder, P. Southam, S. Robinson, A. Bangham, and E. Coen, "Generation of leaf shape through early patterns of growth and tissue polarity.," *Science (New York, N.Y.)*, vol. 335, pp. 1092–1096, Mar. 2012.
21. S. Sauret-Güeto, K. Schiessl, A. Bangham, R. Sablowski, and E. Coen, "JAGGED controls Arabidopsis petal growth and shape by interacting with a divergent polarity field.," *PLoS biology*, vol. 11, no. 4, p. e1001550, 2013.
22. R. Kennaway, E. Coen, A. Green, and A. Bangham, "Generation of diverse biological forms through combinatorial interactions between tissue polarity and growth.," *PLoS computational biology*, vol. 7, p. e1002071, June 2011.
23. R. Dyson, L. Band, and O. Jensen, "A model of crosslink kinetics in the expanding plant cell wall: Yield stress and enzyme action," *Journal of Theoretical Biology*, vol. 307, no. 0, pp. 125 – 136, 2012.

24. A. Nili, H. Yi, V. H. Crespi, and V. M. Puri, "Examination of biological hotspot hypothesis of primary cell wall using a computational cell wall network model," *Cellulose*, vol. 22, no. 2, pp. 1027–1038, 2015.
25. M. G. Heisler, O. Hamant, P. Krupinski, M. Uyttewaal, C. Ohno, H. Jönsson, J. Traas, and E. M. Meyerowitz, "Alignment between pin1 polarity and microtubule orientation in the shoot apical meristem reveals a tight coupling between morphogenesis and auxin transport," *PLoS Biol*, vol. 8, p. e1000516, Jan 2010.
26. G. W. Bassel, P. Stamm, G. Mosca, P. Barbier de Reuille, D. J. Gibbs, R. Winter, A. Janka, M. J. Holdsworth, and R. S. Smith, "Mechanical constraints imposed by 3D cellular geometry and arrangement modulate growth patterns in the Arabidopsis embryo.," *Proceedings of the National Academy of Sciences*, p. 201404616, May 2014.
27. O. Hamant, M. G. Heisler, H. Jönsson, P. Krupinski, M. Uyttewaal, P. Bokov, F. Corson, P. Sahlin, A. Boudaoud, E. M. Meyerowitz, Y. Couder, and J. Traas, "Developmental patterning by mechanical signals in arabidopsis," *Science*, vol. 322, pp. 1650–1655, Dec 2008.
28. A. Sampathkumar, P. Krupinski, R. Wightman, P. Malini, A. Berquand, A. Boudaoud, O. Hamant, H. Jönsson, and E. M. Meyerowitz, "Subcellular and supracellular mechanical stress prescribes cytoskeleton behavior in arabidopsis cotyledon pavement cells," *eLife*, vol. 3, p. e01967, 2014.
29. B. Bozorg, P. Krupinski, and H. Jönsson, "Stress and strain provide positional and directional cues in development," *PLoS Comp Biol*, vol. 10, p. e1003410, 2014.
30. M. Sassi, O. Ali, F. Boudon, G. Cloarec, U. Abad, C. Cellier, X. Chen, B. Gilles, P. Milani, J. Friml, T. Vernoux, C. Godin, O. Hamant, and J. Traas, "An Auxin-Mediated Shift toward Growth Isotropy Promotes Organ Formation at the Shoot Meristem in Arabidopsis.," *Current biology : CB*, vol. 24, pp. 2335–2342, Sept. 2014.
31. F. Boudon, J. Chopard, O. Ali, B. Gilles, O. Hamant, A. Boudaoud, J. Traas, and C. Godin, "A computational framework for 3D mechanical modeling of plant morphogenesis with cellular resolution.," *PLoS computational biology*, vol. 11, p. e1003950, Jan. 2015.
32. L. A. Taber, "Biomechanics of growth, remodeling, and morphogenesis," *Applied Mechanics Reviews*, vol. 48, pp. 487–545, Aug 1995.
33. R. L. Robertson, "Boundary identifiability of residual stress via the dirichlet to neumann map," *Inverse Problems*, vol. 13, pp. 1107–1119, 1997.
34. P. Sahlin and H. Jönsson, "A modeling study on how cell division affects properties of epithelial tissues under isotropic growth," *PLoS ONE*,

vol. 5, p. e11750, Jan 2010.
35. S. Besson and J. Dumais, "Universal rule for the symmetric division of plant cells," *Proc Natl Acad Sci USA*, vol. 108, pp. 6294–9, Mar 2011.
36. D. Kierzkowski, N. Nakayama, A.-L. Routier-Kierzkowska, A. Weber, E. Bayer, M. Schorderet, D. Reinhardt, C. Kuhlemeier, and R. S. Smith, "Elastic Domains Regulate Growth and Organogenesis in the Plant Shoot Apical Meristem," *Science*, vol. 335, pp. 1096–1099, mar 2012.
37. K. Alim, O. Hamant, and A. Boudaoud, "Regulatory role of cell division rules on tissue growth heterogeneity.," *Frontiers in plant science*, vol. 3, p. 174, jan 2012.

IV

ANISOTROPIC GROWTH IN PLANTS CAN RESULT FROM STRESS FEEDBACK ON WALL MATERIAL AND STRAIN-REGULATED GROWTH

Behruz Bozorg [1] and Henrik Jönsson [1,2,3].

[1] Computational Biology & Biological Physics, Lund University, Sölvegatan 14A, SE 223 62 Lund, Sweden.
[2] Sainsbury Laboratory, Cambridge University, Bateman Street, CB2 1LF Cambridge, United Kingdom.
[3] Department of Applied Mathematics and Theoretical Physics (DAMTP), University of Cambridge, Cambridge, United Kingdom.

LU TP 16-15 (submitted 2016)

Sizes and shapes of plants and their organs are essential for their functions and evolutionary fitness. Given the lack of cell migration and apoptosis plant form is created by heterogeneous and anisotropic growth. To gain a quantitative understanding of the genetics and physics behind morphogenesis is still one of the main challenges in biology.

Using computational morphodynamics models we show how a feedback between stresses and cell wall anisotropy together with a strain-based growth signal can lead to shapes seen in different plant tissues. In particular, we show that the competing idea of stress-based growth ultimately leads to shapes dissimilar to most plant organs. Further, we combine morphogen and strain-based signals for growth and elucidate how such models can generate different organ shapes and sizes. Finally, we also show how stress-feedback on material anisotropy and cell-layer organized growth together with strain-based growth are able to explain the reversal of the direction of cortical microtubules for a transiently elongating organ, as has been reported in for example hypocotyls and roots.

This work provides an improved quantitative description of plant cell growth. Using this model, we show that a combination of general and cell-type specific

hypotheses of molecular and physical interactions act in concert to regulate morphogenesis via strain-based growth in plants.

IV.1 INTRODUCTION

Plants have an astonishing variety of beautiful shapes generated mainly by heterogeneous and anisotropic growth [1]. Growth is driven by turgor pressure, guided by genetic and hormonal signals, and the anisotropic shapes are generated by the alignment of stiff cellulose fibers in specific directions [2]. In 1965, James Lockhart defined a growth rule for plant cells, where the elongation rate of cells is proportional to the pressure above a yield threshold [3]. Varieties of such growth model have recently been used in highly detailed [4], spring-based [5], and 2D descriptions of plant cell walls [6, 7].

While turgor pressure is providing the main forces for promoting growth, plant cell walls are the main factor for restricting growth and providing shapes via anisotropies in material stiffness [8, 9]. The cell wall is a composite material, where the stiff cellulose fibers are interconnected by xyloglucan molecules and sitting in a pectin matrix [8]. Growth is suggested to happen due to the breakage of connections between the cellulose fibers, which leads to a microscale sliding of wall components. An influx of water keeps the turgor pressure high while new material is added to keep the cell walls at roughly the same thickness [3, 9]. Still, the growth process and the wall material configuration are both highly complex and the development of an optimal quantitative description continues to be a challenge [10, 11].

Anisotropic growth is suggested to mainly be a result of the strong alignment of the cellulose fibers in patterns orthogonal to the growth directions [2]. The plant cells can control the direction since the cellulose fibrils are synthesised along tracks following the directions of cortical microtubules (MTs) [12, 13]. Several mechanisms have been suggested for regulating the directions of MTs, including light, auxin, and physical stresses, and they are all dependent on dynamical severing events where MTs are cut in a process dependent on katanin proteins [14–16]. While changing light conditions or auxin concentrations might not directly provide a directional cue, using the maximal principal stress as a cue can provide both magnitude and direction [17–19], and the correlation between maximal stress direction and MT alignment has been shown both at the tissue and subcellular scales [17, 20].

The cell pressure transforms into strains and stresses in the cell walls. Given the 3D extension of the walls and the anisotropy in terms of stiffness of the wall material, maximal strain and stress directions may not agree between walls of a cell or even within a single cell wall [18]. Hence, it be-

comes important to correctly interpret the growth rule defined by Lockhart [3] in terms of strain and stress and to understand the consequences for morphogenesis depending on the selected signal for growth. While Lockhart explicitly used stress for the wall elongation rates, as he was analysing elongation in a single dimension, either stress or strain would have worked. In addition, genes and hormones are involved in regulating plant growth [21, 22], and a combined description is essential for quantitatively being able to understand morphogenesis.

Several recent models include growth processes for plant development beyond simple spring descriptions. At the tissue scale, finite element models have been used to generate mainly 2D shapes of plant organs where growth has been promoted by morphogen [23, 24], or mechanical signals [25]. A 3D effort combines morphogen signals with a Lockhart description of growth [6] to show that mechanics can translate the maximal growth to regions away from maximal morphogen levels. Another 3D example was used to show that the outgrowth of primordia at the shoot can be promoted by making the wall material isotropic at the primordia site [7, 26]. Neither of these models includes cell divisions, which recently was included in a non-mechanical geometrical description of embryo development [27].

Here, we develop a modeling framework where we can test different hypotheses for promoting growth, based on previous work [18, 28]. We apply the model to different plant tissues, to investigate hypotheses for growth based on stress, strain and molecular inputs. First, we compare the shapes generated when growth is promoted by strain or by stress. Then, we analyse the shape of the shoot and the initial primordia formed at the shoot when a combination of morphogen and mechanical-based signals is promoting growth. We also compare loosening of the wall material as a growth mechanism with a change in yield threshold. Finally, we propose a rule for growth together with a stress feedback on material anisotropy that is able to predict the reversal of microtubules at the growth of anisotropic organs, following what has been reported in hypocotyls and roots [15, 29].

IV.2 RESULTS

IV.2.1 *Growth promoted by elastic strain can predict growth domains compatible with plant tissues*

The distribution of stresses and their anisotropies in a pressurised epidermis is resulting from the shape of the organs and cells [17, 20, 30]. The curvature determines the direction, size and anisotropic properties of stresses (Fig. V.1A), while material anisotropy in different domains can be inferred

from alignment properties of microtubules[13, 17]. Given the stresses and material properties, a strain field arises. Analysing the growth rules for small elements of a material is useful for understanding the complicated deformations at tissue scale that are the integral of small and simpler increments. Such reduction, has the advantage of having countable number of variables and parameters for building the fundamental hypotheses for how growth is regulated. To better understand the differences between strain and stresses as potential growth signals, we take advantage of such simplification and analyse a planar element (Figs. V.1 B-F). We consider measures of force and deformation as stress and strain values and anisotropies (first and second principal components), when both material anisotropy, κ (Eq. 2) and stress anisotropy, α (Eq. 1), vary within a range between 0 (isotropic) to 0.8 (highly anisotropic) (Fig. V.1B-F).We assume constant overall material elasticity across the tissue. Maximal stress and strain can be perpendicular or parallel in different regions in the parameter space (black and white domains in Fig. V.1D), and the values of strain and stress show completely different behaviours (Figs. V.1 B,E vs. C,F). While the stress value (and direction) always follow the loading forces and has no dependence on material anisotropy (Fig. V.1 C), the strain shows a more complex behavior, where either large loading forces or large material anisotropy can lead to large strains (Fig. V.1 B). The large material anisotropy causes the maximal strain to be perpendicular to the maximal force direction (Fig. V.1 D).

By noticing the approximate degrees of tissue anisotropy and stress anisotropies in different domains of the plant shoot (Fig. V.1A, [17]), these regions can be represented in the parameter space of the patch analysis (Figs. V.1 B-F). The central zone (CZ) at the very apex has isotropic forces (given the isotropic curvature), and no clear anisotropy in material stiffness. The curvature gradually decreases in the radial direction when tracing a path from the CZ via the periphery of the shoot (PZ), to the stem region (S). This leads to increased anisotropies in materials and stresses, where $\alpha = 0.5$ is expected at S given the close to cylindrical shape. Finally, the largest anisotropic forces are predicted at the boundary (B) between the shoot and an initiating primordium.

Interestingly, both strain and stress magnitudes increase when moving from CZ via PZ to S (Figs. V.1 B, C), and this correlates with growth rates reported [31]. However, when analysing maximal strain and stress values, the corresponding directions need also to be considered (Fig. V.1D. Then there is quite a striking difference: the maximal strain direction is radial in PZ and axial in S, which predict plant growth patterns [31], while the maximal stress direction is circumferential in these regions. In CZ both stress and strain are low, and isotropic as reported for growth in experiments [31].

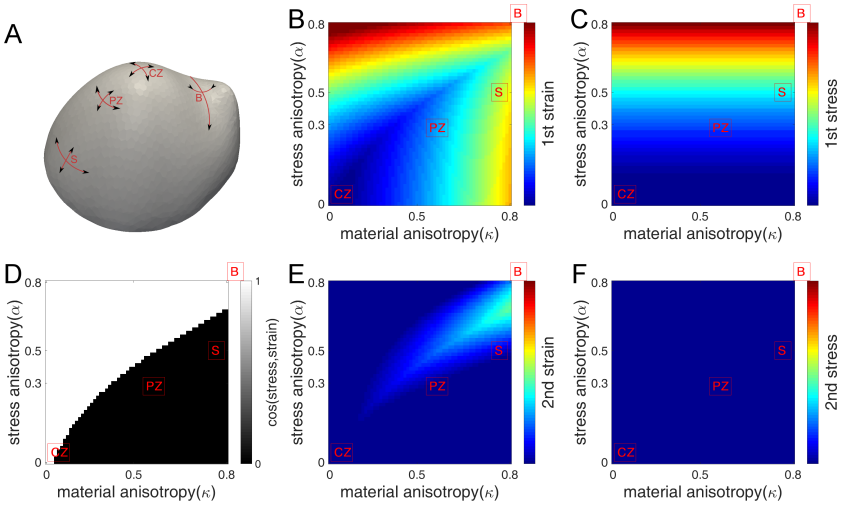

Figure IV.1: **Comparing the strength of stress and strain signals versus different values of stress and material anisotropy** (A) A representation of the shape in the shoot apical meristem. The key domains with distinct material and stress anisotropies are marked with CZ as central zone, PZ as peripheral zone, S as stem and B as boundary between shot and primordium. In each domain arrows are indicating the direction and values of principal stresses. (B,E) The strength of 1st (B) and 2nd (E) strain signal is shown versus different values of stress and material anisotropy for a planar patch of material. Different domains marked in (A) are marked using approximate values of stress and material anisotropy. (C,D) similar to B and E but for the strength of 1st and 2nd eigenvalues of stress. (D) Relative direction of maximal stress and strain versus stress and material anisotropy. Those are perpendicular in the black region and parallel in the white region.

Possibly, the boundary sits outside of the analysed domain in the parameter space, as the stress anisotropy (and possibly material anisotropy) is high. The boundary is a special case since the stresses are not fully determined by curvature of the epidermis. Due to the negative curvature the internal tissue becomes an important player for resisting stresses.

Using a patch simulation and testing large ranges of loading forces and material anisotropies, it was possible to show similarities and differences between using stress or strain as signal for plastic growth. In particular, while the maximal values have some agreements, the two signals predict completely opposite growth directions in the PZ and S, where the simulations indicate that a strain model is in more agreement with measured growth directions.

IV.2.2 *Correct interpretation of Lockhart's growth model is required to generate correct growth patterns in plant tissues*

The detailed analysis of how stresses and strains change for different loading forces and material properties from the previous section is of great importance since such anisotropic properties of material and stresses are both present in the plant epidermis. The analysis indicates that Lockhart's pressure description of growth regulation needs a careful interpretation to predict growth magnitudes and directions in a more complex tissue situation. To understand how strain and stress signals used as plastic growth promoters act on a tissue scale, we developed a cell-based model of an epidermal tissue where any mechanical and non-mechanical signal can be used to promote growth (Methods, [28]). We used a template of the epidermis, which was pressurised from the inside (Fig. V.2A), and where each cell has the same material model and the same growth and division rules (Methods). It is the dynamical shape of the tissue that will lead to stress and strain patterns for a single cell that then can feedback on growth of this cell, while cells still interact mechanically with neighboring cells to maintain the continuity of the whole tissue. Equation11 is used to regulate growth in individual cells using principal values and directions of stress or strain.

Applying plastic growth induced by stress leads to a spherical shape after a period of growth (Fig. V.2B). This is since any anisotropy in the curvature will generate an anisotropy in stress and extending the material more in this high-stress direction will act to make the curvature more isotropic (until a perfect spherical shape is achieved). Interestingly, using an isotropic material or dynamical anisotropic material based on a stress feedback, which potentially can hold back extension in most stressed directions, gives the same result. This is because the stress pattern does not depend on material anisotropy (Fig. V.1C, but only on the loading forces that would not change when changing material.

If an isotropic material is used, strains and stresses are behaving exactly the same, and if strain is provided as a growth signal together with an isotropic material, again a more spherical shape would appear (cf. Fig. V.2B). However, applying a strain based promotion of plastic growth together with an anisotropic material where stress feeds back to the material (anisotropic) stiffness, can lead to amplification of shape anisotropy (Fig. V.2C). The stress feedback mechanism makes the material stiffer in the direction of larger stress (curvature), and this can lead to higher strain values in the axial direction. Such behavior occurs in a particular range of anisotropic

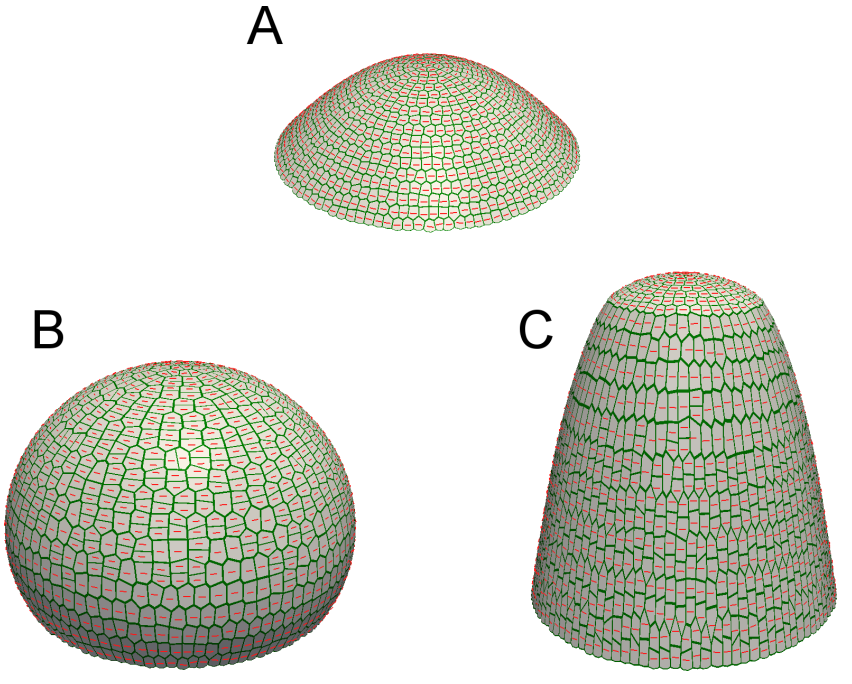

Figure IV.2: **Stress versus strain as growth signal.** The template is pressurised where there is a stress based growth or strain based growth dynamics with a constant yield threshold. The cells divide after reaching a threshold size. The division takes place close to the shortest path within each cell. (A) The dome-like template which is used as the initial state of the simulation. (B) The final state of stress based growth after a finite growth period. Using the isotropic or anisotropic material does not alter the final state noticeably. (C) the final state of strain based growth together with stress feedbak to the direction and degree of anisotropy[18]

.

stress and anisotropic material stiffness, where maximal strain is perpendicular to maximal stress (black region in Fig. V.1D). In the case of a cylindrical symmetry (stress anisotropy $\alpha \approx 0.5$), which is very common in plants, a material anisotropy (κ) above about 0.5 would lead to axial plastic growth if the growth is promoted by strain. Generally this mechanism can amplify or at least maintain the anisotropic curvature of the organ surfaces.

In summary, the model predicted that if mechanical signals are used as the main promoter of plastic growth, a combination of growth promoted by strain and material anisotropy promoted by stress leads to the generation

of typical plant organ shapes. This means a reinterpretation of Lockhart's original idea where he discussed the pressure-driven cell growth in terms of a stress-based cell wall elongation [3].

IV.2.3 *A combination of strain and morphogen as input to growth prescribes the shape and size of the tissue*

In the previous section, the aim was to discern between different mechanical inputs for plastic growth by comparing the resulting shapes. In those simulations, all cells in the tissue behaved with exactly the same mechanical rules. There is also a cell-type specific component to growth, and we aim to address how this affect tissue shape by assuming that a morphogen can influence the system by altering material properties and/or growth parameters. The morphogen can be interpreted as genetic or hormonal contributions, e.g. [21, 22].

First, we noticed that in the strain-induced growth simulation, which resulted in an appropriate stem elongation, the tissue has a quite flat meristem region (Fig. V.2C). Different plant species have differently shaped meristems, and the vegetative meristem in *Arabidopsis* is one example of a flat meristem [32]. Still, a paraboloid has been shown to provide an excellent quantitative fit to the meristem surface shape for a large collection of meristems of different sizes [33], and it is not trivial to generate these more dome-like shapes in the strain-based simulations. The reason for the flat structure is the lack of growth at the apex (Fig. V.2C), due to a strain lower than the yield threshold. The threshold was set to avoid radial growth in the stem region, and decreasing the threshold would lead to mainly axial but also a radial component of growth at the stem.

Some radial growth at the stem might not be problematic, but the simulation pinpoints that a cell-type specific component to growth might be needed for a more complex regulation of growth [21]. We explored a scenario of a combined strain and morphogen input to the regulation of growth by producing a diffusing morphogen at the center of the CZ (Methods). In this case, the morphogen reduced the strain yield threshold at high concentrations (Eq. 16). This results in higher growth rates in the central domain and a more dome-like shape (Fig. IV.3 A, cf. Fig. V.2 C), visually more resembling an *Arabidopsis* inflorescence shape [33]. Strikingly, adjusting the morphogen production rate is directly influencing the meristem size and thereby the stem radius (Fig. IV.3 B).

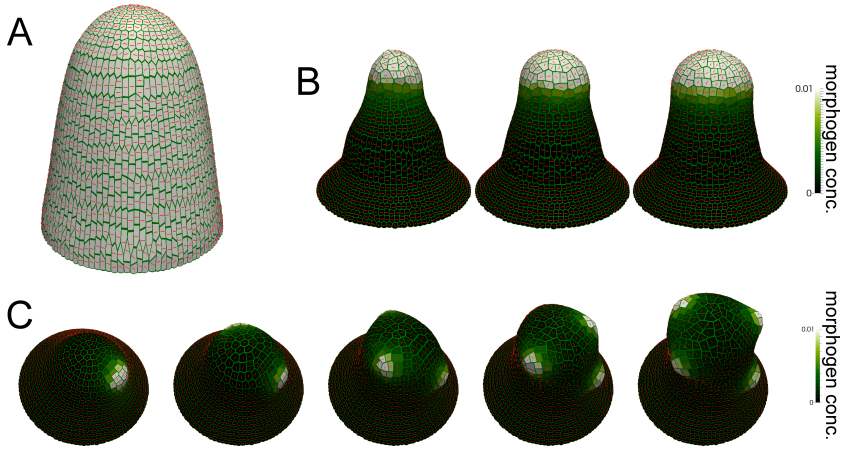

Figure IV.3: **Addition of morphogen to strain based growth.** A) Similar to Fig. V.2C together with dependence of the growth threshold on a morphogen concentration. B) By changing the production rate of the morphogen it is possible to regulate the stem size. Here, the production rate is increased from left to right. The template and all other model parameters are the same in the three different cases. C) A second morphogen is employed to destroy the fiber component of the composite material in the cell wall. By successive addition of morphogen production to the patches of cells in the peripheral zone a phyllotactic pattern is generated.

Next, a second morphogen was added at the sites of primordia initiation in the PZ (Fig. IV.3 C). While there is a change of stress patterns from circumferential around the shoot to circumferential around the primordia, and increased growth in the primordia, the CZ part is relatively unaffected. This morphogen can be interpreted as the plant hormone auxin [34], and the effect of auxin was to lower the stiffness of the wall material (Eq. 15), as proposed experimentally [35]. In this implementation the reduction is via the fiber content and will result in lower stiffness in general, but also more isotropic material [26].

We used two examples how a morphogen could effect the growth rate by changing material properties in the wall (Eqs. 15, 16). Our experience is that while the morphodynamical changes induced by these alterations are quite similar, they are useful in terms of interpreting the mechanism in the context of other experiments. While, auxin has been suggested to weaken the walls, atomic force microscopy has been used to show that the CZ actually has cells with stiffer walls [36]. Hence we implemented the threshold-lowering mechanism for the morphogen produced in this region.

We showed that the effect of morphogens can be added by adjusting different growth parameters with similar effects, and that the combination of morphogens and strain as input signals for growth rates allows for a tunable system for morphogenesis. In particular, we showed how different meristems shapes and sizes could be generated.

IV.2.4 *Cell layer specific growth can predict microtubular dynamics in transiently elongating plant cells*

In multiple cases of transient cell elongation in plant tissues, for example in hypocotyls and roots, the elongation direction is perpendicular to the MT and fiber directions, and there is a correlation between the reduction of growth and reorientation of the MTs in the elongating direction [29, 37]. Whether the reduction in elongation rate is caused by the MT reorientation is still under debate [38].

Given that the geometry of the tissue is not changing drastically during these events, it is of interest to see if a model using strain induced growth together with a stress feedback on material anisotropy is able to predict such dynamical events for the MTs. To investigate this, we model this system by pressurizing a cylinder, resembling a hypocotyl or root epidermis (Fig. IV.4A). Similar to the stem region in our previous simulations, material anisotropy can be adjusted such that maximal strain is in the longitudinal direction, although the maximal stress is in the circumferential (hoop) direction (Fig. IV.4A). Adding plastic growth promoted by the strain does not change this stress pattern (Fig. IV.4B). Similarly, if plastic growth would be halted again, the stress pattern would not change, and the reorientation of the MTs would not be predicted by a stress feedback model on MT directions.

So far, the model has only taken into account the growth of the epidermal cells, although several layers contribute to the tissue growth. In particular, tissue-cutting experiments suggest the internal cell layers to be under compression in the longitudinal direction, compared to the epidermal tissue [30]. This can be interpreted as the internal cell layers exert a 'force' on the epidermis in the longitudinal direction. For the cases when epidermal and internal layers are either not growing or both growing (Figs. IV.4 D, E), the stress patterns look the same (Figs. IV.4 A, B). However, if the growth is halted in the epidermal layer while the internal cells are still expanding (Fig. IV.4 F), a reversal of the stress can appear (Figs. IV.4 C, G).

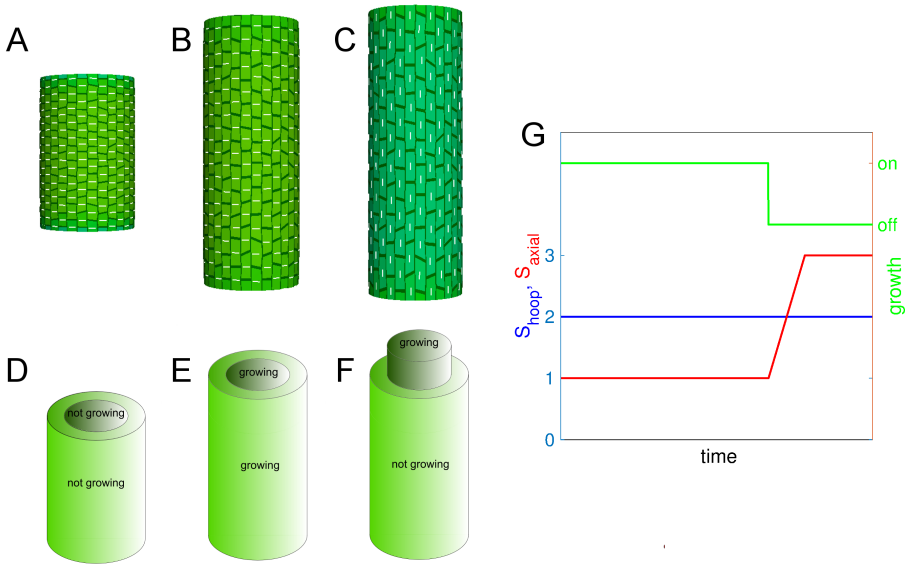

Figure IV.4: **MT dynamics during transient cell elongation** A hollow pressurized cylinder as a model for a hypocotyl/root is used togther with strain based growth. A) initial state. B) The state after a period of growth. C) The result of halting growth together with application of an additional axial force applied in the form of pressure to the system. D,E,F) Illustrations for the assumptions that are made in A,B and C, respectively. The reversal of direction of microtubules might be assumed as the result of interaction between a growing interior and non-growth epidermal cell layer. (G) A plot showing the values of stresses in hoop and axial directions as well as the status of the growth process. On the left side of the plot stresses results from isotropic pressure while the growth mechanism is on. Moving towards right in the plot we reach a time where growth is halted in the epidermis. From here on we add an additional axial force to the system while it is gradually increasing.

In summary, by adding cell-layer specific growth to the model, inspired by expansion data [30], the stress can be used as a predictor for MT directions also in the dynamical situation of transient cell elongation [29, 37].

IV.3 DISCUSSION

We have defined a growth description that is able to predict morphogenesis in several plant tissues. The unifying idea is to use strain as a regulator of growth, and by this generate anisotropic shapes (Fig. IV.5). This

highlights the need of a specific interpretation of the Lockhart model [3], where pressure above a yield threshold defined the elongation rate. Since Lockhart related the pressure to stresses and stress yield thresholds in the walls, it is a reinterpretation, but in his one-dimensional case, the strain and stress would behave similarly. The cell pressure will generate both strains and stresses in the walls, and in a situation of isotropic wall material the maximal principal directions of these would agree. In the cases we have investigated, walls can be anisotropic, and stresses and strains can be perpendicular [18] (Fig. V.1). In particular, the use of strain for defining growth instead of stress becomes important to predict published growth data (Fig. V.1) [31], both in terms of magnitude and directions.

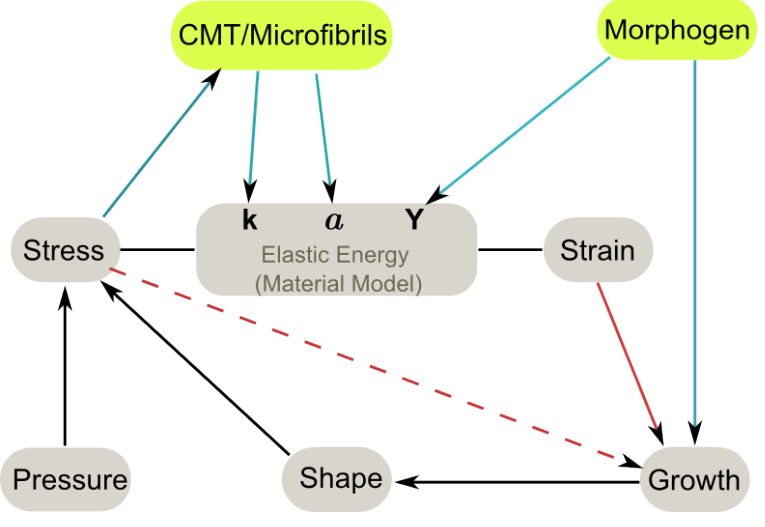

Figure IV.5: **Possibilities for modelling growth** Y is the overall elasticity, k represents mechanical anisotropy and a is the vector of anisotropy direction. CMT is the short term for Cortical Microtubules. Mechanical parameters and variables are in gray boxes and biological variables are in green boxes. Morphogen represents any biological component that can regulate the growth process. This includes the plant hormone auxin. The arrows and lines in black show physical connections. There are strong experimental evidences for blue arrows that show the potential feedback mechanisms between mechanical and biological components of the system. The red arrows are mechanical candidates for growth regulation.

We also showed that the implementation of growth, either by loosening wall stiffness, or by changing the yield threshold can lead to very similar shapes, and importantly, that a strain based growth by itself is not able

to generate all possible shapes. For this, we propose a combined signal for growth, where the strain input is integrated with morphogen signals where the size and shape of the tissue after growth is highly tunable. In our examples meristem shapes varied from flat to dome-shaped (Fig. V.2). The morphogen was in this case provided from the apex, and the shapes resemble those found when modeling tip-growing cells [39], although at a different scale. In addition a second morphogen was shown to provide primordia growth by adjusting cellulose fibers [26], with a reorganisation of the stress patterns surrounding the buds.

An interesting dynamics of wall material anisotropy is given in slender organs where cells elongate for a finite time, like the hypocotyl or the root [29, 37]. Interestingly, as seen by visualising microtubule directions, the fibers are aligning transversely during the initial phase of highly anisotropic growth in the longitudinal direction. At the time of growth decrease, the microtubules reorient towards the longitudinal direction, and it is not well understood how this is regulated, neither if the reorientation is causal of the halted growth [38]. We have previously shown that under the assumption of tension in the epidermal tissue, a stress feedback would robustly align the microtubules in a transverse direction [18]. Here, we show that this is still the case if plastic growth driven by strain is added. This is also the case if growth from the internal cell layers provides a longitudinal force onto the epidermal cells. But this is true only as long as new material is continuously added, and the reversal, seen in experiments, comes from the stopping of addition new wall material in the epidermal cells (Fig. IV.4). Our model clearly predicts that the halting of growth in the epidermis leads to the reorientation of the wall anisotropy, which in turn counteract growth, hence generating a positive feedback system for halting growth. While the additional cell-layer hypothesis is needed for predicting correct MT dynamics in this case, the added hypothesis is based on data on residual stresses in epidermis vs. internal cell layers [30].

Several growth models for plant tissue in 2D and 3D have been developed recently. We argue that the way they grow the tissue lack several important features for an optimal quantitative description of plant tissue growth. Either they continuously remove stresses to avoid complications [23, 25], or they grow edge elements independently, which can lead to a non-consistent description if anisotropic material is taken into account [6]. Also, compared with the effort in [7], which is the most similar model to ours, we propose our description is simplified by being reference system free, and we have a well defined algorithm to keep the strain field at cell divisions [28]. Our model is compatible with anisotropic growth of anisotropic material and allows for tracking residual stresses and keep strain fields after remeshing,

which is essential for large deformations. As such, the model provides an approach to truly investigate plant cell growth by combining morphogen and mechanical signals as dynamical inputs.

IV.4 MODELS

We extended material models and growth and division models from previous efforts [5, 17, 18, 28].

Measures of stress and material anisotropy

We measure stress anisotropy via

$$\alpha = 1 - \frac{S_{min}}{S_{max}}, \tag{1}$$

where S_{min} and S_{max} are the smallest and largest eigenvalues of the stress tensor. Similarly we introduce material anisotropy by

$$\kappa = 1 - \frac{Y_T}{Y_L}, \tag{2}$$

where again Y_T and Y_L are the smallest and largest elasticity constants of the material in the material coordinate system of the planar element. The assumption of constant overall material elasticity can be expressed as

$$Y_L + Y_T = Y_{overall} \tag{3}$$

where $Y_{overall}$ is constant.

IV.4.1 *Material models of anisotropic tissue*

We use St. Venant-Kirchoff description for the isotropic elastic energy [18],

$$W_{iso} = \frac{\lambda}{2}(tr\boldsymbol{E})^2 + \mu tr\boldsymbol{E}^2 \,, \tag{4}$$

where $\boldsymbol{E}$ is the Green-Lagrange strain tensor and λ and μ are the Lame coefficients of the material. We assume plane stress condition where the Lame constants can be expressed as

$$\lambda = \frac{Y\nu}{1-\nu^2}, \quad \mu = \frac{Y}{2(1+\nu)} \,, \tag{5}$$

where Y and ν are the Young modulus and Poisson ratio, respectively. For anisotropic material we add the following correction to the energy

$$W_{aniso} = \frac{\Delta\lambda}{2} \langle a|\boldsymbol{E}|a\rangle \, tr\boldsymbol{E} + \Delta\mu \langle a|\boldsymbol{E}^2|a\rangle \,, \tag{6}$$

where $|a\rangle$ is the anisotropy vector, which shows the direction in the material with the largest elasticity constant. The $\Delta\lambda$ and $\Delta\mu$ are the differences between longitudinal and transverse Lame coefficients which are in turn related to Young modulus in longitudinal and transverse directions and Poisson ratio.

Elements are triangular plates under plane stress condition that provide an adequate description for the epidermis [18]. The stress tensor can then be calculated via

$$\mathbf{S} = \frac{\partial W}{\partial \mathbf{E}} \,, \tag{7}$$

where $W = W_{iso} + W_{aniso}$. For spatial discretisation, we use triangular plates[18].

IV.4.2 *Regulating tissue anisotropy by stress feedback*

For regulating material anisotropy in the simulations for Figs. V.2-IV.4, we use the direction of maximal stress and stress anisotropy measure from Eq. 1. In the model it is assumed that the overall elastic strength of the material is maintained according to Eq. 3. Longitudinal and transverse Young moduli are updated via simple Euler steps in time as

$$\Delta Y = K^Y_{rate} \Delta t (Y_{new} - Y_{old}) \,, \tag{8}$$

where K^Y_{rate} determines the rate of update, Δt is the time step, Y_{old} refers to current values and Y_{new} indicates the new values of longitudinal and

transverse Young moduli. Young moduli can be evaluated from the relation between stress and material anisotropy via

$$Y_L = Y_{Matrix} + 0.5(1 + \frac{\alpha^n}{(1-\alpha)^n K^n + \alpha^n}) Y_{Fiber} \ ,$$
$$Y_T = Y_{Matrix} + 0.5(1 - \frac{\alpha^n}{(1-\alpha)^n K^n + \alpha^n}) Y_{Fiber} \ , \tag{9}$$

where K and n are model parameters and Y_{Matrix} and Y_{Fiber} are Young moduli of the isotropic matrix and anisotropic fiber part, respectively.

The update for anisotropy direction is done based on

$$\Delta |a\rangle = K^a_{rate} \Delta t (|S_m\rangle - |a\rangle) \ , \tag{10}$$

where $|a\rangle$ is the current anisotropy direction vector and $|S_m\rangle$ is the maximal stress direction vector. K^a_{rate} again sets the time delay.

IV.4.3 *Continuous growth using mechanical signals*

For stress or strain-based growth the growth tensor, can be defined as

$$f_g = K^G_{rate} \Sigma_i \mathcal{R}(S_i - S_{th}) |S_i\rangle \langle S_i| \ , \tag{11}$$

where S_i and $|S_i\rangle$ are the i^{th} principal value and vector of strain or stress in the resting configuration [28]. S_{th} is the strain or stress threshold for growth. K_{rate} is the growth rate and $\mathcal{R}$ is the ramp function defined by

$$\mathcal{R}(x) \quad = \quad \begin{cases} 0 & if \ \ x \leq 0 \ , \\ x & if \ \ x > 0 \ . \end{cases} \tag{12}$$

IV.4.4 *Cell division*

For cell division a volume threshold is considered above which cells divide. The division rule we use is the shortest path in the cell that halves the cell [5]. However the effect of division rule on deformations in tissue scale is not studied in this paper.

After each division we re-mesh the new cell walls and the resting shape of new elements are approximated via

$$L = [\Sigma_i (1 - 2\mathcal{S}_i) \langle l | \mathcal{S}_i \rangle^2]^{\frac{1}{2}} , \tag{13}$$

where $\mathcal{S}_i$ and $|\mathcal{S}_i\rangle$ are the i^{th} eigenvalue and eigenvector of the Almansi tensor averaged over the elements of the mother cell and $|l\rangle$ is the corresponding element edge vector in the current configuration [28].

IV.4.5 *Morphogen concentration*

The dynamics of the concentration of morphogens in the cells is based on constant production of the morphogen in one or a few cells at the tip where the production rate is constant. The morphogen is degraded in all cells and moves passively between cells according to a diffusion-like equation. For a cell with index i this can be formulated via

$$\frac{dC_i}{dt} = k_p^i - k_d C_i + k_D \Sigma_{j=1\ldots n} L_{ij} (C_j - C_i) , \tag{14}$$

where k_p^i is the production rate and is non zero only for one or a few cells at the tip. k_d is the degradation rate and k_D is the diffusion (or permeability) constant. The index j refers to one of the n neighbours of cell i and L_{ij} is the interface between the cell i and its j^{th} neighbour. The sum over the cell neighbours is in fact discretised form of $\nabla^2 C$ and introduces the diffusion between adjacent cells.

IV.4.6 *Reduction of stiffness versus growth threshold by morphogen*

The effect of a morphogen on growth was implemented in two ways. It can reduce the elasticity constant of the material

$$Y_{Fiber} = Y_{Max} + (Y_{Min} - Y_{Max}) \frac{C^n}{K^n + C^n} , \tag{15}$$

where C is the morphogen concentration, K and n are parameters of the nonlinear Hill function, Y_{Fiber} is the elasticity constant of the fiber network in the wall (Eq. 9) and Y_{Max} and Y_{Min} are the limits for elasticity constant when $C = 0$ and $C = \infty$ respectively.

Another implementation we used is the impact of morphogen on the growth threshold

$$S_{th} = S_{thMax} + (S_{thMin} - S_{thMax}) \frac{C^n}{K^n + C^n} \ . \tag{16}$$

This equation is the same as Eq. 15, which now is used for growth threshold S_{th} and its upper and lower limits(S_{thMax}, S_{thMin}).

AVAILABILITY

The software used for the simulations are available upon request (http://dev.thep.lu.se/Organism). File describing the models, the initial geometries and solver configurations are provided as Supplemental Information.

AUTHOR CONTRIBUTIONS

Both authors designed models and experiments. BB implemented and simulated all models. Both authors analysed data. Both authors wrote and edited the paper.

ACKNOWLEDGEMENTS

This work was supported by the Swedish Research Council (VR2013:4632), the Gatsby Charitable Foundation (GAT3395/PR4), and the Knut and Alice Wallenberg Foundation via project ShapeSystems (KAW2012.0050).

REFERENCES

1. D. Barabe and R. Jean, *Symmetry in plants*. World Scientific Publishing Co Pte Ltd, 1998.
2. P. B. Green, "Mechanism for plant cellular morphogenesis," *Science*, vol. 138, no. 3548, pp. 1404–1405, 1962.
3. J. A. Lockhart, "An analysis of irreversible plant cell elongation," *Journal of Theoretical Biology*, vol. 8, no. 2, pp. 264 – 275, 1965.
4. R. Dyson, L. Band, and O. Jensen, "A model of crosslink kinetics in the expanding plant cell wall: Yield stress and enzyme action," *Journal of Theoretical Biology*, vol. 307, no. 0, pp. 125 – 136, 2012.
5. P. Sahlin and H. Jönsson, "A modeling study on how cell division affects properties of epithelial tissues under isotropic growth," *PLoS ONE*, vol. 5, p. e11750, Jan 2010.

6. G. W. Bassel, P. Stamm, G. Mosca, P. Barbier de Reuille, D. J. Gibbs, R. Winter, A. Janka, M. J. Holdsworth, and R. S. Smith, "Mechanical constraints imposed by 3D cellular geometry and arrangement modulate growth patterns in the Arabidopsis embryo," *Proceedings of the National Academy of Sciences of the United States of America*, vol. 111, no. 23, pp. 8685–8690, 2014.
7. F. Boudon, J. Chopard, O. Ali, B. Gilles, O. Hamant, A. Boudaoud, J. Traas, and C. Godin, "A computational framework for 3d mechanical modeling of plant morphogenesis with cellular resolution," *PLoS Comput Biol*, vol. 11, pp. 1–16, 01 2015.
8. D. J. Cosgrove, "Growth of the plant cell wall.," *Nature reviews. Molecular cell biology*, vol. 6, pp. 850–61, nov 2005.
9. T. I. Baskin, "Anisotropic expansion of the plant cell wall," *Annu Rev Cell Dev Biol*, vol. 21, pp. 203–22, Jan 2005.
10. D. J. Cosgrove, "Plant cell wall extensibility: connecting plant cell growth with cell wall structure, mechanics, and the action of wall-modifying enzymes.," *Journal of experimental botany*, vol. 67, pp. 463–476, Jan. 2016.
11. S. A. Braybrook and H. Jönsson, "Shifting foundations: the mechanical cell wall and development," *Current Opinion in Plant Biology*, vol. 29, pp. 115 – 120, 2016. Growth and development.
12. T. Arioli, L. Peng, A. S. Betzner, J. Burn, W. Wittke, W. Herth, C. Camilleri, H. Höfte, J. Plazinski, R. Birch, A. Cork, J. Glover, J. Redmond, and R. E. Williamson, "Molecular Analysis of Cellulose Biosynthesis in Arabidopsis," *Science*, vol. 279, pp. 717–720, Jan. 1998.
13. H. E. McFarlane, A. Döring, and S. Persson, "The Cell Biology of Cellulose Synthesis," *Annual Review of Plant Biology*, vol. 65, pp. 69–94, Apr. 2014.
14. M. Uyttewaal, A. Burian, K. Alim, B. Landrein, D. Borowska-Wykręt, A. Dedieu, A. Peaucelle, M. Ludynia, J. Traas, A. Boudaoud, D. Kwiatkowska, and O. Hamant, "Mechanical stress acts via katanin to amplify differences in growth rate between adjacent cells in Arabidopsis.," *Cell*, vol. 149, pp. 439–51, apr 2012.
15. J. J. Lindeboom, M. Nakamura, A. Hibbel, K. Shundyak, R. Gutierrez, T. Ketelaar, A. M. C. Emons, B. M. Mulder, V. Kirik, and D. W. Ehrhardt, "A mechanism for reorientation of cortical microtubule arrays driven by microtubule severing.," *Science (New York, N.Y.)*, vol. 342, pp. 1245533–1245533, Dec. 2013.
16. X. Chen, L. Grandont, H. Li, R. Hauschild, S. Paque, A. Abuzeineh, H. Rakusová, E. Benková, C. Perrot-Rechenmann, and J. Friml, "Inhibition of cell expansion by rapid ABP1-mediated auxin effect on micro-

tubules.," *Nature*, vol. 516, pp. 90–93, Dec. 2014.
17. O. Hamant, M. G. Heisler, H. Jönsson, P. Krupinski, M. Uyttewaal, P. Bokov, F. Corson, P. Sahlin, A. Boudaoud, E. M. Meyerowitz, Y. Couder, and J. Traas, "Developmental patterning by mechanical signals in arabidopsis," *Science*, vol. 322, pp. 1650–1655, Dec 2008.
18. B. Bozorg, P. Krupinski, and H. Jönsson, "Stress and strain provide positional and directional cues in development," *PLoS Comp Biol*, vol. 10, p. e1003410, 2014.
19. B. Bozorg, P. Krupinski, and H. Jönsson, "Morphogenesis can be guided by the dynamic generation of anisotropic wall material optimizing strain energy," *LU TP*, pp. 16–12, 2016.
20. A. Sampathkumar, P. Krupinski, R. Wightman, P. Milani, A. Berquand, A. Boudaoud, O. Hamant, H. Jönsson, and E. M. Meyerowitz, "Subcellular and supracellular mechanical stress prescribes cytoskeleton behavior in *Arabidopsis* cotyledon pavement cells," *eLife*, vol. 3, p. e01967, apr 2014.
21. E. Coen, A.-G. Rolland-Lagan, M. Matthews, J. A. Bangham, and P. Prusinkiewicz, "The genetics of geometry," *Proc Natl Acad Sci USA*, vol. 101, pp. 4728–4735, Apr 2004.
22. M. G. Heisler, O. Hamant, P. Krupinski, M. Uyttewaal, C. Ohno, H. Jönsson, J. Traas, and E. M. Meyerowitz, "Alignment between pin1 polarity and microtubule orientation in the shoot apical meristem reveals a tight coupling between morphogenesis and auxin transport," *PLoS Biol*, vol. 8, p. e1000516, Jan 2010.
23. E. E. Kuchen, S. Fox, P. B. De Reuille, R. Kennaway, S. Bensmihen, J. Avondo, G. M. Calder, P. Southam, S. Robinson, A. Bangham, and E. Coen, "Generation of leaf shape through early patterns of growth and tissue polarity.," *Science*, vol. 335, pp. 1092–1096, Mar. 2012.
24. S. Sauret-Güeto, K. Schiessl, A. Bangham, R. Sablowski, and E. Coen, "JAGGED controls Arabidopsis petal growth and shape by interacting with a divergent polarity field.," *PLoS biology*, vol. 11, no. 4, p. e1001550, 2013.
25. N. Hervieux, M. Dumond, A. Sapala, A.-L. Routier-Kierzkowska, D. Kierzkowski, A. H. Roeder, R. S. Smith, A. Boudaoud, and O. Hamant, "A mechanical feedback restricts sepal growth and shape in arabidopsis," *Current Biology*, 2016.
26. M. Sassi, O. Ali, F. Boudon, G. Cloarec, U. Abad, C. Cellier, X. Chen, B. Gilles, P. Milani, J. Friml, T. Vernoux, C. Godin, O. Hamant, and J. Traas, "An Auxin-Mediated Shift toward Growth Isotropy Promotes Organ Formation at the Shoot Meristem in Arabidopsis.," *Current biology*, vol. 24, pp. 2335–2342, Sept. 2014.

27. S. Yoshida, P. Barbier de Reuille, B. Lane, G. W. Bassel, P. Prusinkiewicz, R. S. Smith, and D. Weijers, "Genetic Control of Plant Development by Overriding a Geometric Division Rule," *Developmental cell*, vol. 29, pp. 75–87, Apr. 2014.
28. B. Bozorg, P. Krupinski, and H. Jönsson, "A continuous growth model for plant tissue," *LU TP*, pp. 16–13, 2016.
29. S. Pietra, A. Gustavsson, C. Kiefer, L. Kalmbach, P. Hörstedt, Y. Ikeda, A. N. Stepanova, J. M. Alonso, and M. Grebe, "Arabidopsis SABRE and CLASP interact to stabilize cell division plane orientation and planar polarity," *Nature communications*, vol. 4, Nov. 2013.
30. Z. Hejnowicz, A. Rusin, and T. Rusin, "Tensile tissue stress affects the orientation of cortical microtubules in the epidermis of sunflower hypocotyl," *J PLant Growth Regul*, vol. 19, pp. 31–44, 2000.
31. D. Kwiatkowska, "Surface growth at the reproductive shoot apex of arabidopsis thaliana pin-formed 1 and wild type.," *Journal of experimental botany*, vol. 55, pp. 1021–32, may 2004.
32. I. Steeves, T nad Sussex, *Pattern in plant development*. Cambridge University Press, 1989.
33. J. Gruel, B. Landrein, P. Tarr, C. Schuster, Y. Refahi, A. Sampathkumar, O. Hamant, E. M. Meyerowitz, and H. Jönsson, "An epidermis-driven mechanism positions and scales stem cell niches in plants," *Science Advances*, vol. 2, p. e1500989, Jan. 2016.
34. D. Reinhardt, T. Mandel, and C. Kuhlemeier, "Auxin regulates the initiation and radial position of plant lateral organs.," *The Plant cell*, vol. 12, pp. 507–518, Apr. 2000.
35. D. L. Rayle and R. E. Cleland, "The Acid Growth Theory of auxin-induced cell elongation is alive and well.," *Plant physiology*, vol. 99, pp. 1271–1274, Aug. 1992.
36. P. Milani, V. Mirabet, C. Cellier, F. Rozier, O. Hamant, and A. Boudaoud, "Matching patterns of gene expression to mechanical stiffness at cell resolution through quantitative tandem epiflourescence and nanoindentation," *Plant Physiology*, pp. 1399–1408, 2014.
37. K. Zandomeni and P. Schopfer, "Reorientation of microtubules at the outer epidermal wall of maize coleoptiles by phytochrome, blue-light photoreceptor, and auxin," *Protoplasma*, vol. 173, no. 3-4, pp. 103–112, 1993.
38. T. I. Baskin, "Auxin inhibits expansion rate independently of cortical microtubules.," *Trends in plant science*, vol. 20, pp. 471–472, Aug. 2015.
39. J. Dumais, S. L. Shaw, C. R. Steele, S. R. Long, and P. M. Ray, "An anisotropic-viscoplastic model of plant cell morphogenesis by tip growth," *Int J Dev Biol*, vol. 50, pp. 209–222, 2006.

V

A MODEL ANALYSIS OF MECHANISMS FOR RADIAL MICROTUBULAR PATTERNS AT ROOT HAIR INITIATION SITES

Pawel Krupinski [1], Behruz Bozorg [1], André Larsson [1], Stefano Pietra [2], Markus Grebe [3,2] and Henrik Jönsson [1,4,5].

[1]Computational Biology and Biological Physics, Department of Astronomy and Theoretical Physics, Lund University, Lund, Sweden
[2] Umeå Plant Science Centre, Department of Plant Physiology, Umeå University, Umeå, Sweden
[3] Department of Plant Physiology, Univeristy of Potsdam, Golm, Germany
[4] Sainsbury Laboratory, University of Cambridge, Cambridge, United Kingdom
[5] Department of Applied Mathematics and Theoretical Physics, University of Cambridge, Cambridge, United Kingdom

LU TP 16-14 (submitted 2016)

Plant cells have two main modes of growth generating anisotropic structures. Diffuse growth where whole cell walls extend in specific directions, guided by anisotropically positioned cellulose fibers, and tip growth, with inhomogeneous addition of new cell wall material at the tip of the structure. Cells are known to regulate these processes via molecular signals and the cytoskeleton. Mechanical stress has been proposed to provide an input to the positioning of the cellulose fibers via cortical microtubules in diffuse growth. In particular, a stress feedback model predicts a circumferential pattern of fibers surrounding apical tissues and growing primordia, guided by the anisotropic curvature in such tissues. In contrast, during the initiation of tip growing root hairs, a star-like radial pattern has recently been observed. Here, we use detailed finite element models to analyze how a change in mechanical properties at the root hair initiation site can lead to star like stress patterns in order to understand whether a stress-based feedback model can also explain the microtubule patterns seen during root hair initiation. We show that two independent mechanisms, individually or combined, can be sufficient to generate radial patterns.

In the first, new material is added locally at the position of the root hair. In the second, increased tension in the patch area provides a mechanism. Finally, we describe how a molecular model of Rho-of-plant (ROP) GTPases activation driven by auxin can position a patch of activated ROP protein basally along a 2D root epidermal cell plasma membrane, paving the way for models where mechanical and molecular mechanisms cooperate in the initial placement and outgrowth of root hairs.

V.1 INTRODUCTION

Most higher plants do not display cell migration and need to generate optimal shapes by adjusting growth both in terms of magnitude and directions. Two main modes of growth are prevailing across the plant kingdom [1, 2]. The first is diffuse growth where whole cells or tissues are expanding quite homogeneously, although often anisotropically. The other mode of growth is tip growth, where expansion appears in a focused region of a cell. The growth is dependent on environmental signals and guided by cells genetic and hormonal interactions [3]. Still, to effectuate the growth, manipulation of the stiff cell walls surrounding all cells is necessary [4].

The plant cell wall can be seen as a complex composite material composed mainly of cellulose microfibrils, pectins and xyloglucans [1, 4]. Intricate connections between these wall components and their effect on the mechanical properties of the cell wall are not yet completely understood. Similarly, the way in which the plant dynamically controls composition and properties of its cell walls to form different organs to their appropriate shape is a matter of extensive research [5]. Cortical microtubules serve as the guiding tracks for deposition of cellulose microfibrils and in consequence cells can control anisotropy of its wall stiffness [6, 7]. This in turn relates to directionality of anisotropic growth of a tissue and influences stresses at subcellular to tissue scales [1, 8, 9]. For tip-growing root hairs, the cellulose fibers have been shown to be randomly oriented at the very tip, while organized longitudinally away from the tip where there is also a formation of a secondary wall [10–12]. In tip growth, high rates of wall material deposition are promoting the localized growth [13].

Several signals regulating the dynamic orientations of the cortical microtubules have been suggested, including environmental, molecular and mechanical regulation [3, 14–18], and for diverse input signals micotubule severing is important part of the orientation process as shown by katanin mutants [15, 17, 19–21]. The *Arabidopsis* hypocotyl displays a strong growth response to light. Hypocotyl microtubules were recently shown to quickly reorient from transverse to longitudinal after being exposed to blue light

and this reorganization was dependent on katanin [15]. Treatment with the phytohormone auxin has been shown to induce changes in microtubule orientations [16], which more recently has also been reported for *Arabidopsis* roots and hypocotyls [17]. Again the reorientation is quick [17], but it is yet to be understood whether growth is affected in such treatments.

For several of the suggested input cues orienting microtubules it is unclear how the input provides a directional signal. Mechanical stresses and strains could serve that purpose. Mechanical stresses in the walls have been suggested to provide a directional signal where cortical microtubules orient along the maximal principal stress direction, both at the tissue and at the subcellular levels in shoots, leaves and flowers in *Arabidopsis* [18, 19, 22]. Such feedback loop between stress and direction of material anisotropy has been implemented in models which have verified its ability to produce robust regulation of anisotropic growth [23]. In particular, such a model correctly predicts the circumferential arrangement of microtubules (and tissue scale stresses) around the sites of primordia outgrowth in the shoot apical meristem and towards the stem tissue.

In tip growing cells, the growth is much more localized to a specific site of the cell wall. As mentioned above, the microtubules are randomly organized at the tip, and growth is rather promoted by vigorous local deposition of the new material to the site of outgrowth. At the tip there is a region of the cytosol less abundant in large organelles and with targeted secretion of wall material seen by enriched presence of secretory vesicles [2, 24, 25]. Pectin deposited to the tip is further de-esterified and rigidified by calcium cross-linking, promoted by high levels of calcium at the tip [26]. In particular, the addition of wall material, and hence the cell wall thickness at the tip is oscillating and is out of phase with growth rates, altering thick walls with high growth rates [27]. Also actin has been shown to play prominent role in wall elongation process [13]. When measuring the rigidity of pollen tubes using cellular force microscopy, the apparent reduced stiffness at the tip was attributed to the respective geometrical change [28]. Computational models of tip growth connect deformation to the addition of material, the use of anisotropic wall material, and strain-based growth [29]. In addition, the inclusion of pectin chemistry provides means to have parameter space regions determining steady and oscillatory growth in model [30]. Moreover models including details of osmotic pressure alterations discuss possible role of pressure as a driving force for oscillatory tip growth [31], as suggested by experimental data [32, 33].

We are particularly interested in the process of root hair initiation. A transcriptional network for root hair cell differentiation in *Arabidopsis* has been identified [34], defining alternating cell files of root hair cells (trichoblasts)

and non root hair cells (atrichoblasts). The differentiation of root hair cells has been modeled, suggesting different mechanisms [35–37]. While root hair initiation often fails in genetic perturbations of components of these networks, these proteins are not known to provide information of the polar position of root hair initiation site on the lateral membrane of epidermal cells. Similarly, auxin has been suggested to identify files of root hair cells. Its supply is facilitated, at least in part, by auxin influx mediators throughout non root hair cells files [38].

More interesting for the subcellular localization of the root hair, an intracellular auxin gradient has been proposed to be informative in the positioning of root hairs on the lateral membrane of hair cells, close to their basal (rootward) end [39]. One of the earliest markers of the basal initiation site is the activated Rho-of-plants (ROP) GTPases [39–42]. The ROP localization has been also found to correlate with positioning of lobes and necks in pavement cells where ROP is activated by auxin [43]. The ROP proteins are likey to be important for the correct placement and outgrowth of root hairs as suggested by dominant-interference and overexpression studies [40, 41]. The activation dynamics of ROP proteins in root hair cells have been modeled using a reaction-diffusion type of model where auxin at the subcellular level is assumed to promote activation of ROP [44]. Together with a positive self-feedback of ROP-activation this was sufficient to generate peaks of activated ROPs at the root-tip oriented (basal) ends of cells lateral membrane in a 1D model, predicting the positioning of root hair initiation in wild type as well in selected mutants.

Also the actin and microtubular cytoskeleton networks are important for correct root hair formation [45–47]. When microtubules were imaged together with PIP5K3, an early root hair initiation marker [48], microtubules were reported to orient into a radial pattern surrounding the root hair initiation site [49]. Similar to other microtubule organizing events, this was disrupted in mutants defective in the SABRE and CLASP genes required for microtubule organization. Also, the basal positioning of root hairs as well as the polar localization of the ROP patches were perturbed in different combinations of loss-of-function mutants, indicating a regulatory role of microtubular patterning for polar ROP placement. Consistent with this view, the procuste1/cesA6 mutant defective in a cellulose synthase subunit displays alterations in polar ROP and root hair placement [50], resembling the defects in sabre mutants suggesting a requirement for both correct microtubule organization and cellulose microfibril synthesis during polar root haor initiation. In addition, ROPs have been reported to be activated by auxin and regulate microtubular patterning in pavement cells [43, 51]. Hence, an intricate feedback mechanism between ROPs and microtubules

connecting also auxin and wall mechanics seems to be at the core of root hair initiation and growth (Fig. V.1A).

Altogether, the ROP and microtubular data indicate a complex feedback between molecular and cytoskeletal dynamics during root hair initiation, and computational modeling is essential to understand the behavior. In particular, current data raise the question if a correlation between microtubule organization and principal stress direction is sustained in the case of the root hair initiation, as has been observed before in diffuse growth (Fig. V.1A). In diffuse growth of organ formation, auxin is accumulated at the site of outgrowth, leading to the loosening of cell wall material. In effect we observe around the outgrowth region circumferential stress orientation and corresponding microtubule pattern. Here, we extend the previously published 1D ROP model to 2D to confirm it can provide a mechanism for correct placing of an activated ROP patch correctly along root hair cell. We then investigate whether the previously suggested mechanical stress feedback on microtubule directions can predict the patterns seen at root hair initiation sites by analyzing mechanical scenarios of tip growth that can produce radial stresses patterns.

V.2 RESULTS

The results reported in this communication present two connected mechanisms concerning root hair outgrowth. Firstly we consider the process by which the site of the root hair outgrowth can be specified within a cell, by the localization of activated ROP into a small patch. Secondly we examine if the initiation of root hair growth can be explained by mechanical perturbations in such a patch and in agreement with experimental data. We consider several scenarios and analyze the emerging pattern of stresses in comparison with experimentally observed microtubule organization.

V.2.1 *An auxin-driven ROP-activation model can guide the activated membrane-localized ROP into a basally localized patch in the 2D epidermal cell wall membrane*

We developed a 2D single cell model where the cycling of ROP from an inactive to an active form is influenced by an auxin gradient (Methods, Red box in Fig. V.1A). The model is an extension of a previously published 1D model of ROP cycling [44]. We discretize the cell into several compartments between which the ROPs are allowed to diffuse, assuming a faster movement of inactive ROPs, which reside in the cytosol, compared to the active ROPs which are connected to the membrane. We assume that ROPs are

created in their inactive form and subsequently activated by auxin to become the active membrane-bound form. Further, the active form of ROP is subject to constant degradation. Also included in the model is a non-linear self-activation of activate ROP. All reactions follow simple mass action and diffusion descriptions (Eqs. 1-3).

First we tested whether such a molecular model is able to create a peak of active ROP, marking the site of root hair outgrowth, at the correct location in the epidermal cell membrane. We expect the peak to locate close to the basal end of the lateral membrane, even when considering a full 2D description of this membrane. Indeed, a patch of active ROP localize at the basal end of the lateral membrane (Fig. V.2A), slightly away from the cell wall, consistent with previous experimental findings [39–41]. The patch first appears near the cell boundary where the level of auxin is predicted to be highest, after which it moves a small distance away from the cell boundary where it becomes stable. To confirm the importance of the auxin gradient for the localization of the peak, we simulated the model with constant auxin in the lateral direction (Fig V.2B – D). The basal bias for the ROP patch is lost, and depending on the auxin level, a single central peak, several peaks spread across the cell, or a low activation of ROP throughout the cell was found. Interestingly, phenotypes as multiple hairs, more apical root hair positions and loss of root hairs has been found in mutants suggested to alter intracellular auxin levels and or gradients [39, 52–54]. The model parameters of the simulation with a gradient was set such that it generates a gradient of about 20%, showing that the gradient does not need to be steep to generate enough bias to the ROP dynamics. While the intracellular gradient has yet to be measured in experiments, the gradient is well within ranges suggested in tissue models of auxin in the root [38, 55].

Our model confirms, in a 2D setting, that a sub-cellular auxin-dependent activation of ROPs promoted by an intracellular auxin gradient together with intracellular transport is sufficient to create convergence of active ROPs, placing the site of root hair formation to the center close to the basal end of the outer epidermal cell plasma membrane. The active ROP is an early marker of root hair initiation and we will use this to investigate how such a patch may influence mechanical properties of the cell wall such that a root hair can be initiated, and whether this can lead to a star-like pattern of stresses.

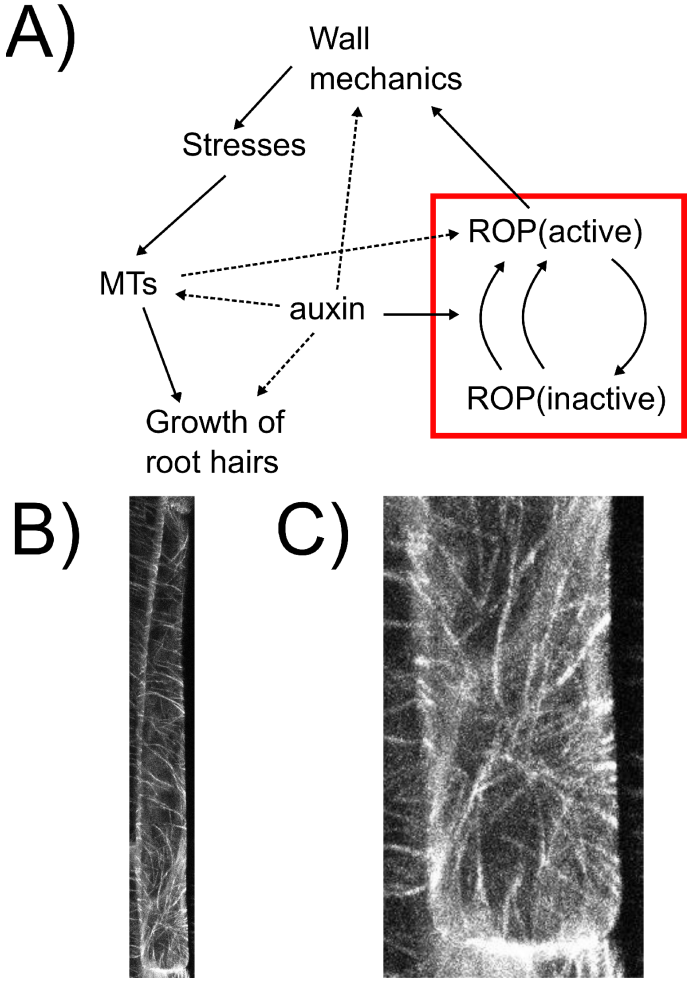

Figure V.1: **Root initiation is dependent on ROP activation and microtubular dynamics.** A) Model diagram including feedback between cycling of ROPs and mechanical properties via microtubular dynamics of the root hair initiation process. Solid lines represent mechanisms explicitly modeled, dashed lines are implicitly in the models or suggested in the literature. The red box represents the ROP model tested in 2D and the arrow from the ROP to mechanics are evaluated by testing different hypotheses. B) Pattern of cortical microtubules in plant epidermal cell visualized by RFP-TUB6. In the top part a mainly transverse pattern of microtubules can be seen, while a star-like radial pattern around the root hair initiation site can be seen at the lower end. C) magnification of the radial pattern in the lower part of the cell from (B).

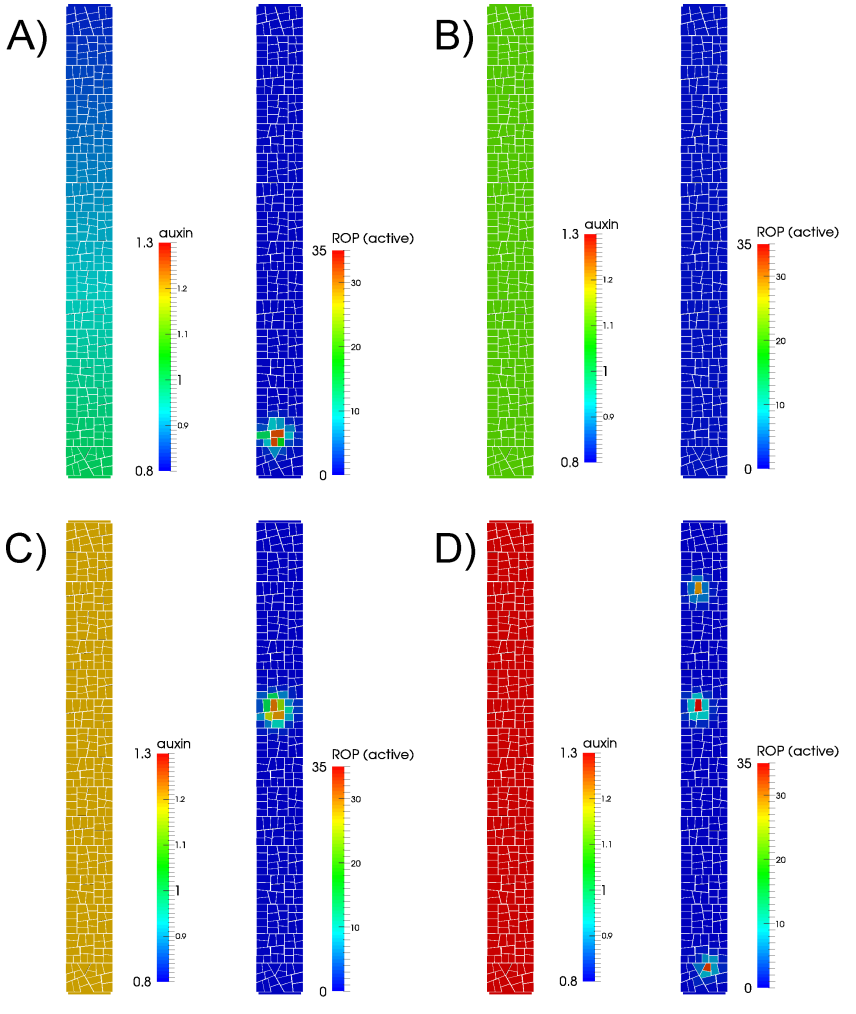

Figure V.2: **Auxin gradient and pattern of active ROP in model of auxin-driven ROP-activation.** A) When an auxin gradient is present, active ROPs can localize centrally at the basal side on the cell, similar that is seen in experiments. B) A low activation of ROPs is seen for a constant auxin level of 1.1, with no clear peaks of active ROP forming. C) For a constant auxin level at 1.2, the active ROP peak localizes to a position close to the center of the cell. D) For a constant auxin level of 1.3, several ROP peaks appear throughout the cell.

V.2.2 *Altering mechanical stiffness locally at the root hair initiation site can guide stresses from circumferential to radial*

The mechanical aspects of root hair growth are analyzed by means of a finite element model of the epidermal wall of a rectangular cell and from changing material properties in a small region representing an activated ROP patch.

A simulation of rectangular epidermal wall under turgor pressure results in the stress pattern in which the first principal stress component is mostly oriented perpendicularly to the long axis of the cell Fig. V.3A). That correlates well with the orientation of microtubules observed in close to rectangular epidermal walls of the *Arabidopsis* root (Fig. V.1B, [49]). Note that this result pertains to the cell scale stresses and is independent of the root tissue curvature where a pressurized cylindrical root shape would also produce highest stresses in the circumferential direction, e.g. [23]. Hence, the simulation suggest that cellular stresses can complement tissue scale stresses to provide a directional cue for microtubules in roots and other elongated tissues with elongated cells. Note that there are deviations in the general stress patterns in proximity of basal and apical ends of the outer wall of the root hair cell (Fig. V.3A). While such a pattern could provide a mechanical bias for root hair initiation, the effect can be affected by the specific material model choice.

More intriguingly, in experiments deviation from this pattern in microtubule orientation appears at the site of subsequent root hair outgrowth, where a star-like pattern around the initiation point can be observed (Fig. V.1C, [49]). We extended the model to analyze whether mechanical perturbations in a localized patch can reconcile the experimental observations of microtubule organization with stress patterns surrounding the patch. We localize the site of the root hair outgrowth to a circular region which can have different mechanical properties. We assume that the outer edges of the cell wall are fixed in space and the loading forces arise from turgor pressure. We have previously shown that assumption of local loosening the pressurized cell wall(s) lead to circumferential pattern of tissue scale stresses surrounding the loosened region [18]. A similar principle applies for the simulation of local loosening of a root epidermal cell wall (Fig. V.3B), which shows circumferential maximal principal stress around the loosened region. Such loosening is suggested to be a prerequisite, for example, for the diffuse growth in plant meristems and it is supposed to be a result of breaking the bonds that link the cellulose fibers or of processes that affect the pectin matrix[4, 5].

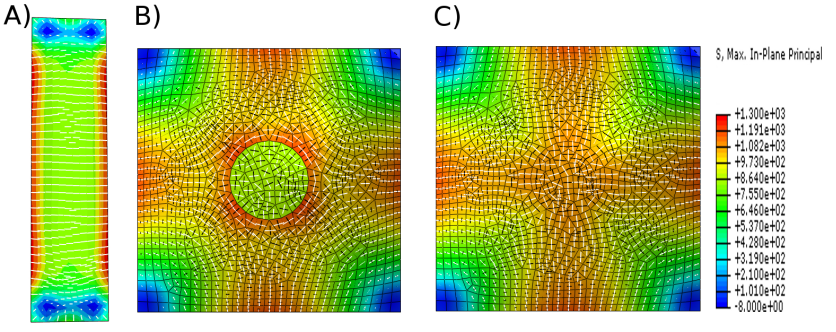

Figure V.3: **Principal stress directions predicted by finite element models in root hair cells.** White bars show the direction of the maximal principal stress, the black bars indicate minimal principal stress directions and the color represents the maximal stress magnitude. A) Pattern of maximal principal stress in epidermal wall of pressurized rectangular cell bears resemblance of micrutubular pattern of ruffly rectangular root cell except of the region of subsequent root hair outgrowth. B) In case of softened material in the center of patch we observe circumferential alignment of maximal principal stress around this region. C) Increasing the Young modulus of the material in the same region leads to radial organization of maximal principal stress around center.

In tip growing cells rapid deposition of new wall material and complex pectin chemistry may alter mechanical properties at the tip [2, 56, 57]. We hypothesize, that such rapid deposition of new material and reorganization of cell wall components, at least temporarily can lead to local stiffening of the cell wall. Indeed, under the assumption of local stiffening of the material we obtain a radial pattern of maximal stress in the surrounding region (Fig. V.3C), which is matching the microtubule pattern seen *in vivo* (Fig. V.1C, [49]). This simulation suggests a phase of local stiffening, by addition of more wall material or by changes to the wall properties preceding the localized growth phase of the root hair. Interestingly, such suggestion is in parallel with observations of changes in thickness off the cell wall in pollen tube tips which show oscillatory behavior and thickening prior to the growth phase [27].

We explored the idea that the quick addition of material connected to root hair initiation might, at least transiently, lead to stiffer walls at the initiation site, and our model predicted radial stresses surrounding such a region. In such scenario stresses correlate with the star-like microtubule patterns seen in root hair cells before root hairs grow out.

V.2.3 *Heterogeneous forces can generate radial stress patterns surrounding a root hair initiation site*

Another mechanism that may contribute to tip growth is a differential pressure model [32, 33], possibly driven by strong cytosolic streaming together with heterogeneous cytoskeletal crowding. While a pressure difference within a root epidermal cell might be hard to envision a heterogeneous force distribution at the wall might still be possible, where for example the cytoskeleton could exert forces on the site of outgrowth leading to increased loading of this region. Application of increased outward forces in a patch can lead to radial stresses around the outgrowth site in our simulation (Fig. V.4A). We increase loading forces by increasing pressure in the small region in the simulations up to 200% of the pressure value in remaining part of a cell.

Next we test in our model combination of previously analyzed mechanisms of local material or loading force changes during root hair initiation. Strikingly, the forces locally increased at the site of outgrowth can lead to radial stress pattern even for the case of elastically softened material in the outgrowth region (Fig. V.4B, cf. Fig. V.3B). This however depends on the relation between difference in Young modulus and pressure in both regions in such a way that there exist a threshold where transition between circumferential and radial stress pattern occurs. This possibility of combing local material softening with locally increased forces at a tip growth site allows for a mechanism in which the structure of the cell wall changes, similarly to the scenario suggested for diffuse wall growth, allowing greater wall extensibility and, at the same time, local forces exerted by the cytoskeleton contribute to tip growth.

Finally, if locally increased forces and local material stiffening are combined a slightly stronger (more anisotropic) radial stress pattern results (Fig. V.4C). This scenario can be of interest since there is the possibility that cytoskeleton reorganization during tip growth itself leads to local stiffening of the cell wall material.

In summary, the finite element model predicts that radial stress patterns are possible surrounding a small region where increased forces are applied. This can be realized independently of any heterogeneous or anisotropic material properties in such a region.

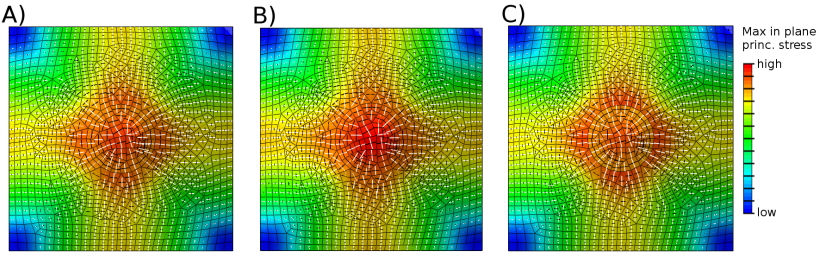

Figure V.4: **Principal stress directions predicted by finite element models in root hair cells.** White and black bars show maximal and minimal respectively principal stress directions in finite element models when loading forces are locally increased in the region of predicted root hair outgrowth. The color represents the maximal stress magnitude. A) Principal stress directions predicted by finite element models in the case of locally increased pressure in the center when material properties are kept constant. B) The radial pattern can appear also when the material in the patch is made elastically softer. C) The mechanisms yielding radial stress alignment can be combined without destruction of the radial stress pattern. The image presents combination of elastically stronger center together with locally increased forces. The radial pattern of maximal principal stress is still evident.

V.3 DISCUSSION

The importance of growth for morphogenesis in plants has lead to a large interest in how cortical microtubules organize into patterns regulating cellulose deposition and subsequent growth. The classic model is that the microtubules organize like hoops around a barrel to generate anisotropic growth [8].

Our study was inspired by the strikingly different pattern of microtubules seen at the initiation of root hairs, where a radial pattern is found around the initiation site (Fig. V.1, [49]). Importantly, we acknowledge that the root initiation process involves a complex combination of molecular and mechanical patterning (Fig. V.1A). Hence, our first aim was to investigate a mechanism for marking the site of the root hair outgrowth in a molecular 2D model based on a previous 1D effort [44]. An early marker for the site where a root hair is initiated is a peak of active ROP protein [41]. Our simulations demonstrate that an internal auxin gradient promoting ROP activation together with self-activating feedback is sufficient to correctly place the peak centrally at the basal side of the epidermal wall (Fig. V.2A).

We then investigated how a localized change to mechanical properties affects stresses surrounding this region, in particular, if a radial star-like pattern of microtubules (Fig. V.1C,[49]) can be predicted by stress patterns.This appeared plausible since it has previously been reported that microtubular patterns correlate with maximal stress directions at subcellular and at tissue scales [18, 19]. For example, the outgrowth of primordia at the shoot apical meristem leads to a circumferential pattern of microtubules and the intracellular patterns of stresses can be used to predict microtubular patterns in the complex shapes of leaf epidermal pavement cells. We presented two different scenarios that could lead to radial pattern of stresses during tip growth reconciling the alignment of microtubules and stresses in this case of root hair initiation. Firstly, the quick addition of material could lead to a stiffening of the wall, and we could show that this can lead to radial stress patterns (Fig. V.2C). This can be related to observations of alternating phases of tip growth and wall thickening at the tip [27]. Although this may occur at a different time scale during root hair initiation, only about 50% of analyzed cells showed that behavior, which could indicate that it represents a transient state [49]. A competing idea suggested for tip growth is that the forces exerted on the wall at the tip are changing [32]. When applied to a patch in the epidermal wall, this was also able to generate radial patterns of stresses (Fig. V.3). Importantly, the radial pattern can be achieved independently of changes in cell wall stiffness.

Since our results show that either local alteration of material properties of the cell wall or the active interaction with cytoskeleton may lead to the radial pattern of stresses around the place of root hair outgrowth, it would be interesting to measure wall stiffness at this site for example by using atomic force microscopy.

While we have stressed the importance of looking at several processes when analyzing root hair initiation (Fig. V.1A), our computational simulations have been divided into the processes of ROP patch formation (Fig.V.2) and of ongoing mechanical changes (Figs. V.3-V.4). A main challenge will be to integrate these into a single model where both ROP activation is necessary for root hair initiation [41], and correct microtubular dynamics are necessary for correct ROP positioning [49]. Induced chemical or genetic perturbations followed by live imaging can provide additional dynamical data to generate improved insight into the process, and computational modeling of the interactions will be essential to understand the consequences of direct or indirect mechanisms of several combined feedback regulations.

V.4 METHODS

V.4.1 *Plant growth and imaging*

Plant growth medium and conditions were as described [39]. Seeds were surface sterilized and stratified at 4 C for 3 days before plating on MS plates (1 MS medium, 1% sucrose, 0.8% plant agar, 1 M morpholinoethanesulphonic acid, pH 5.7). Seedlings were grown vertically at 23 C day and 18 C night under 16 h light/8 h dark photoperiod and subjected to analysis after 5 days. Confocal imaging followed [49]. Cortical microtubules were imaged in epidermal cells of seedlings expressing pUBQ1:RFP-TUB6 [58]. Z stacks of planes at 0.53 μm distance intersecting the periclinal face of the cell were acquired and employed to generate maximum intensity projections.

V.4.2 *ROP activation model*

We developed a ROP activation model based on a previously published model [44]. The model describes the ROP dynamics in 2D close to the epidermal cell membrane of a root trichoblast. The ROP activation is influenced by an auxin (A) gradient produced by a source-sink model in which auxin is allowed to diffuse and is subject to a constant degradation rate. Based on the assumption of an basipetal auxin flow in the epidermis (due to reported fluxes and gradients), auxin is produced in the basal part of the cell, representing auxin influx, and degraded at the apical side of the cell, representing auxin outflux. The auxin dynamics are described by

$$\frac{dA}{dt} = D_a \Delta A + t + s_{in} - s_{out} - qA \,, \tag{1}$$

where s_{in} is the auxin production at the source and s_{out} is the auxin degradation at the sink. Further, q is the auxin degradation rate, D_a is the rate of auxin diffusion and t is a general auxin production. For the simulation with a non-constant auxin gradient, the parameter t is set to zero (Table V.1). In the simulations with constant auxin levels, all parameters are zero except for the general production rate t and the degradation rate q. The ROPs can be in an 'inactive' form (R_i) moving in the cytosol, or in an 'activated' form (R_a) where it sits in the membrane less prone to move. In addition to a constant activation of the ROPs with rate k_1 and an inactivation with rate c there is also an auxin-dependent activation with the rate k_2 that depends

also on the active ROP concentration, creating a positive feedback. The full ROP dynamics are described by

$$\frac{dR_a}{dt} = \begin{cases} D_1\Delta R_a + a - rR_a - pR_a + R_i \cdot \left(k_1 + k_2 R_a^2 A\right) - cR_a & \text{if boundary} \\ D_1\Delta R_a + a - rR_a + R_i \cdot \left(k_1 + k_2 R_a^2 A\right) - cR_a & \text{otherwise} \end{cases} \tag{2}$$

$$\frac{dR_i}{dt} = D_2\Delta R_i + b - eR_i - R_i \cdot \left(k_1 + k_2 R_a^2 A\right) + cR_a \tag{3}$$

where D_1 and D_2 are the diffusion rates of active and inactive ROP respectively. a is the production rate of active ROP, b the production rate of inactive ROP while r is the degradation rate of active ROP and e is the degradation rate of inactive ROP. Active ROPs are degraded at the cell boundary (compartments that has the background as a neighbor) with a rate p, corresponding to active ROPs diffusing out of the cell. We assume that ROP is only produced in its inactive form and only degraded in its active form (Table V.1). Transport between compartments is assumed to be proportional to the difference in concentrations, with spatial factors being included in the diffusion constant. The auxin simulation was run first, and the resulting auxin gradient was used in the ROP simulation. Both simulations were run until the system was in equilibrium. We discretized the 2D surface into 286 polygonal compartments, and spatial factors are added to the transport rates given the different sizes of the compartments and their neighbor cross sections. All simulations use a 4th order Runge-Kutta solver and was implemented in an in-house developed open source software (http://dev.thep.lu.se/organism), available upon request. Files defining the models, the initial configuration, and the solver parameters are provided as Supplementary Information.

V.4.3 *Mechanical simulations and material model*

We used finite element models for all mechanical simulations using quadrilateral shell elements in Abaqus (Dassault Systemes, 2012). The finite element method is based on linearization of virtual work δW equation

$$\delta W = \int_V \boldsymbol{S} : \delta\dot{\boldsymbol{E}} dV - \int_V \boldsymbol{f_0} \cdot \delta\boldsymbol{v} dV - \int_{\partial V} \boldsymbol{t_0} \cdot \delta\boldsymbol{v} dA = 0\,, \tag{4}$$

where $\boldsymbol{S}$ is a second Piola-Kirchhoff stress tensor and $\dot{\boldsymbol{E}}$ is time derivative of its work conjugate Green-Lagrange strain tensor. The two last terms of Eq. 4 contribute to the external virtual work component and $\boldsymbol{f_0}$ and $\boldsymbol{t_0}$ represent

Table V.1: Model parameters for the ROP activation model.

Symbol	Value	Description
D_a	5.0 length^2/s	diffusion rate of auxin
t	0.0 conc/s	production of auxin throughout the cell
s_{in}	0.25 conc/s	auxin source production rate
s_{out}	0.3 conc/s	auxin sink degradation rate
q	$2.0 \cdot 10^{-5}$ 1/s	degradation rate of auxin
D_1	0.01 length^2/s	diffusion rate of active ROP
a	0 conc/s	production rate of active ROP
r	0.01 1/s	degradation rate of active ROP
p	0.01 1/s	rate of boundary degradation of active ROP
k_1	0.01 1/s	rate of constant ROP activation
k_2	0.015 1/(conc^3 s)	rate of auxin-dependent ROP-autoactivation
c	0.1 1/s	rate of constant ROP inactivation
D_2	1.0 length^2/s	diffusion rate of inactive ROP
b	0.01 conc/s	production rate of inactive ROP
e	0 1/s	degradation rate of inactive ROP

body force per undeformed unit volume and traction per undeformed unit area, respectively. For hyperelastic materials second Piola-Kirchhoff stress tensor can be calculated from strain energy function U as a derivative with respect to Green-Lagrange strain tensor

$$\boldsymbol{S} = \frac{\partial U}{\partial \boldsymbol{E}} \,. \tag{5}$$

In Saint Venant-Kirchhoff model strain energy function takes form

$$U = \frac{1}{2}\lambda(tr\boldsymbol{E})^2 + \mu \boldsymbol{E} : \boldsymbol{E} \,, \tag{6}$$

where λ and μ are Lamé coefficients related to Young modulus E_Y and Poisson ratio ν by formulas

$$E_Y = \frac{\mu}{\lambda + \mu}(2\mu + 3\lambda) \tag{7}$$

$$\nu = \frac{\lambda}{2(\lambda + \mu)} \,. \tag{8}$$

We applied standard isotropic elastic material in Abaqus with Young modulus of 100 MPa. In softened regions we used Young modulus of 70 MPa and in stiffened regions 130 MPa. We assumed turgor pressure of 0.2 MPa. In all cases we used Poisson ratio of 0.2.

CONFLICT OF INTEREST STATEMENT

The authors declare that the research was conducted in the absence of any commercial or financial relationships that could be construed as a potential conflict of interest.

AUTHOR CONTRIBUTIONS

SP and MG designed and analysed experiments. PK, AL, BB, HJ designed and analyzed models and simulations. PK and BB developed and simulated mechanical models. AL developed and simulated the molecular model. All authors wrote and edited the paper.

FUNDING

This work was funded by the Knut and Alice Wallenberg Foundation via grant ShapeSystems (KAW 2012.0050) to MG and HJ, the Gatsby Charitable Foundation (GAT3395/PR4) to HJ and the Swedish Research Council (VR2013-4632) to HJ,

REFERENCES

1. T. I. Baskin, "Anisotropic expansion of the plant cell wall," *Annu Rev Cell Dev Biol*, vol. 21, pp. 203–22, Jan 2005.
2. C. M. Rounds and M. Bezanilla, "Growth Mechanisms in Tip-Growing Plant Cells," *Annual review of plant biology*, vol. 64, pp. 243–265, Apr. 2013.
3. X. Chen, S. Wu, Z. Liu, and J. Friml, "Environmental and endogenous control of cortical microtubule orientation.," *Trends in cell biology*, Mar. 2016.
4. D. J. Cosgrove, "Growth of the plant cell wall.," *Nature reviews. Molecular cell biology*, vol. 6, pp. 850–61, nov 2005.
5. S. A. Braybrook and H. Jönsson, "Shifting foundations: the mechanical cell wall and development.," *Current opinion in plant biology*, vol. 29, pp. 115–120, Jan. 2016.

6. T. Arioli, L. Peng, A. S. Betzner, J. Burn, W. Wittke, W. Herth, C. Camilleri, H. Höfte, J. Plazinski, R. Birch, A. Cork, J. Glover, J. Redmond, and R. E. Williamson, "Molecular Analysis of Cellulose Biosynthesis in Arabidopsis," *Science*, vol. 279, pp. 717–720, Jan. 1998.
7. H. E. McFarlane, A. Döring, and S. Persson, "The Cell Biology of Cellulose Synthesis," *Annual Review of Plant Biology*, vol. 65, pp. 69–94, Apr. 2014.
8. P. B. Green, "Mechanism for Plant Cellular Morphogenesis," *Science*, vol. 138, pp. 1404–1405, Dec. 1962.
9. I. B. Heath and A. Geitmann, "Cell Biology of Plant and Fungal Tip Growth–Getting to the Point," *The Plant Cell Online*, vol. 12, pp. 1513–1517, sep 2000.
10. E. Newcomb and H. Bonnet, "Cytoplasmic Microtubule and Wall Microfibril Orientation in Root Hairs of Radish," *The Journal of Cell Biology*, vol. 27, no. 3, pp. 575–589, 1965.
11. M. Akkerman, M. A. W. Franssen-Verheijen, P. Immerzeel, L. D. E. N. Hollander, J. H. N. Schel, and A. M. C. Emons, "Texture of cellulose microfibrils of root hair cell walls of Arabidopsis thaliana, Medicago truncatula, and Vicia sativa.," *Journal of Microscopy*, vol. 247, pp. 60–67, July 2012.
12. S. Park, A. L. Szumlanski, F. Gu, F. Guo, and E. Nielsen, "A role for CSLD3 during cell-wall synthesis in apical plasma membranes of tip-growing root-hair cells.," *Nature cell biology*, vol. 13, pp. 973–980, Aug. 2011.
13. A. Geitmann, B. N. Snowman, A. M. C. Emons, and V. E. Franklin-Tong, "Alterations in the Actin Cytoskeleton of Pollen Tubes Are Induced by the Self-Incompatibility Reaction in Papaver rhoeas," *The Plant Cell Online*, vol. 12, pp. 1239–1251, July 2000.
14. T. Hogetsu, "Re-formation of microtubules in closterium ehrenbergii meneghini after cold-induced depolymerization," *Planta*, vol. 167, no. 4, pp. 437–443, 1986.
15. J. J. Lindeboom, M. Nakamura, A. Hibbel, K. Shundyak, R. Gutierrez, T. Ketelaar, A. M. C. Emons, B. M. Mulder, V. Kirik, and D. W. Ehrhardt, "A mechanism for reorientation of cortical microtubule arrays driven by microtubule severing.," *Science*, vol. 342, pp. 1245533–1245533, Dec. 2013.
16. K. Zandomeni and P. Schopfer, "Reorientation of microtubules at the outer epidermal wall of maize coleoptiles by phytochrome, blue-light photoreceptor, and auxin," *Protoplasma*, vol. 173, no. 3-4, pp. 103–112, 1993.

17. X. Chen, L. Grandont, H. Li, R. Hauschild, S. Paque, A. Abuzeineh, H. Rakusová, E. Benková, C. Perrot-Rechenmann, and J. Friml, "Inhibition of cell expansion by rapid ABP1-mediated auxin effect on microtubules.," *Nature*, vol. 516, pp. 90–93, Dec. 2014.
18. O. Hamant, M. G. Heisler, H. Jönsson, P. Krupinski, M. Uyttewaal, P. Bokov, F. Corson, P. Sahlin, A. Boudaoud, E. M. Meyerowitz, Y. Couder, and J. Traas, "Developmental patterning by mechanical signals in arabidopsis," *Science*, vol. 322, pp. 1650–1655, Dec 2008.
19. A. Sampathkumar, P. Krupinski, R. Wightman, P. Malini, A. Berquand, A. Boudaoud, O. Hamant, H. Jönsson, and E. M. Meyerowitz, "Subcellular and supracellular mechanical stress prescribes cytoskeleton behavior in arabidopsis cotyledon pavement cells," *eLife*, vol. 3, p. e01967, 2014.
20. M. Uyttewaal, A. Burian, K. Alim, B. Landrein, D. Borowska-Wykret, A. Dedieu, A. Peaucelle, M. Ludynia, J. Traas, A. Boudaoud, D. Kwiatkowska, and O. Hamant, "Mechanical Stress Acts via Katanin to Amplify Differences in Growth Rate between Adjacent Cells in Arabidopsis," *Cell*, vol. 149, pp. 439–451, Apr. 2012.
21. M. Sassi, O. Ali, F. Boudon, G. Cloarec, U. Abad, C. Cellier, X. Chen, B. Gilles, P. Milani, J. Friml, T. Vernoux, C. Godin, O. Hamant, and J. Traas, "An Auxin-Mediated Shift toward Growth Isotropy Promotes Organ Formation at the Shoot Meristem in Arabidopsis.," *Current biology*, vol. 24, pp. 2335–2342, Sept. 2014.
22. N. Hervieux, M. Dumond, A. Sapala, A.-L. Routier-Kierzkowska, D. Kierzkowski, A. H. K. Roeder, R. S. Smith, A. Boudaoud, and O. Hamant, "A Mechanical Feedback Restricts Sepal Growth and Shape in Arabidopsis," *Current Biology*, vol. 26, p. 1019–1028, Apr. 2016.
23. B. Bozorg, P. Krupinski, and H. Jönsson, "Stress and strain provide positional and directional cues in development," *PLoS Comp Biol*, vol. 10, p. e1003410, 2014.
24. M. E. Galway, J. W. Heckman, and J. W. Schiefelbein, "Growth and ultrastructure ofArabidopsis root hairs: therhd3 mutation alters vacuole enlargement and tip growth," *Planta*, vol. 201, no. 2, pp. 209–218, 1997.
25. A. Lovy-Wheeler, L. Cárdenas, J. G. Kunkel, and P. K. Hepler, "Differential organelle movement on the actin cytoskeleton in lily pollen tubes," *Cell Motility and the Cytoskeleton*, vol. 64, pp. 217–232, mar 2007.
26. A. Sanati Nezhad, M. Packirisamy, and A. Geitmann, "Dynamic, high precision targeting of growth modulating agents is able to trigger pollen tube growth reorientation.," *The Plant Journal*, vol. 80, pp. 185–195, Oct. 2014.

27. S. T. McKenna, J. G. Kunkel, M. Bosch, C. M. Rounds, L. Vidali, L. J. Winship, and P. K. Hepler, "Exocytosis precedes and predicts the increase in growth in oscillating pollen tubes.," *The Plant Cell*, vol. 21, pp. 3026–3040, Oct. 2009.
28. H. Vogler, C. Draeger, A. Weber, D. Felekis, C. Eichenberger, A.-L. Routier-Kierzkowska, A. Boisson-Dernier, C. Ringli, B. J. Nelson, R. S. Smith, and U. Grossniklaus, "The pollen tube: a soft shell with a hard core.," *The Plant Journal*, vol. 73, pp. 617–627, Feb. 2013.
29. J. Dumais, S. L. Shaw, C. R. Steele, S. R. Long, and P. M. Ray, "An anisotropic-viscoplastic model of plant cell morphogenesis by tip growth.," *The International journal of developmental biology*, vol. 50, no. 2-3, pp. 209–222, 2006.
30. E. R. Rojas, S. Hotton, and J. Dumais, "Chemically mediated mechanical expansion of the pollen tube cell wall.," *Biophysical journal*, vol. 101, pp. 1844–1853, Oct. 2011.
31. A. E. Hill, B. Shachar-Hill, J. N. Skepper, J. Powell, and Y. Shachar-Hill, "An osmotic model of the growing pollen tube.," *PLoS ONE*, vol. 7, no. 5, p. e36585, 2012.
32. L. Zonia, "Spatial and temporal integration of signalling networks regulating pollen tube growth.," *Journal of experimental botany*, vol. 61, pp. 1939–1957, Apr. 2010.
33. L. J. Winship, G. Obermeyer, A. Geitmann, and P. K. Hepler, "Under pressure, cell walls set the pace.," *Trends in plant science*, vol. 15, pp. 363–369, July 2010.
34. J. Schiefelbein, S.-H. Kwak, Y. Wieckowski, C. Barron, and A. Bruex, "The gene regulatory network for root epidermal cell-type pattern formation in Arabidopsis.," *Journal of experimental botany*, vol. 60, no. 5, pp. 1515–1521, 2009.
35. M. Benítez and E. R. Alvarez Buylla, "Dynamic-module redundancy confers robustness to the gene regulatory network involved in hair patterning of Arabidopsis epidermis.," *Bio Systems*, vol. 102, pp. 11–15, Oct. 2010.
36. N. S. Savage, T. Walker, Y. Wieckowski, J. Schiefelbein, L. Dolan, and N. A. M. Monk, "A mutual support mechanism through intercellular movement of CAPRICE and GLABRA3 can pattern the Arabidopsis root epidermis.," *PLoS Biology*, vol. 6, p. e235, Sept. 2008.
37. M. Benítez, N. A. M. Monk, and E. R. Alvarez Buylla, "Epidermal patterning in Arabidopsis: models make a difference," *Journal of Experimental Zoology Part B: Molecular and Developmental Evolution*, vol. 316B, no. 4, pp. 241–253, 2011.

38. A. R. Jones, E. M. Kramer, K. Knox, R. Swarup, M. J. Bennett, C. M. Lazarus, H. M. O. Leyser, and C. S. Grierson, "Auxin transport through non-hair cells sustains root-hair development," *Nature Cell Biology*, vol. 11, pp. 78–84, 01 2009.
39. U. Fischer, Y. Ikeda, K. Ljung, O. Serralbo, M. Singh, R. Heidstra, K. Palme, B. Scheres, and M. Grebe, "Vectorial information for arabidopsis planar polarity is mediated by combined aux1, ein2, and gnom activity," *Current Biology*, vol. 16, pp. 2143–2149, 2006.
40. A. J. Molendijk, F. Bischoff, C. S. V. Rajendrakumar, J. Friml, M. Braun, S. Gilroy, and K. Palme, "Arabidopsis thaliana rop gtpases are localized to tips of root hairs and control polar growth," *EMBO Journal*, vol. 20, no. 11, pp. 2779–2788, 2001.
41. M. Jones, J.-J. Shen, Y. Fu, H. Li, Z. Yang, and C. S. Grierson, "The arabidopsis rop2 gtpase is a positive regulator of both root hair initiation and tip growth.," *The Plant Cell*, vol. 14, no. April, pp. 763–776, 2002.
42. J. Xu and B. Scheres, "Dissection of Arabidopsis ADP-RIBOSYLATION FACTOR 1 Function in Epidermal Cell Polarity," *The Plant Cell Online*, vol. 17, pp. 525–536, feb 2005.
43. T. Xu, M. Wen, S. Nagawa, Y. Fu, J.-G. Chen, M.-J. Wu, C. Perrot-Rechenmann, J. Friml, A. M. Jones, and Z. Yang, "Cell surface- and rho GTPase-based auxin signaling controls cellular interdigitation in Arabidopsis.," *Cell*, vol. 143, pp. 99–110, Oct. 2010.
44. R. J. H. Payne and C. S. Grierson, "A theoretical model for rop localisation by auxin in arabidopsis root hair cells.," *PLoS ONE*, vol. 4, p. e8337, 2009.
45. C. Ringli, N. Baumberger, A. Diet, B. Frey, and B. Keller, "ACTIN2 is essential for bulge site selection and tip growth during root hair development of Arabidopsis.," *Plant physiology*, vol. 129, pp. 1464–1472, Aug. 2002.
46. Y. Bao, B. Kost, and N. H. Chua, "Reduced expression of alpha-tubulin genes in Arabidopsis thaliana specifically affects root growth and morphology, root hair development and root gravitropism.," *The Plant journal*, vol. 28, pp. 145–157, Oct. 2001.
47. C. S. Kiefer, A. R. Claes, J.-C. Nzayisenga, S. Pietra, T. Stanislas, A. Huser, Y. Ikeda, and M. Grebe, "Arabidopsis AIP1-2 restricted by WER-mediated patterning modulates planar polarity," *Development*, vol. 142, pp. 151–161, jan 2015.
48. H. Kusano, C. Testerink, J. E. M. Vermeer, T. Tsuge, H. Shimada, A. Oka, T. Munnik, and T. Aoyama, "The Arabidopsis Phosphatidylinositol Phosphate 5-Kinase PIP5K3 is a key regulator of root hair tip growth.," *The Plant Cell*, vol. 20, pp. 367–380, Feb. 2008.

49. S. Pietra, A. Gustavsson, C. Kiefer, L. Kalmbach, P. Hörstedt, Y. Ikeda, A. N. Stepanova, J. M. Alonso, and M. Grebe, "Arabidopsis SABRE and CLASP interact to stabilize cell division plane orientation and planar polarity," *Nature communications*, vol. 4, Nov. 2013.
50. S. K. Singh, U. Fischer, M. Singh, M. Grebe, and A. Marchant, "Insight into the early steps of root hair formation revealed by the procuste1 cellulose synthase mutant of Arabidopsis thaliana," *BMC Plant Biology*, vol. 8, no. 1, p. 57, 2008.
51. Y. Fu, T. Xu, L. Zhu, M. Wen, and Z. Yang, "A ROP GTPase signaling pathway controls cortical microtubule ordering and cell expansion in Arabidopsis.," *Current biology*, vol. 19, pp. 1827–1832, Nov. 2009.
52. J. D. Masucci and J. W. Schiefelbein, "The rhd6 mutation of arabidopsis thaliana alters root-hair initiation through an auxin- and ethylene-associated process.," *Plant physiology*, vol. 106, pp. 1335–1346, 1994.
53. M. Grebe, J. Friml, R. Swarup, K. Ljung, G. Sandberg, M. Terlou, K. Palme, M. J. Bennett, and B. Scheres, "Cell polarity signaling in arabidopsis involves a bfa-sensitive auxin influx pathway," *Current Biology*, vol. 12, no. 02, pp. 329–334, 2002.
54. Y. Ikeda, S. Men, U. Fischer, A. N. Stepanova, J. M. Alonso, K. Ljung, and M. Grebe, "Local auxin biosynthesis modulates gradient-directed planar polarity in arabidopsis.," *Nature cell biology*, vol. 11, no. 6, pp. 731–738, 2009.
55. R. Swarup, E. M. Kramer, P. Perry, K. Knox, H. M. O. Leyser, J. Haseloff, G. T. S. Beemster, R. Bhalerao, and M. J. Bennett, "Root gravitropism requires lateral root cap and epidermal cells for transport and response to a mobile auxin signal," *Nature cell biology*, vol. 7, pp. 1057–1065, 11 2005.
56. M. Bosch, "Pectin Methylesterases and Pectin Dynamics in Pollen Tubes," *The Plant Cell*, vol. 17, pp. 3219–3226, dec 2005.
57. C.-Y. Pang, H. Wang, Y. Pang, C. Xu, Y. Jiao, Y.-M. Qin, T. L. Western, S.-X. Yu, and Y.-X. Zhu, "Comparative Proteomics Indicates That Biosynthesis of Pectic Precursors Is Important for Cotton Fiber and Arabidopsis Root Hair Elongation," *Molecular & Cellular Proteomics*, vol. 9, pp. 2019–2033, sep 2010.
58. C. Ambrose, J. F. Allard, E. N. Cytrynbaum, and G. O. Wasteneys, "A CLASP-modulated cell edge barrier mechanism drives cell-wide cortical microtubule organization in Arabidopsis," *Nature Communications*, vol. 2, p. 430, aug 2011.